Plant and Process Safety, 6. Risk Analysis

ULLMANN'S ENCYCLOPEDIA OF INDUSTRIAL CHEMISTRY

Ulrich Hauptmanns, Schönebeck, Germany

Michael Schatzmann, Universität Hamburg, Hamburg, Germany

Axel Schönbucher, Universität Duisburg-Essen, Lehrstuhl für Technische Chemie I, Essen, Germany

Stefan Schälike, Bundesanstalt für Materialprüfung (BAM), Reaktionsfähige Stoffe und Stoffsysteme, Berlin, Germany

Risk is the possibility of suffering damage. In engineering it may be quantified and is assessed as a combination of the expected frequency of an undesired event, e.g., in case of process plants a fire, an explosion, or a toxic release, and the damage associated with this event. Every possibility to suffer damage is a risk if it is uncertain whether it will become reality. Damage and uncertainty therefore are the two elements which determine a risk. If the magnitude of damage and the uncertainty of its occurrence can be quantified, then a number may be assigned to the corresponding risk, the risk number. Frequently, this number refers to a

10.1002/14356007.q20_q05

certain period of exposure, for example, one year. It is then called "risk per year".

Nevertheless it is difficult to assess the risk from a process plant, because accidents are rare events. Therefore, one cannot extrapolate from the number of occurrences in one year to the number expected during the next, as, for example, with the number of flu cases, a procedure called actuarial approach. Hence, the assessment must be based on the knowledge of details. An accident is decomposed into small steps starting with the initiating event (e.g., the failure of the coolant pump of a reactor for an exothermal reaction) up to the damage caused. Expected frequencies, respectively probabilities are then assigned to these steps. The general procedure is shown in Figure 1.

It consists of four steps [1]:

1. Event sequences: All event sequences contributing to the risk must be described in detail. This is done by using event trees in combination with fault trees. The various event sequences resulting from an initiating event, D_i (e.g., the failure of an operational component or a human error), consist of concatenations of sub-events A_1 A_2, . . ., I_1, I_2,. . ., which describe the failure (A) or functioning (I) of technical systems. For example: Release of chlorine following pipe rupture due to overpressure. Each sequence represents a scenario, i.e., a potential development of the future.
2. Characteristics: In this step the results of the different event sequences are described. This is done in terms of the parameters of the event characteristics which are essential for assessing the damage (e.g., intensity of a possible explosion, level of heat and smoke generation, etc.). These are quantified by means of experimental observations or model calculations. Depending on the range of values of the above-mentioned parameters and their significance for an assessment of the damage the results are divided into classes or categories k_1, k_2 . . ., k_n for the sake of simplification. These categories represent the initial and boundary conditions for the calculations to be performed for assessing the magnitude of damage. An example for such a boundary condition is a leak of chlorine from a cross section of 10 cm^2, at a release height of 10 m, and with a pressure difference of 500 kPa, which represents a category covering all chlorine leaks smaller than 10 cm^2.
3. Exposure sequences: In this step all processes are described according to time, location, intensity, and probability (exposure sequences E_1,. . ., E_N) through which the event

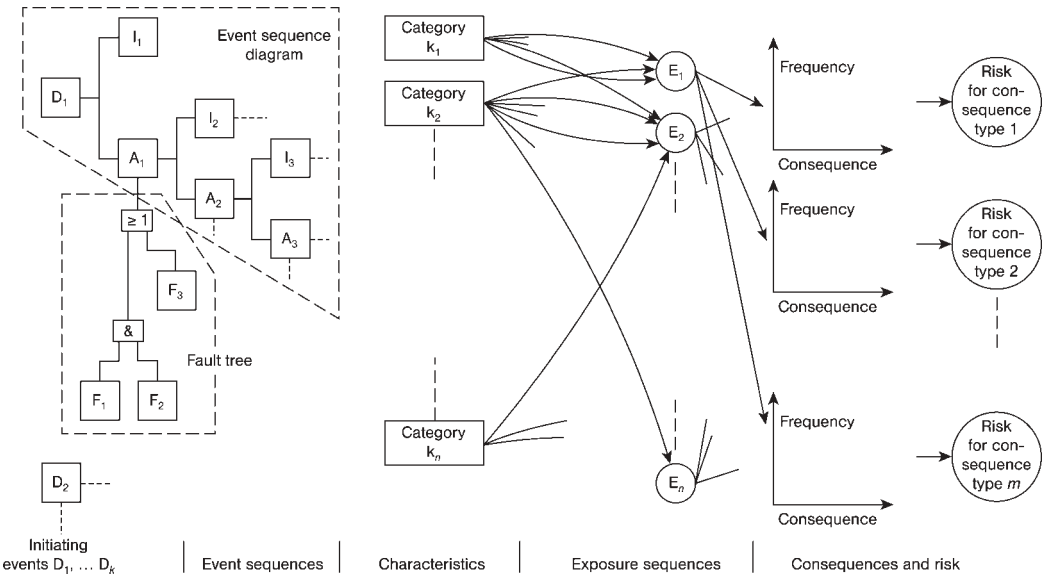

Figure 1. Outline of a risk assessment based on detailed knowledge of event and exposition sequences (from [1])

characteristics could have a detrimental effect on a single person or a group of persons, on the environment, or on valuable assets. An example is a dispersion calculation for released chlorine to assess how many people are exposed to which concentrations during which period of time. In this assessment measures like staying indoors or evacuation may be accounted for.

4. Damage and risk: In this step the relation between the intensity of the damaging effects and all damages resulting therefrom is described. Firstly, the amount of damage is assessed. For example, x fatalities or y cases of acne following chlorine exposure. To calculate the risk, the damage and its expected frequency of occurrence are combined, e.g., $10^{-6} \times$ fatalities per year caused by chlorine exposure.

Steps (1) and (2) constitute the analysis of the plant, which sheds light on how unwanted events may occur and which areas of the design exhibit weaknesses compared with others. After eliminating potential weaknesses, a safety technologically balanced design should result, i.e., all sequences leading to the undesired event should make more or less the same contribution to it and not be dominating. This part of the analysis is addressed in Chapter 1.

Steps (3) and (4) are the consequence calculations, which lead to an assessment of the damage caused by the undesired events. Their treatment is the subject of Chapter 2.

In conclusion it may be stated that risk is assessed by examining in detail a limited number of scenarios which are considered to be representative for the infinity of conceivable scenarios. In a formalized way risk may be represented by Equation (1) [2]

$$R_n = \langle S_n, f_n, d_n \rangle \quad n = 1, \ldots, N \tag{1}$$

where S_n describes an event sequence which is a possible answer to the question "what can happen?", f_n is its expected frequency of occurrence, and d_n represents its consequences, i.e., category and magnitude of damage; N is the number of event sequences taken into account in determining the risk. Theoretically, N would be arbitrarily large, since arbitrarily many event sequences are conceivable. In practice, however, event sequences are not taken into account if they are so unlikely that their occurrence may be excluded on the grounds of numerical estimates or of common sense.

Completeness can of course not be proved. However, if good records on accidents exist, the expected frequency of occurrence of an event that has not yet occurred in the type of plant under investigation may be obtained with the help of Equation (19). If the result is below the value obtained from the sequences which are taken into account, it may safely be neglected even if one assumes that no safety barriers for coping with it are present (probability of barrier failure 1).

Uncertainties are unavoidable in determining frequencies of occurrence and magnitudes of damage. They are normally accounted for in risk analyses; details may be found in [3–5].

Risk analysis consists of a qualitative assessment complemented by quantification. In what follows pertinent methods of analysis are described.

1. Process and Plant Safety Analysis

1.1. Qualitative Methods

A number of methods are available for identifying sources of hazards and initiating events, some of which were developed specifically for chemical plant analysis. They are often called systems analysis methods. OSHA lists the following methods of safety analysis [6]:

- What-if analysis?
- Checklists
- What-if analysis/checklists
- Hazard and operability study (HAZOP)
- Failure mode and effects analysis (FMEA)
- Fault tree analysis (FTA)
- Other appropriate methodologies

Numerous other methods exist; in most cases they are modifications of the procedures mentioned. It must be kept in mind that these methods merely serve to organize existing input knowledge in such a way that the output may be used as a basis for a safety-related decision. They are an aid to the analysts' imagination and require thought experiments to be performed. Safety analysis is a multidisciplinary task covering all areas involved in the design of a plant.

In addition, it normally deals with nonstationary regimes. It requires comprehensive information on the process and the plant, usually provided by P&I diagrams and descriptions of the process and the plant design etc.

The interrelationships between different sources of information and the systems analysis methods are illustrated by Figure 2, where the safety team leader is assumed to be a process engineer. It should be noted that a safety analysis is called qualitative (despite the use of model calculations and experimental results) as long as no probabilities or expected frequencies are assigned to the results.

An assumption usually underlying all methods is that the design of the system is safe if all of its components work as required. However, it is advisable to check in the context of the safety analysis whether this assumption is true or not.

Some of the methods are presented in more detail below. A comprehensive account with references and examples is found in [8].

All methods have in common that they trigger thought experiments. These can only be carried out with success if the analyst, or preferably the group of analysts, has the necessary background knowledge, for example, in engineering, physics, and chemistry.

1.1.1. What If? Analysis

The "what if? method" involves asking a series of questions beginning with this phrase as a means of identifying hazards. Questions such as

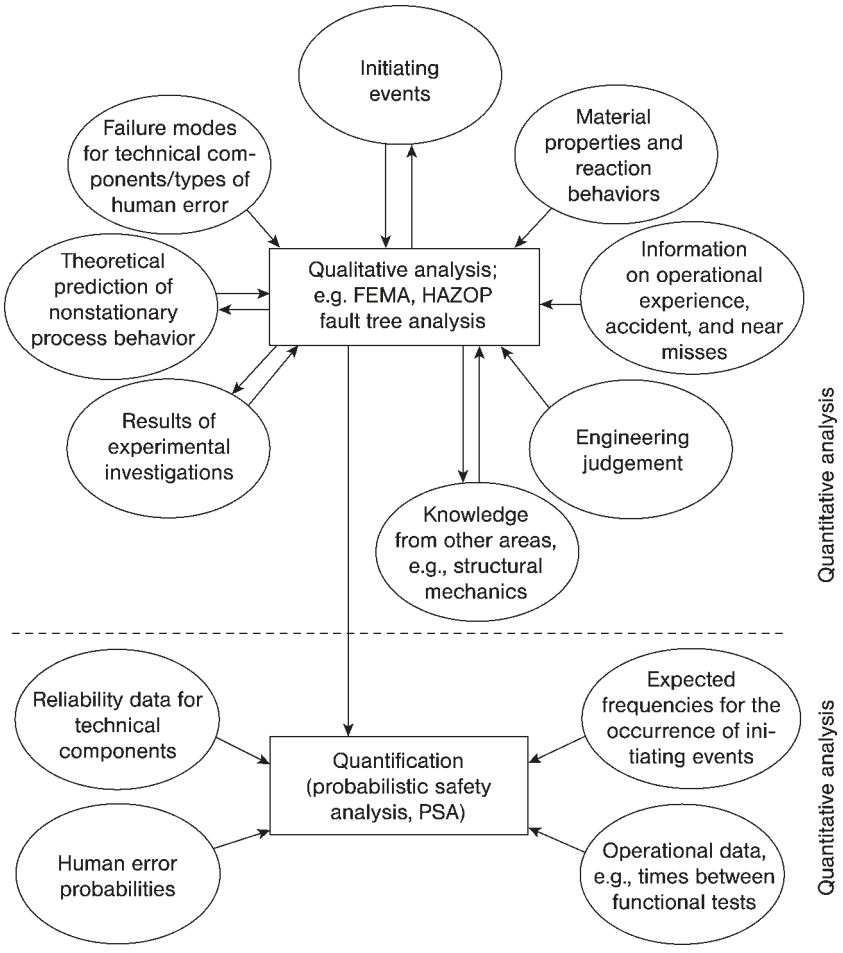

Figure 2. Relationship between different areas of knowledge and methods of safety analysis (after [7]).

- What if the pump stops?
- What if the temperature sensor fails?

are asked. Other similar questions may be posed as well.

The method involves a review of the whole design by a team using a list of predetermined questions.

1.1.2. Checklists

Checklists represent a systematic account of past experience. They are a reminder of aspects which should be controlled. Checklists may have any desired degree of detail and be adapted to the purpose in question. They allow an examination of safety-relevant questions with little effort. Checklists are used to identify hazard potentials by examining every component and subsystem in terms of the topics included in the list.

The application of checklists is appropriate for comparable situations. However, the possibility of overlooking problems exists. The procedure is therefore mainly used to prepare the application of other methods of analysis.

Often checklists are formulated to require a simple "yes" or "no" as the answer. It is more useful to formulate open questions like "is the safety relief adequate?" instead of asking "is there a relief valve?". The former incites the analyst to use his knowledge of engineering, chemistry, etc. A method for assessing the safety culture on the basis of openly formulated questions is presented in [9].

1.1.3. Failure Mode and Effects Analysis (FMEA)

The failure mode and effects analysis [10] is an inductive qualitative or semiquantitative method for identifying hazardous states. It enables one to determine the consequences of different failure modes of components for other components, the process, and the technical system. It is equipment- rather than process-oriented.

Its objective is to identify weaknesses in the design of systems and interfaces. It is focused on single failures causing an unwanted state and reveals whether a backup exists or not. Hence, it shows whether measures must be taken to eliminate weaknesses of the design. If the extension FMECA (failure modes, effects, and criticality analysis) is performed, in addition the criticality, i.e., the expected frequency and associated damage of the unwanted state are estimated.

The corresponding format requires the following topics to be addressed (1) component, (2) failure or error mode, (3) effects on other components, (4) effects on the whole system, (5) detection method, (6) compensating provisions and remarks, and in case of an FMECA additionally (7) severity, and (8) expected frequency.

Failures of active (e.g., a control valve) and passive (e.g., a pipe or a pump casing) components as well as operators' actions are investigated. The method is best suited to analyze series systems. It is inductive and appropriate for preparing a fault tree analysis (cf. 1.2.2), which is a deductive method and better suited for systems with both series and parallel structures.

1.1.4. Hazard and Operability (HAZOP) Studies

The HAZOP (hazard and operability) study method [11, 12], which was developed in the 1960s by ICI in the UK, is especially suited for analyses of process plants. Its German version is known as PAAG [13]. The study is performed by a multidisciplinary team using the guide words presented in Table 1. Based on a comprehensive description of the plant and the process, every part is systematically questioned. The objective is to discover deviations from the intention of the design and to identify associated causes and consequences. The design intent is

Table 1. Guide words for a HAZOP study

Guide Word	Meaning
NO or NOT	Complete negation of the design intent
MORE	Quantitative increase
LESS	Quantitative decrease
AS WELL AS	Qualitative modification/increase
PART OF	Qualitative modification/decrease
REVERSE	Logical opposite of the design intent
OTHER THAN	Complete substitution

Table 2. Time-related guide words

Guide Word	Meaning
EARLY	Relative to the clock time
LATE	Relative to the clock time
BEFORE	Relating to order or sequence
AFTER	Relating to order or sequence

examined, for example, with respect to process parameters such as flow, temperature, pressure, and concentration. In general it suffices to consider the pipes connecting the equipment because deviations which become manifest there are usually caused by malfunctions of the equipment they connect.

The analysis may be applied to both continuous and batch processes and should include startup and shutdown. For the latter additional time-related guide words may be useful (Table 2).

In general the guide words apply to plant functions and—with the possible exception of REVERSE—to substances as well. If necessary, they must be modified accordingly.

The analysis is to be carried out by a group of experts with different backgrounds. Areas like process and safety engineering, process control, electrical and civil engineering, plant design and operation should be represented. The group should be chaired by a person familiar with the analysis technique but not necessarily specialized in the process under investigation.

The procedure is illustrated by the following example.

System Description. The cooling system, which is shown in Figure 3, consists of two loops, the coolant tank (1), two redundant pumps in each loop (P1A, P1B and P2A, P2B), and the heat exchanger (2). The latter is connected to a refrigerating unit. In one of the loops the coolant, whose temperature is −5°C, is pumped by one of the pumps P2A or P2B from the cold side of the coolant tank to the consumers of the production process. After extracting heat from the consumers the coolant is pumped back into the warm side of the coolant tank.

The second loop serves to transport the coolant from the warm side of the coolant tank through the evaporator (2) where it is cooled to −5°C. Transport is effected by either pump P1A or P1B. After passing through the evaporator the coolant is returned to the cold side of the coolant tank. The coolant temperature is lowered from 1 to −5°C in the heat exchanger. The heat is removed by evaporation of a halogenated hydrocarbon in the refrigerating unit, whose details are not shown in Figure 3. The cooling unit is controlled by temperature switch TS 4001. It ensures the appropriate temperature of the coolant (−5°C), which is returned from the refrigerating unit to the cold side of the coolant tank.

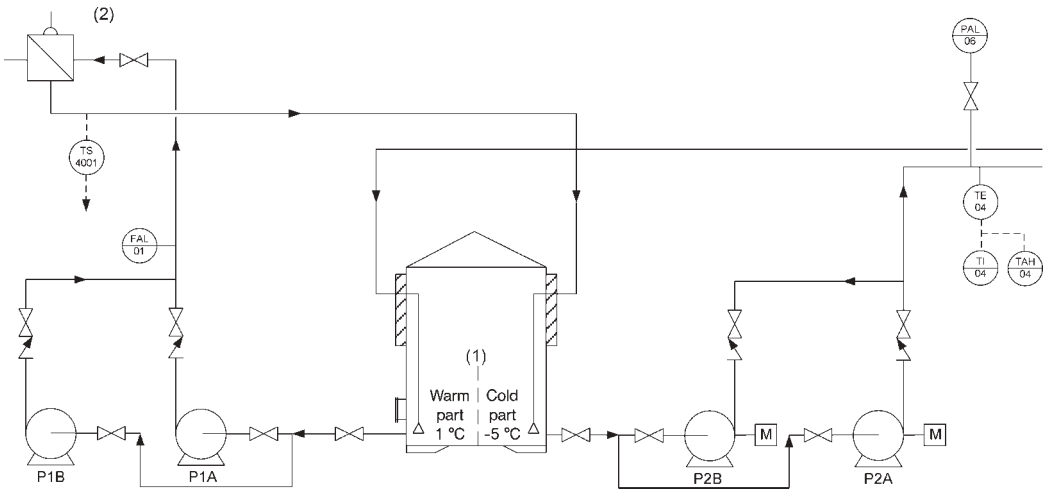

Figure 3. P&I diagram of the cooling system of a plant for producing hexogen [14, 15]

The flow in the warm loop is monitored by flow switch FAL 01, which provides an alarm in the control room on low flow. Both temperature and pressure of the cold loop are monitored. Instrument TI04 indicates the temperature in the control room, giving an alarm signal for high temperature via TAH04. If the pressure in the loop is too low, instrument PAL 06 gives an alarm. The operating handbook contains the instructions for actions to be taken after perceiving any of the alarms.

Cooling failures, if undiscovered or unattended, would lead to the exothermal process downstream not being cooled adequately. This would cause a runaway reaction if the reactor safety devices failed as well.

HAZOP Study. The HAZOP study is shown in Table 3.

It should be noted that

- For realizing the required action the information about its necessity must be available, e.g., by an alarm (here indicated under the heading consequences)
- It is important to make sure that the time for detection and realizing the required action is sufficiently large to prevent a dangerous state

1.2. Qualitative Methods Appropriate for Quantification

1.2.1. Event Tree Analysis

Event tree or event sequence analysis is an inductive method. Starting from a defined initiating event (e.g., pipe rupture, failure of energy supply) and depending on the functional success or failure of the operating and safety systems (barriers) required for coping with it, its different possible consequences are determined [16]. The paths of events resulting therefrom are combined in an event tree, as shown in Figure 4. It is useful to distinguish between plant-internal and plant-external events:

- Plant internal events are, for example:
  - Mechanical failures of active components (e.g., pumps) and passive components (e.g., pipes and tanks)
  - Malfunctions or failures of process control equipment
  - Failure of the supply of electricity or other media to equipment
  - Human error
- External events are, for example:
  - Natural events such as lightning, earthquakes, and flooding
  - Impacts from other hazardous installations in the vicinity (e.g., industrial plants)
  - Impacts from transportation media (e.g., aircraft crash or explosion of a passing tank car or truck)
  - Sabotage

Since it is impossible to treat all conceivable initiating events, it suffices to deal with the important ones, i.e., those which dominate with respect to frequency of occurrence and/or consequences.

The expected frequencies of the initiating events are in general derived from observation. Either estimates are directly obtained from operational experience (e.g., for the occurrence of pipe leaks) or the initiating event is decomposed into such subevents for which operational experience is available. The frequency of occurrence is then assessed by fault tree analysis (cf. Section 1.2.2). Additionally, there are cases where one has to rely on expert judgment.

Depending on the countermeasures required and the operational and safety systems available for these measures, their failure results in bifurcations of possible event sequences. These are represented by the event tree. Every path through such a tree represents a scenario, i.e., a possible development of the future triggered by the initiating event.

Which of the systems must maintain their function and which ones are demanded is assessed by simulating the dynamic behavior of the process. The simulation is based on mathematical models for physical and chemical processes. Each branch of the event tree is the static description of an event proceeding in time. The process is represented by a few bifurcations where, depending on the failure (downward branch) or functioning (upward branch) of the required system, the further course of the process is determined.

Table 3. HAZOP study for the system of Figure 3 (guide words which do not proceed were left out after examination)

Guide word	Deviation	Possible causes	Consequences	Action required
			Coolant flow from the heat exchanger to the cold part of tank 1	
NO or NOT	No flow	P1A failure	Depletion of contents of cold part; flow alarm via FAL01	Activation of reserve pump P1B
MORE	Abnormally high temperature	Refrigerating unit failed	Cold part gradually warms up; alarm via TAH 04	Shutdown of plant; repair of refrigerating unit
LESS	Less flow	Pipe leak	Depletion of contents of cold part: detection on walk-around	Shutdown of plant; repair of pipe
			Coolant supply from the cold part of tank 1 to the process	
NO or NOT	No flow	P2A failure	No supply to the process; pressure alarm via PAL06	Activation of reserve pump P2B
LESS	Less flow	Pipe leak	Insufficient cooling of process	Emergency trip of plant; repair of pipe
			Coolant flow from the process to the warm part of tank 1	
NO or NOT	No flow	P2A failure	No return to tank, depletion of warm part; pressure alarm via PAL06	Activation of reserve pump P2B
LESS	Less flow	Pipe leak	Depletion of warm part of tank; detection on walk-around	Repair of pipe
			Coolant flow from the warm part of tank 1 to the heat exchanger	
NO or NOT	No flow	P1A failure	Depletion of contents of cold part; flow alarm via FAL01	Activation of reserve pump P1B
LESS	Less flow	Pipe leak	Depletion of contents of cold part: detection by FAL01, if before instrument, on walk-around or TS 4001	Shut-down of plant; repair of pipe

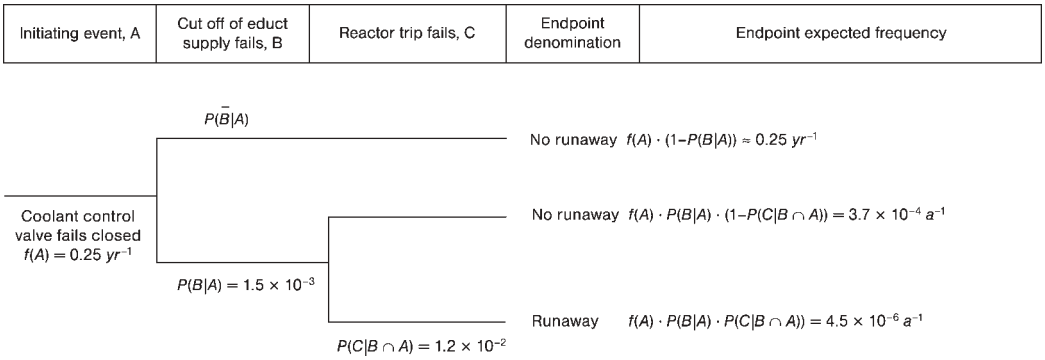

Figure 4. Event tree showing the consequences of the failure of the coolant control valve of a reactor for an exothermal reaction (quantification based on assumed frequencies and conditional probabilities)

To determine the minimum requirements for fulfilling a success criterion (e.g., 75% of pump flow must be available for sufficient cooling) frequently information from accident simulations which have been carried out in other contexts is used, e.g., the licensing procedure. The event tree analysis for the technical systems of a plant may be divided into two tasks:

- The analyses dealing with the event sequence, as far as it is determined by the functioning of the operational and safety systems
- The analyses which deal with the event sequences resulting from the assumption that the operational and safety systems fail; these concern events within the plant up to the release of hazardous substances and energy

Event trees are based on binary logic, i.e., components and systems either function fully or fail completely. Possible intermediate states are assigned to one of the two, normally the failed state. The material bases for the logic structure are results from plant dynamic calculations, experimental results, and engineering judgment.

In performing an event tree analysis the following aspects must be observed:

- Mutual dependencies may exist. For example, the countermeasures following an initiating event may not be completely independent.
- Secondary failures may occur, i.e., for any event of a sequence a possible impact from previous events must be accounted for. If, for example, a fluid flowing from a leak impacted a sensor of a protective system, the possible increase of its failure probability must be accounted for.

Hence, all probabilities assigned to events are conditional probabilities depending on the outcome of events prior to the one under consideration; independent probabilities may be used if the impact of dependencies is negligible.

The following steps must be performed (based on [17])

Qualitative analysis

1. Identify (and define) a relevant accidental (initiating) event that may give rise to unwanted consequences
2. Identify the barriers that are designed to deal with each particular accidental event
3. Construct the event tree
4. Describe the (potential) resulting accident sequences

Quantification

- Determine the frequency of the accidental event and the (conditional) probabilities of the branches in the event tree
- Calculate the probabilities/frequencies for the identified consequences (outcomes)
- Compile and present the results from the analysis

The description of event tree analysis given here is based on the analysis of plant internal sequences. Note, however, that event trees are fundamental for describing accident

consequences, e.g., the events following the release of a flammable substance like fires or explosions (cf. Chap. 2).

1.2.2. Fault Tree Analysis

Fault tree analysis [18–20] is a deductive method, which usually serves for quantification. Just like all methods of systems analysis it requires in the first place a qualitative investigation of the system under analysis. After system failure or more generally the undesired or unwanted event (e.g., toxic release) has been defined, logic relationships with the so-called primary or basic events are identified and represented by a fault tree (Fig. 5). The primary event may represent the failure of a technical component, an operator error, an impact from outside like flooding or the spreading of a fire from neighboring installations.

Fault tree analysis is a complete procedure. Due to its deductive nature it yields all combinations of events leading to the undesired event if it is consistently applied. Limitations are not inherent in the process of analysis but result from a possible lack of knowledge and care by the analyst. Obviously, a fault tree analysis cannot reveal phenomena which are unknown at the time of its execution.

The fault tree represents the result of the qualitative part of the analysis. This is based on questions such as "How can this happen?". These questions enable one to firstly relate the undesired event with the failure of sub-systems functions such as cooling or energy supply. Successively these failures are broken down into the failures of sub-sub-systems, etc. until the level of the primary events is reached. Hence, only portions of the plant of a size which can be handled by the human intellect at any one time are analyzed; they are then logically connected with the analyses of other portions.

In general, a variety of failure combinations of various components or events such as human error are obtained which make sub-systems fail. The failure of a sub-system may either directly cause the undesired event or do so in combination with failures of other sub-systems, components or human error. The combinations are described by logical AND and OR gates. The output of an OR gate is true if any one, several or all of its inputs are true (inclusive OR); the AND gate requires all of its inputs to be true in order for its output being true.

Thus complex relations within systems are described by using binary logic, which considers only the functioning or failure of components, or the occurrence or nonoccurrence of events. This, together with a suitable graphical presentation, permits a transparent and comprehensive treatment, even of very large technical systems. The fault tree is the logical model of a technical process with regard to the undesired event. Specific problems like human error, dependent failures, and external events (e.g., the impact of an explosion blast wave on the system) can be accounted for. Dependence is especially important because it may weaken or disable layers of protection. Fault tree analysis is particularly suited for the investigation of systems whose design fulfils the single failure criterion and which therefore can only fail as a consequence of multiple failures. Depending on the effort to be invested varying degrees of detail including coarse or screening analyses are possible (cf. Sections 1.7, and→ Plant and Process Safety, 7. Risk Calculations, Chap. 1).

The fault tree represents a simplified model of the system with regard to the undesired event. Its advantage is that the influence of components on one another and the consequences of their failure, human error, and impact from outside on the system may be accounted for. To model an entire system accounting for the process parameters (e.g., pressure, temperature, concentration, mass flow, etc.) and their evolution with time after the occurrence of the primary event usually proves too difficult. Nevertheless the knowledge of the time-dependent behavior of the physical, chemical, or other relevant process parameters (e.g., biological) following the occurrence of a primary event is necessary. This knowledge is reflected by the logical structure of the fault tree, i.e., the choice of AND or OR gates. The latter is supported, for example, by decisions on whether temperatures or pressures occur during the accident event sequence which exceed material limits. The knowledge on system behavior in general stems from dynamic calculations of material loads, experiments, or engineering judgment. The latter should be exerted with conservatism, i.e., an unfavorable result for the system should be used.

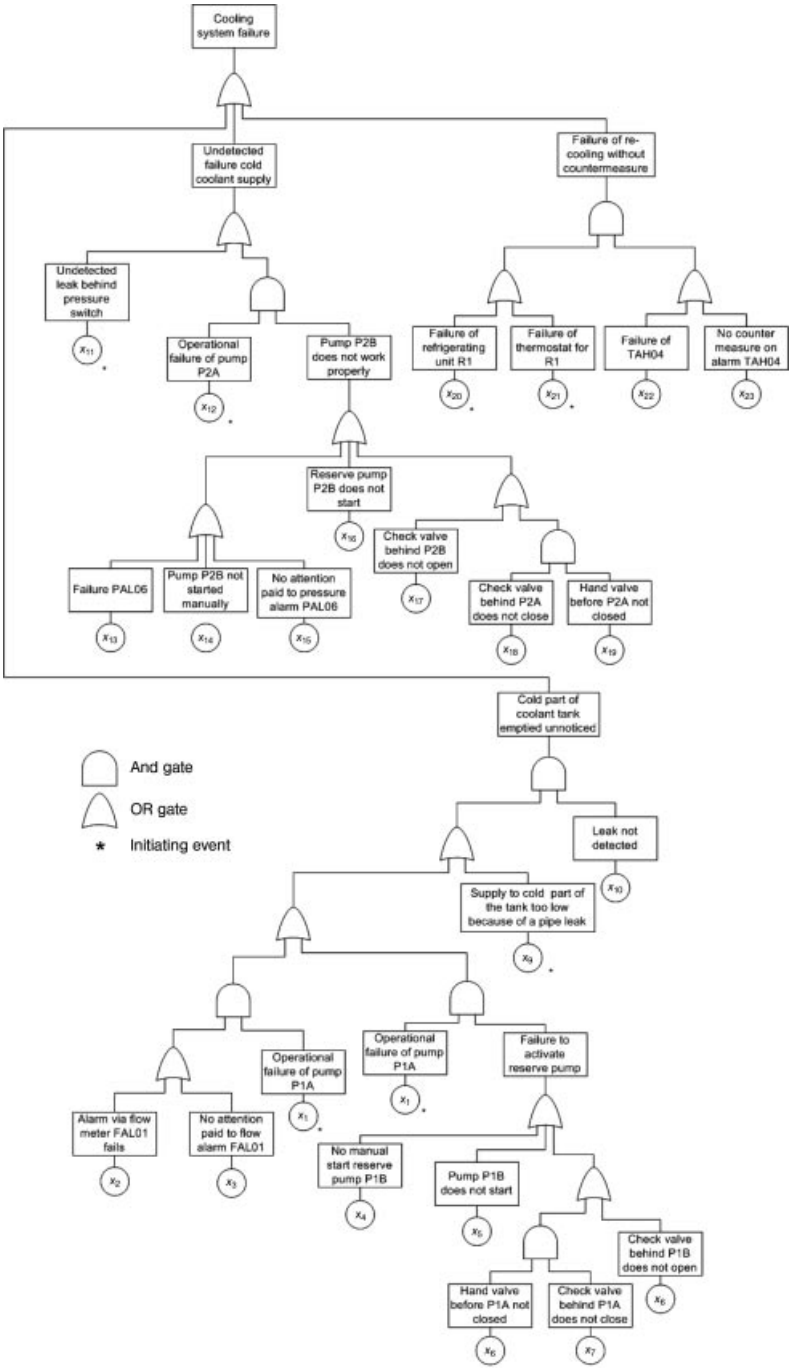

Figure 5. Fault tree for the failure of the cooling system of Figure 3 [21]
x_i, $i = 1, \ldots, 22$ are binary indicator variables describing the state of the component, i.e., $x_i = 1$ failed, $x_i = 0$ working)

When performing a fault tree analysis it is generally assumed that all components are designed, built, and installed such that they fulfill their function if they work properly. For example, one supposes that a relief valve has a cross section which is sufficient to maintain the pressures within the equipment to be protected by discharge within permissible limits. The assumption of correct functioning must be checked in the context of the analysis, especially if failure combinations are considered which may lead to loads beyond the design limits of the components. In such a case correct functioning may not be assumed. An example is a pressure switch exposed, after the breach of a steam pipe, to temperatures and air humidities for which it is not designed.

Fault tree analysis may be used during the design of a plant and thus influence its final configuration. It may be used as well to assess existing designs. In the latter case knowledge is gained on the efficiency of existing design procedures and their potential improvements. Fault tree analysis should especially be used if there is little operational experience with a type of a plant. In such a case the probability of plant failure may not be derived from records on operation (actuarial approach) but must be assessed starting from probabilities for the occurrence of primary events. In any case the expression of the undesired event in terms of primary events reveals possibly existing design weaknesses which cannot be discovered if the actuarial approach is used.

When determining the failure probabilities of components use is made of the circumstance that many items of the same type of component are used and that several plants use the same type of component. Additionally, components usually fail more frequently than the systems in which they are installed. Hence, sufficient operational experience (number of component failures and operating time) can be collected in relatively short periods of time. Although the possibility exists to assess the failure probability of a plant directly if the number of a plant type and the operating experience is sufficiently large, fault tree analysis does not lose its value. It provides insight into system structure, enables one to identify design weaknesses and to judge the effectiveness of planned remedial actions. Such knowledge cannot usually be obtained from records on a specific type of plant. In general it may be stated that fault tree analysis searches for the conditions of plant failure and hence may be regarded as the antithesis of the design process, which aims at identifying the conditions for functioning. Hence it is useful for identifying design weaknesses in both its qualitative and quantitative parts. Eventually, the synthesis of design and safety analysis leads to a better plant.

The following steps are required for carrying out a fault tree analysis:

1. Familiarization with the process and plant using the corresponding descriptions, R&I diagrams, information from the plant designer and operator, etc.
2. Determination of the undesired and initiating events by using checklists, information on material properties, reports on events, and studies of similar plants.
3. Development of the fault tree or trees.
4. Preparation of probabilities for the failure of technical components, human error, and external impacts.
5. Numerical evaluation of the fault tree or trees.
6. Valuation of the results, proposals for improvements, if necessary, and renewed evaluation of the fault tree(s) after having introduced the improvements in them

Fault trees for complex technical systems can only be evaluated with computer programs. Basically, two different methods are distinguished

- Simulation methods
- Analytical methods (cf. [22]).

Simulation methods may either be used for directly simulating system reliability parameters or for identifying the minimal cut sets of the fault tree. Analytical methods serve to determine the minimal cut sets.

A *minimal cut set* is a combination of components whose simultaneous failure is just sufficient to make the system fail. (The word "component" is used to denote any primary event, and the expression "system failure" to signify the undesired event.) Mathematically speaking, it represents a necessary and sufficient

condition for a system failure. In general, several minimal cut sets exist for a technical system. Each of them constitutes a possible mode of its failure.

The decomposition of a fault tree into its minimal cut sets provides information about the logical structure of the system under consideration. In this way, it is possible to determine which component failures alone or in combination with others make the system fail (minimal cut sets with one or several components). The number of failure modes of the system to which a component contributes can also be determined (number of minimal cut sets in which it figures). This information is the basis for identifying weaknesses of the system; for example, minimal cut sets comprising just one component indicate the absence of redundancies. Yet, their relevance can only be judged properly if probabilities are attached to them. To assess the failure probability of the system, its structure function, which describes mathematically the failure of a system in terms of the failure of its components, is formed by using the minimal cut sets of its fault tree. Failure probabilities of the components [e.g., according to Eq. (2) or (10)] are then introduced into this function and thus the failure probability of the system is obtained (c.f. [23]).

1.3. Quantitative Analysis

1.3.1. Failure Rates

Engineering systems are made up of components such as valves, pumps, pipes, measuring devices, control loops, etc. These must fulfill certain tasks within the system. If they do not comply with these tasks because their technical properties have changed in such a way that they lie outside the regions of tolerance of the system, they have failed. Hence, the design of the system determines when a component is considered to have failed. For this reason a fault-forgiving design is desirable [24]. There are many reasons for component failures, e.g., fabrication flaws, corrosion, overload, unfavorable environment, and wear, to name just a few. It is known that components fail after a certain period of time, but this knowledge concerns the average. The point in time of failure of an individual component cannot be predicted.

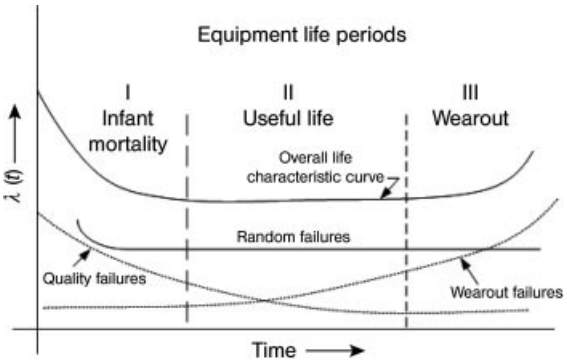

Figure 6. Contributions to component failure rate $\lambda(t)$ [25]

Hence, models describing the operational behavior of components are statistical in nature. The failure behavior is then characterized by the failure rate, whose time dependence is in general described by the so-called bathtub curve, as shown in Figure 6.

The failure rate is composed of contributions representing different failure causes as explained below.

Period I: Early Failures. This period represents early failures due to hidden manufacturing or material defects. It is also called the period of infant mortality and is usually eliminated by product testing with the intention of rejecting substandard components. Substandard components which escape this procedure are identified by observing their behavior during production and then replaced. Hence, it may be assumed that period I is not relevant for plant operation.

Period II: Random Failures. This period with its constant failure rate represents random failures of such nature that future failures do not depend on past operation. These random failures are caused mainly by random fluctuations of operating and environmental conditions which cause loads which exceed design strength.

Period III: Wear-Out Failures. During this period the failure rate increases. This is due to physical and chemical changes during the deployment of the component, which reduce its strength. In general, maintenance strategies provide for replacement before wear-out becomes

manifest. However, prediction of the beginning of wear-out is not possible, and replacement relies on engineering judgment. Hence, there is good reason to assume that components in operation are inscribed in period II and therefore characterized by a constant failure rate [$\lambda(t) = \lambda = \text{const.}$].

Note that the curve of Figure 6 also applies to piece parts. Therefore one or several piece parts may have reached period III whilst the remainder is still in period II. Replacement of these piece parts would then make the component "as good as new".

If λ is constant, component lifetimes τ are described by an exponential distribution (Eq. 2)

$$F(t) = P\{\tau \le t\} = 1 - e^{-\lambda} t \quad t \ge 0 \tag{2}$$

for the component failure probability and

$$\bar{F}(t) = P\{\tau > t\} = 1 - F(t) \quad t \ge 0 \tag{3}$$

for its survival probability, also called reliability.

The corresponding probability density function is obtained by differentiating Equation (2) with respect to t

$$f(t) = \frac{dF(t)}{dt} = \lambda e^{-\lambda} t \tag{4}$$

The average lifetime of a component, also called mean time to failure (MTTF), is obtained by

$$E[\tau] = T = \int_0^\infty t \cdot f(t)\mathrm{d}t = \int_0^\infty \exp(-\lambda t)\mathrm{d}t = -\left[\frac{1}{\lambda} \cdot \exp(-\lambda t)\right]_0^\infty = \frac{1}{\lambda} \tag{5}$$

Hence, the average lifetime in the case of a constant failure rate is equal to the inverse of its failure rate. The important property of the exponential distribution is that the probability of failure in the future does not depend on its past history. It can be proved that the exponential distribution is the only one with a constant failure rate; hence the indication of a constant failure rate (e.g., in a collection of reliability data) makes the use of the exponential distribution mandatory.

1.3.2. Constant Failure Probabilities

Sometimes components are to be treated which have to fulfill their task at a certain moment in time. For example, an emergency Diesel generator must go into operation when the supply from the grid fails. Occasionally components must be modeled which only function during certain periods of time, for example, during charging and discharging operations.

The probability of a component to function at a certain instant in time is called availability on demand p

$$p = \text{const.} \quad (0 \le p \le 1) \tag{6}$$

Its complement, i.e., the probability that a component fails at a certain instant in time or has failed before and not been repaired is called unavailability or probability of failure on demand:

$$u = 1 - p \quad (0 \le u \le 1) \tag{7}$$

On modeling components which have to fulfill their function on demand it is supposed that the failure is caused by the demand itself, for example, by overload or wrong handling.

If component behavior is described by a failure rate, the assumption is that corrosion, dirty environment, etc. are at the root of failure. Such influences are also present during standby (e.g., of components of safety systems). If they cause a failure it manifests itself on demand. Therefore, frequently failure rates are also used to describe standby components. However, the numerical values may differ from those applicable to their operating phases.

1.4. Methods for Increasing Reliability

An important objective of safety analyses is to point out ways to increase the survival probability of technical systems. One possibility is redundancy, i.e., more components than actually needed are installed; they lead to AND gates in a fault tree. Another measure frequently encountered is the installation of reserve components which take over the function of the main component in case that it should fail. A distinction is made between hot reserve (redundancy) and cold reserve. A component running in neutral that takes over a function after just a short delay is called warm reserve.

The following model describes a cold reserve under the ideal condition that

- The need to activate the reserve component is noticed with probability 1 (normally an instrument switches on the reserve component or an alarm prompts an operator to switch on the reserve component)
- The reserve component starts with probability 1, i.e., it is available
- The change to the reserve component is such that there is no interruption of the operation

The failure probability of a system of two components $q_S^{(2)}(t)$ described by the same failure rate then is

$$q_S^{(2)}(t) = 1-e^{-\lambda}t(1+\lambda t) \quad t \geq 0 \tag{8}$$

A relaxation of the above conditions leading to a more realistic model of the system can be achieved by using fault trees.

1.4.1. Maintenance Models

If components are not repaired, unavailability and failure probability are identical. If they are repaired, this is no longer true. A low unavailability is not identical with a low failure probability. For example, an imaginary cable car stops running several a times a day, but is restored within minutes; it then has a low unavailability but a high failure probability. Which of the two parameters is appropriate to characterize a component or a technical system depends on the circumstances. Sometimes both parameters are required. An emergency Diesel generator needs high availability (probability to start) and a high survival probability (functioning until the grid supply is restored, i.e., until mission time t).

Repair on Failure. If components of a standby system announce their failure or components are essential for plant operation, it is assumed that the failure is detected immediately. If additionally the following requirements are satisfied:

- Repair is started immediately after failure
- Component lifetimes are exponentially distributed
- Repair times are exponentially distributed
- Repair leads to a state "as good as new"

we obtain the asymptotic unavailability

$$u = \frac{T_r}{T_r+T} = \frac{\lambda}{\lambda+\mu} \tag{9}$$

where T_r is the average time needed for repair (mean time to repair: MTTR), and μ the repair rate $\mu = 1/T_r$. If there is a delay until the failure becomes known and further delays until the repair is initiated, the sum of the repair time and all other delays may replace T_r. This is known as mean downtime (MTD); it allows one to account for the total time during which the component is not available. Time-dependent results for this case may be obtained by using the theory of Markov processes [26]. Additionally, this enables one to model even more complex situations of maintenance. If the assumption of exponentially distributed lifetimes, repair times, etc. is to be relaxed, analogous results are obtained by using renewal theory [27].

1.4.2. Recurrent Functional Tests

Components of a technical system are often tested in certain time intervals. This applies especially to standby components, whose state (functioning or failed) can only be established in this way, unless the component failure is self-announcing.

The mathematical model makes use of the following assumptions:

- Component lifetimes are exponentially distributed
- The time interval between functional tests θ is constant
- Failures are only discovered on test
- The time needed for the test and a possibly required repair or replacement is much smaller than the average lifetime of the component and hence taken to be equal to 0
- If the component has failed, it is either replaced or repaired in such a way that it is "as good as new", i.e., lifetimes are distributed with the same failure rate as before the repair.

We then have the unavailability

$$u(t) = 1-\exp[\lambda(t-n\theta)] \quad t \geq 0; \quad n = 0, 1, \ldots \tag{10}$$

In Equation (10) n is the whole-numbered part of the quotient t/θ. This leads to the

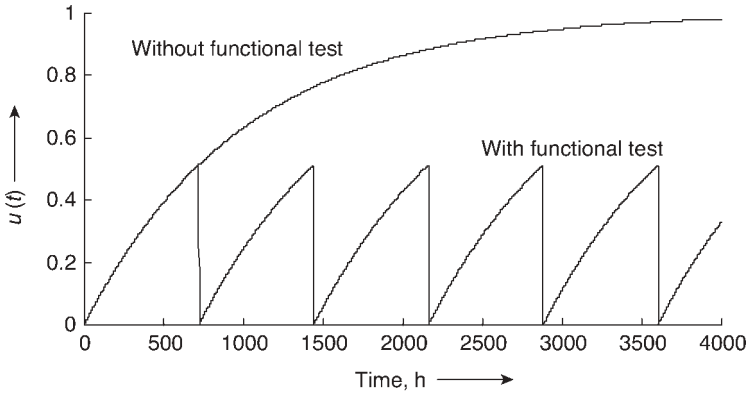

Figure 7. Time-dependent unavailability of a component with $\lambda = 1000 \times 10^{-6} \cdot h^{-1}$ with and without functional tests in time intervals $\theta = 720$ h

so-called sawtooth curve, which is shown in Figure 7.

The maximum unavailability results immediately before the test, i.e.

$$u_{max} = 1 - \exp(-\lambda\theta) \tag{11}$$

and the time-averaged unavailability is

$$\bar{u} = \frac{1}{\theta} \cdot \int_{\theta}^{\theta} \{1 - \exp[-\lambda(t - n\theta)]\} \cdot dt = 1 + \frac{1}{\lambda\theta}[\exp(\lambda\theta) - 1] \tag{12}$$

A component with an exponentially distributed lifetime cannot be improved by maintenance. An improvement would be equivalent to a reduced failure rate. In the present model the unavailability is equal to 0 after every test. If the component works when tested it is new, because $\lambda = $ const. means it does not age. If the component has to be repaired the "as good as new" hypothesis is required to ensure an unavailability of 0.

Since failure rates usually are numerically small, the arguments in the previous formulae are often $\ll 1$. In such a case, the approximation

$$\exp(x) \approx 1 - x$$

holds. This is frequently used, for example in [28, 29]. Then the expressions of Table 4 result. When using them it is advisable to check whether the argument is actually $\ll 1$ or not.

1.5. Reliability Data

For applying the above equations reliability data, i.e., component failure rates and failure probabilities, are required. Their quality determines to a considerable extent the quality of the results of a probabilistic analysis.

The reliability data applied should ideally stem from the plant under investigation, i.e., they should be plant-specific. Whilst this objective may be achieved for analyses of nuclear power stations (cf. [30]), it may not yet be realized for plants from the process industry.

One should at least strive to apply data from the same type of industry in analyses for which plant specific-data are not available. This suggests that key factors of influence on component lifetime such as the type of component used, its working conditions and environment, as well as

Table 4. Approximate expressions for reliability parameters

Parameter	Equation	Denomination in [24, 25]	Approximation
Unavailability	(2)		$\lambda \cdot t$
Availability	(3)		$1 - \lambda \cdot t$
Unavailability of a system with reserve	(8)		$1 - [1 - (\lambda \cdot t)^2]$
Unavailability	(9)		$\lambda \cdot T_r$ (if $\lambda \cdot T_r \ll 1$)
Maximum unavailability	(11)	Probability of failure on demand (PFD)	$\lambda \cdot \theta$
Time-averaged unavailability	(12)	Average probability of failure on demand (PFD_{avg})	$\lambda \cdot \theta / 2$

the maintenance procedures applied are at least similar. It is well known that even these relaxed requirements may rarely be satisfied in the case of process plants. This calls for a collection and evaluation of reliability data, which should be governed by strict quality assurance [31, 32].

When detailed fault tree analyses are carried out reliability data are required at component level. The main published sources are [33–37]; not all of them refer to the process industry, a problem which is addressed in Section 1.8. If risk-based studies are to be performed (see → Plant and Process Safety, 7. Risk Calculations, Section 7.1) aggregates like pipes with valves and fittings, columns, vessels, etc. are considered as a single unit. Failure rates are then supposed to cover all sorts of malfunctions and refer to the loss of containment [38, 39].

Frequentist Reliability Data Evaluation. Usually the lifetime observation process is considered to be a Poisson process [40]. Hence, the lifetimes of the individual components are taken as exponentially distributed, i.e., failures are regarded as random events such that the past does not influence future behavior. The components are characterized by constant failure rates λ. (For simplicity's sake the word "component" is used here to denote components, aggregates, or sub-components.)

The maximum likelihood estimator under these hypotheses is given by

$$\lambda = \frac{k}{mt} \tag{13}$$

In Equation (13) k is the number of failures of a specific failure mode observed, m the number of components at risk, and t the corresponding relevant time of observation.

The number of components at risk m constitutes the group of components which are considered to be technically similar and to be working under comparable conditions. This is the real-world approximation to the statistician's requirement of identical components working under identical conditions. As a result, the judging analyst considers them to form a sufficiently homogeneous class so that they can be described by the same distribution with the same parameter λ.

The relevant time of observation reflects the time during which the conditions determining the failure rate prevail. However, this does not imply that failures cease to be random. For example, a component exposed to a corrosive environment would be expected to exhibit a higher failure rate than an identical one working under noncorrosive conditions. Nevertheless, the moment of its failure cannot be predicted.

The following choices are available:

- Calendar time: $t = T_c$, time during which the items were observed
- Plant operation time: $t = T_p$, time during which the plant was in operation
- Component operation time: $t = T_e$, time during which the item was in operation

Bayesian Reliability Data Evaluation. The Bayesian approach [41] nowadays represents the state of the art for evaluating reliability data. It rests upon the theorem of BAYES

$$f(\lambda/E) = \frac{f(\lambda)L(E/\lambda)}{\int_0^\infty f(\lambda)L(E/\lambda)\mathrm{d}\lambda} \tag{14}$$

where

- $f(\lambda)$ is the prior probability density function (pdf). It reflects the (subjective) assessment of the failure rate before the lifetime observation E is made.
- $L(E/\lambda)$ is the likelihood function. It represents the probability for making observation E under the condition that λ is true.
- $f(\lambda/E)$ is the posterior probability density function (pdf). It represents the synthesis between the knowledge about the failure rate before the lifetime observations were made and the result of the latter. Hence, it is a mathematically consistent expression of a learning process.

The denominator in Equation (14) serves to normalize the result so that the integral of Equation (14) is a probability, i.e., its value lies between 0 and 1.

An important difference between the frequentist and the Bayesian approach is that the former determines a fixed but unknown parameter whilst the latter considers λ to be a random variable. The frequentist estimation of λ provides a value and the corresponding confidence interval. The Bayesian approach, on the other hand, leads to a probability distribution. Both

approaches reflect the fact that the reliability data are uncertain.

The evaluation of fault trees requires additions, subtractions, and multiplications to be performed. These can be carried out according to well-established laws if probability distributions are involved. On the other hand, such rules are lacking for confidence intervals. Thus, the use of the Bayesian approach enables one to propagate uncertainties of input data through fault trees and to have them reflected by the final result.

This is the reason why the Bayesian approach is preferable, even if prior knowledge in the form of previously evaluated data or expert judgment is not available. We then make use of the so-called noninformative prior pdf; the procedure for other types of prior pdfs is described, e.g., in [41].

The present case of a constant failure rate is characterized by the Poisson likelihood function $L(E/\lambda)$

$$L(E/\lambda) = \frac{(\lambda mt)}{k!} \cdot e^{-\lambda mt} \quad t, \quad \lambda \geq 0 \tag{15}$$

which gives the probability of k failures being recorded on observing m components at risk during time t if the failure rate λ applies to this component. Possible choices for t were discussed above.

The corresponding noninformative prior pdf is [41]

$$f(\lambda) \propto \lambda^{-\frac{1}{2}} \tag{16}$$

By introducing this prior pdf and the Poisson likelihood of Equation (15) into Equation (14) it is obtained

$$f(\lambda/E) = \frac{\lambda^{k-1/2} \cdot e^{-\lambda mt}}{\int_0^\infty \lambda^{k-1/2} \cdot e^{-\lambda mt} \cdot d\lambda} \tag{17}$$

and after integration

$$f(\lambda/E) = \frac{\Gamma(k+1, \lambda mt)}{\Gamma(k+1)} \tag{18}$$

In Equations (6)–(18) $\Gamma(k+1, \lambda mt)$ is the incomplete and $\Gamma(k+1)$ the complete Gamma function [42]. The expected value of Equation (18) is

$$M = \frac{2k+1}{2mt} \tag{19}$$

Note that Equation (19) produces a useful result even if no failure ($k = 0$) was observed during time t. This is not true for Equation (13), where the estimate for the failure rate would be 0, a result which would definitely change if the component in question were observed for a longer period of time.

The percentiles of the posterior distribution may be determined by using the relationship between the incomplete Gamma function and the χ^2-distribution [42]

$$\bar{\lambda} = \frac{\chi^2_{(2k+1),(1+\gamma)/2}}{2mt} \tag{20}$$

and

$$\underline{\lambda} = \frac{\chi^2_{(2k+1),(1-\gamma)/2}}{2mt} \tag{21}$$

In the evaluation of reliability data, γ in Equations (20) and (21) is normally taken to be 0.9. Hence, Equation (20) provides the 95th percentile and Equation (21) the 5th percentile of the posterior distribution.

If $\gamma = 0$ is used in either Equation (20) or (21) the distribution median (50% of the values lie below and 50% above) is obtained.

For ease of application in uncertainty propagation the resulting posterior probability functions are often approximated by the log-normal pdfs, since many relevant computer codes use this type of distribution. The procedure is explained below.

Approximation by a Log-Normal Distribution. The pdf of the log-normal distribution is given by

$$f(x) = \frac{1}{\sqrt{2\pi} s\lambda} \cdot \exp\left(\frac{-(\ln\lambda - \mu)^2}{2s^2}\right) \quad \lambda > 0 \tag{22}$$

where λ is the failure rate, μ the mean value of its logarithm, and s the corresponding standard deviation. The distribution is characterized by its expected value

$$M = \exp\left[\mu + \frac{s^2}{2}\right] \tag{23}$$

its median

$$\lambda_{50} = \exp(\mu) \tag{24}$$

and its 5th and 95th percentiles denoted by λ_{05} and λ_{95}, respectively

$$\lambda_{05} = \frac{\lambda_{50}}{K_{95}} \quad \text{and} \quad \lambda_{95} = \lambda_{50} \cdot K_{95} \tag{25}$$

K_{95} is the uncertainty factor, defined as follows:

$$K_{95} = \exp(1.6449 \cdot s) \quad (26)$$

where the value of 1.6449 is the argument of the standard normal distribution corresponding to a probability of 0.95. Hence, as is normally done for failure rates, the factor is chosen such that 90% of the values of λ lie between λ_{05} and λ_{95}.

The approximation of the resulting distribution from the previous section is carried out as proposed in [43]. This implies that the 95th percentiles and the medians of both equations are equated and that the K_{95} factor is calculated by dividing the 95th percentile by the median.

Dependent Failures. Besides independent failures of components, dependent failures may occur [44]. Their consequences may be particularly severe if they affect redundant components or subsystems presenting themselves simultaneously or within a short interval of time such that the failed states coexist. The following types of such failures are distinguished:

1. Failures of two or more redundant components or subsystems caused by functional dependencies, i.e., resulting directly from the structure of the system. For example, functional dependencies may result from a common auxiliary system (e.g., instrument air supply), from a common control device, or from multiply affecting human error.
2. Failures of two or more redundant components or subsystems resulting from a single previous failure. They are called propagating or secondary failures.
3. Failures of two or more similar or identical redundant components or subsystems due to a single shared cause. They are referred to as common-cause failures (CCF).

To adequately treat dependent failures in a reliability analysis, failures of components due to functional dependencies are modeled in the fault trees.

Propagating failures, as far as they cannot be excluded on grounds of spatial segregation or adequate design of the components, should also be modeled in the fault trees (e.g., secondary failures induced by missiles, by pipe whip, or a humid environment). Their modeling may require calculations from a variety of fields, e.g., structural mechanics.

After analyzing the previous two classes of failures there remain those dependent failures which are due to shared causes (CCF; design, construction, or maintenance errors, e.g., unsuitable lubricants in pump bearings). If possible, these should be quantified on the basis of operating experience. Several types of failures must be distinguished in this context:

- Failures which can either occur or be detected only in case of an accident
- Failures detected on demand of a function (in functional tests or in other recurrent system demands)
- Self-announcing failures

Operating experience primarily provides data for the last two types of CCFs, which are detected during the normal operation of the plant. Failures which occur or can be detected only during an accident must usually be predicted by analytical methods. The potential for such failures is, however, likely to be detected if operational requirements or routine functional tests are representative of the requirements on components or systems under accident conditions.

The quantification of CCFs detected during operation or functional tests is difficult, since observations are usually scarce. This may be explained as follows:

- Only a small fraction of component failures are CCFs.
- Causes of system failures which have been detected are usually eliminated. Similar failures will then only recur with an even smaller probability.

If operating experience is not sufficient for the quantification of common cause failures, recourse must be taken to models. Such models are described, for example, in [45, 46], where a detailed account of modeling and parameter estimation is given. Since operational experience with CCF in process plants is virtually nonexistent, only the so-called β factor model is described here. The β factor method is based on the assumption that a constant fraction of all component failures (namely $\beta = 10\%$) are

dependent failures. Hence we have

$$\lambda_{\text{independent}} = \lambda(1-\beta) \quad \lambda_{\text{CCF}} = \lambda\beta \tag{27}$$

The generic β factor of 10%, which is supposed to be valid for all types of components, was derived for the intermeshed one out of two systems formerly used in U.S. nuclear power plants. It also contains contributions from functional dependencies and from inadequate spatial segregation. However, it does not take into account that the probability of a system failure decreases with an increasing number of redundant subsystems or components. Likewise, the influence of administrative measures or of human redundancy on the probability of dependent failures is not included.

A firm establishment of an adequate β factor for process plants would require a comprehensive evaluation of operating experience. Hence, the value of 10% may only serve as a default value until more precise information is available. (A recent evaluation in German process plants suggests a value of $\beta = 0.08$).

1.6. Human Error

The safety analysis of a process plant would be incomplete if human interventions were not accounted for. Humans are involved in process control during startup, production, and shutdown, as well as in maintenance and in coping with incidents and accidents. The extent to which human intervention is required depends on the degree of automation of the plant. The design, construction, and erection of plants are also human activities and hence may be subject to human error.

Human error is defined as an act outside the tolerance bounds. These are determined by the technical boundary conditions and may therefore be influenced by the designer. The analysis includes intentional (the operator believes that he is doing the right thing, although it is wrong) and unintentional error. Malevolence is not addressed. To make a human act successful each of the steps "information", "processing", "decision-making", and "action" must be performed successfully. This highlights the man–machine relationship. The information is usually provided by an alarm, and the next two steps are performed by the operator just as the last step, for which normally a technical device is needed, e.g., a valve.

To analyze human error, classifications are useful. The best known and probably most widely used method for this is THERP (technique for human error rate prediction) [47]. It is the only one for which applications in process industry became known, as stated in the method-comparing study [48]. For this reason only THERP is presented here.

In THERP the following broad classes are distinguished:

- Human error due to the work environment, especially equipment design and written and oral procedures, where it is possible that the demand placed on the operator does not conform to his capabilities and limitations (described by external performance shaping factors, PSFs).
- Human error rooted in the personality (e.g., physical constitution, skills, motivations, expectations) or caused by factors which may be influence by personal decisions (e.g., drinking of alcohol); these are described by internal PSFs.

The following types of human error are normally addressed:

- Error of omission: failure to initiate performance of a system-required task or action
- Error of commission: incorrect performance of a system-required task or action, given that the task or action is attempted, or the performance of some extraneous task or action which is not required by the system and which has the potential for contributing to some system-defined failure
- Error of sequence: performance of a task or action while disregarding the correct sequence
- Time error: performance of a task or action outside the fixed time (e.g., too slow, too fast, too late)
- Extraneous task: task or action which is not required by the system and which has the potential for contributing to some system-defined failure

Furthermore the following distinctions may be made:

- Random error: Action outside the tolerance limits not following a given scheme
- Systematic error: Action outside the tolerance limits following a given scheme
- Sporadic errors: Rare acts outside the tolerance limits.

When quantifying human actions in reliability and risk analyses, humans are regarded as part of the system, i.e., they are treated as a system component. They must fulfill a certain task within a given interval of time, otherwise the "component human" is considered to have failed. Humans are distinct from technical components in that their behavior is characterized by a substantially larger variability and complexity. Therefore, the description of their behavior in terms of reliability parameters is difficult. In particular, complex interdependent actions involving several persons or decision situations are hardly amenable to probabilistic treatment. Furthermore, there is an agreement that only such actions or elements of actions can be described by reliability parameters which refer to skill or rule-based behavior, as defined below.

Operator actions are classified into three categories [49]; based on the definitions in [50], these are:

1. Rule-based actions (or behavior). Behavior in which a person follows remembered or written rules, e.g., performance of written post-diagnosis actions or calibrating an instrument or using a checklist to restore manual valves to their normal operating status after maintenance. Rule-based tasks are usually classified as step-by-step tasks unless the operators must continually divide their attention among several such tasks without specific written cues each time they should shift attention to a different task. In the latter case, in which there is considerable reliance on memory, the overall combination may be classified as a dynamic task, especially in a post accident condition.
2. Skill-based actions (or behavior). The performance of more or less subconscious routines governed by stored patterns of behavior, e.g., the performance of memorized immediate emergency actions to control an incipient runaway or an initiating event like stirrer failure, or the use of a hand tool by a person experienced with the tool. The distinction between skill-based actions and rule-based actions is often arbitrary, but is primarily in terms of the amount of conscious effort involved; in layman terms, the amount of "thinking" required.
3. Knowledge-based actions (or behavior). Behavior which requires one to plan one's actions based on the functional and physical properties of a system.

For the purpose of analysis actions pertaining to the first two areas of behavior are broken down into single elements to a degree such that reliability parameters can be assigned to these elements. Actions inscribed in the third area should normally be anticipated by elaborating pertinent scenarios. The required actions should be laid down in the operating manual so that they then belong to area (1).

In area (3) frequently actions after an accident must be assessed. The HCR method described in [51] is often used to estimate the corresponding nonresponse probability.

The THERP method is composed of four steps:

1. Identification of those failure combinations which will make the system under consideration function or fail, if human error is taken into account.
2. Identification and analysis of the human tasks related to the system function in question (task analysis).
3. Assignment or estimation of the relevant failure probabilities taking into account the specific conditions for the performance of the action by performance shaping factors (PSFs). The basic human error probabilities of [47] are multiplied by these factors, which are greater than 1.
4. Assessment of the influence of human error on the probability of failure combinations (composed of the failure of technical components and human error) and on the unavailability of the system function (as part of the reliability analysis).

Two elements of this method deserve special attention, the task analysis, and the decomposition of a complex action into its constituents.

The task analysis precedes the quantitative evaluation and implies a systematic identification of the parameters which affect human reliability. In performing the decomposition existing dependencies must be identified and accounted for.

The analysis of human actions needed for operating plants is generally performed in the following steps:

- Plant familiarization
  - Collection of information
  - Plant visit
  - Examination of operational regulations/ information from technical systems analysis
- Qualitative evaluation
  - Determination of requirements for the action
  - Valuation of the circumstances for carrying out the action
  - Fixing the objectives
  - Identification of performance shaping factors and interactions influencing human actions
  - Identification of the potential for human error
  - Modeling of human actions
- Quantitative evaluation
  - Determination of probabilities for human error
  - Quantification of performance shaping factors and interactions
  - Assignment of probabilities for error recovery (possibly by a second person)
  - Implementation in the technical systems analysis (e.g., as a primary event in a fault tree)

It is fundamental for assessing human error to identify and describe the human acts with importance for the event sequence under analysis (qualitative assessment). This corresponds to the task analyses, which are characteristic of ergonomic studies. Firstly, the important actions, the moment in time at which they are required and the time period available for their execution must be determined. Furthermore, the requirements for the action, the information necessary, respectively available, and the possibilities of correction in case of omission or faulty execution must be established. Additionally, other factors of important influence on human reliability, such as the state of knowledge on the process in question, ergonomically favorable or disadvantageous layout of the workplace, tools, or the environment are identified. On the basis of this task analysis, reliability data (normally failure probabilities on demand) are assigned to the tasks identified. They stem from the data collection provided in [47] (cf. Table 5). If no data are available, analogies must be used, for example, for "detection by strong ammonia smell" "reaction to a compelling signal".

The uncertainties of the failure probabilities are treated by using log-normal distributions (see Section 1.5). This is an inappropriate choice for a probability, which is defined on [0,1], and was replaced by a β distribution, for example in [52].

Table 5. Excerpt of data for the quantification of human error (5th percentile q_{05}, median q_{50}, 95th percentile q_{95}), according to [47]

Action	Basic probability of failure		
	$q_{H,05}$	$q_{H,50}$	$q_{H,95}$
Response to an alarm with signal horn and light signal	0.00005	0.0001	0.001
Reading an analogue meter	0.01	0.003	0.01
Reading a digital meter	0.0005	0.001	0.005
Discovery of an instrument failure if there is no failure signal	0.02	0.1	0.2
Changing of the position of a manual valve			
with position indicator on the valve	0.0005	0.001	0.01
with position indicator away from the valve	0.001	0.002	0.01
without position indicator	0.003	0.01	0.1
General human error (error of omission or commission)	0.0033	0.01	0.03
Discovery of the wrong position of a valve on control without a checklist	0.1	0.5	0.9

If complex sequences of actions must be analyzed they are decomposed into individual steps down to the level at which data are available.

It is important for the assessment to account for possible dependencies. Such dependencies can exist both between the actions of several persons and several consecutive actions performed by one and the same person (e.g., because of high stress). This is accounted for in [47] by a specific model which enables one to assess probabilities under the condition that the previous act carried out either by another or the same person has failed.

The error probabilities of [47] apply for "optimal" conditions; if these do not prevail they must be modified by performance shaping factors (PSF). In what follows some of the PSFs are described. They lead to multipliers for the basic probabilities >1, if conditions are not "optimal". A method of basing the choice of the multiplier, for which there is little guidance in [47], to a large extent on ergonomic and physiological evidence is presented in [53].

- Ergonomic layout of the control room: An increase in failure probabilities is to be assumed if the arrangement, labeling, and design of the control mechanism are such that error is enhanced. This may be the case, for example, if stereotypes are violated, or if labeling of instruments and buttons is confusing or hardly legible. A stereotype is the expected reaction of a human to an outside influence. For example, turning a button in a clockwise direction is associated with switching off.
- Feedback through indications and alarms: The probability of human failure is reduced if feedback through indications and alarms which render the detection of an error probable exists. The possibility of the discovery of an error is to be taken into account, especially if the operator is warned immediately after committing it. This applies most of all if system response to the error is rapid.
- Human redundancy: A further important way of detecting errors results from human redundancy, i.e., a decision or an act involves more than one person with adequate qualification. Redundancy is assumed as well if a person's acts are also controlled by another.

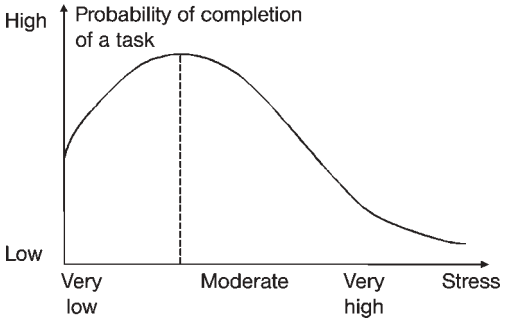

Figure 8. Hypothetical relation between the realization of a task and the existing stress level (according to [47])

- Psychic stress: On assessing human error it must be taken into consideration whether the plant personnel is under stress. Figure 8 shows the hypothetical relationship between stress and human reliability
  - Optimum reliability is attained accordingly in case of moderate stress, which is high enough to fully capture the operator's attention.
  - Low stress decreases the attentiveness because uninteresting and undemanding tasks cause a decrease in attention. Low stress is applicable, for example, to routine control walks.
  - An optimum stress level exists in routine operations in the control room during normal operation of plant, maintenance, and functional tests. These activities do not lead to excessive adaptation nor are they too simple. Therefore, reliable performance may be assumed.
  - Very high stress and hence a high probability for human error reigns shortly after the occurrence of an accident. With increasing time after the accident lower probabilities for human error may be assumed, if the plant is brought under control by appropriate automatic or human interventions during accident progression thereby reducing the stress level.
- Qualification and training of operators: It may normally be assumed that the staff of complex technical installations is carefully selected and hence has a sufficient qualification. This may not apply to the same extent to training before starting to work in the plant; hence, by plant-specific training and recurrent training

the skills and knowledge must be maintained. Whilst often efficient training before employment of personnel takes place, recurrent training is not so frequent. The latter has considerable importance for maintaining the necessary knowledge, especially for handling accident situations.Frequently the effectiveness of existing training programs is not checked. The quality and recurrence of training has therefore to be taken into account in assessing the reliability of the plant personnel.

- Written instructions: Normally lower failure probabilities are assumed for actions based on written instructions. Criteria to assess the quality of written instructions are, for example, good readability and clarity. If instructions concern actions for accident handling, additionally ready access, updating and clearness should be taken into account. Furthermore it should be noted that written instructions exonerate the operator, should the result of following them be negative.
- Dependence of human acts: An important influence factor in assessing human reliability is the interdependence of human acts. Two types are distinguished here: direct and indirect dependence. There is direct dependence if the interdependence is between several acts. Similar tasks carried out by the same operator one after another may serve as an example (e.g., activation of two components, one immediately after the other). Indirect dependence implies that there is interdependence between several acts and a factor of common influence. Such a factor may, for example, be a measuring device wrongly set or calibrated, which is used to calibrate measuring channels. Complete independence of human acts is to be expected if they are totally different or carried out considerably separated as to place and time. Additionally, the dependencies between several operators involved in the same task must be accounted for, as mentioned above.

Apart from THERP numerous other methods were developed. Critical overviews are given in [48] and [50]. More recent methods are ATHEANA [54] and SPAR-H [52]. ATHENEA is based on the behavioral sciences view of human performance comprising four stages, i.e., monitoring and detection, situation assessment, response planning, and response implementation. The human error probabilities were estimated or obtained by eliciting judgments from experts [55]. SPAR-H discusses a general psychological model of human information processing as its basis. Generic error rates and PSF multipliers are apparently based on the authors' observations/reviews of event statistics and on a comparison with data in existing HRA methods.

An application of the THERP methods is presented in the following example [56].

Example: Isolation of a Leak in an Ammonia Pipe. The system shown in Figure 9 serves for transporting ammonia at a temperature of $-30°C$ to a pressurized storage downstream, which supplies ammonia to a production process. A rupture of the pipe is expected to occur with a frequency median of $f_{50} = 7.9 \times 10^{-3}$ a^{-1} ($K_{95} = 10$). If the location of the rupture is such that the leak can be isolated larger releases of ammonia may be prevented by closing the pneumatic valve A.

Valve A can be closed locally (six places) or from the control room. Two operators are present day and night. One of them is to walk through the plant once every hour. The walk-around takes 10 min.

Fault Tree Representation. The probability that the leak is not isolated can be assessed by using the fault tree shown in Figure 10.

The leak is not isolated if

- Valve A is stuck and can therefore not be closed (primary event x_1)
- The solenoid valve fails (primary event x_2)
- The operator does not press the button for closing the valve (undeveloped event x_3)

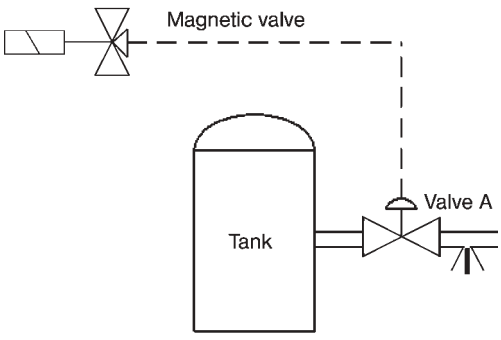

Figure 9. Schematic of storage tank and pipe

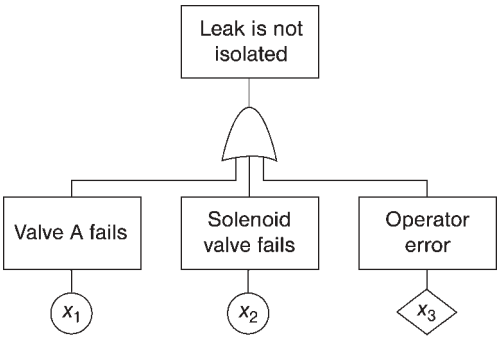

Figure 10. Fault tree for calculating the probability that the leak is not isolated

Reliability Data for Technical Components. For quantifying the fault tree the following reliability data are used:

- Pneumatic valve: $\lambda_{50} = 11.5 \times 10^{-6}$ h^{-1}; error factor $K_{95} = 5$; mean value $\lambda = 18.6 \times 10^{-6}$ h^{-1}
- Solenoid valve: $\lambda = 8.1 \times 10^{-6}$ h^{-1}; error factor $K_{95} = 5$; mean value $\lambda = 13.0 \times 10^{-6}$ h^{-1}

Frequent operational demands on the valve allow one to make the assumption that at least once per week its correct functioning is checked (operational demand as an equivalent for functional test). The unavailability is then calculated according to Equation (12) with $\theta = 168$ h giving:

- Pneumatic valve: $u_1 = 0.0016$
- Solenoid valve: $u_2 = 0.0011$

Calculation of the Probability of Failing to Actuate the Valve. The following tasks must be performed after the leak has occurred:

1. Detection of the leak: It is conceivable to see that the leak has occurred, but only at daytime and if the operator looks out of the window or his colleague is on his walk-around. Therefore, it is assumed conservatively that the leak is only detected by an increased smell of ammonia. An assessment showed that the threshold of smell perception is reached after about 5 min.
2. Closing of valve A: According to the operating manual, valve A must be closed whenever a stronger than usual smell of ammonia is perceived. This is a safety-geared measure. A conflict of interests is not possible because the production is not affected by a temporary interruption of ammonia flow to the pressurized storage. For this reason closing the valve because of a false alarm would not be problematic. The model must account for the fact that we are dealing with a case of human redundancy (two operators). The event tree is presented in Figure 11 and explained in what follows.

It is estimated that the probability of not noticing the smell is $q_{H,50} = 0.001$ (on the basis of a datum for not observing a compelling signal given in [47]). Since at this point in time it is still unclear whether the leak is located such that it can be isolated or not, the resulting high stress is accounted for by a multiplier of 5. Therefore the value used in the evaluation is $q_{H,50} = 0.005$ with an error factor $K_{95} = 3$.

The main operator then fails to close the valve with a probability of $q_{H,50} = 0.01$. Again a stress factor of 5 is applied, so that $q_{H,50} = 0.05$ with $K_{95} = 5$ is used.

The second operator may either be inside the control room or on his inspection walk. He is assumed to comply with his duty only with a probability of 0.5. He spends 5/6 of the remaining time inside the control room as well, so that the total probability of being outdoors is $1-(0.5+0.5\times5/6) \approx 0.08$; an error factor of $K_{95} = 2$ is considered appropriate.

If the second operator is inside the control room his decision on whether there is an increased smell of ammonia or not is influenced by the opinion of his colleague. If the main operator denies the elevated smell, high dependence of the opinion forming process of the second operator is assumed. The corresponding model in [47] gives a conditional probability with a median of 0.5 with an error factor of 2 in this case. If, on the other hand, he is convinced that there is a leak (complementary probability to the foregoing assessment) he carries out the act of closing analogously to his colleague if he had diagnosed the situation properly, as explained above.

If the second operator is outdoors he will analyze the situation the same way as the control operator, because in this case they are assumed to act independently.

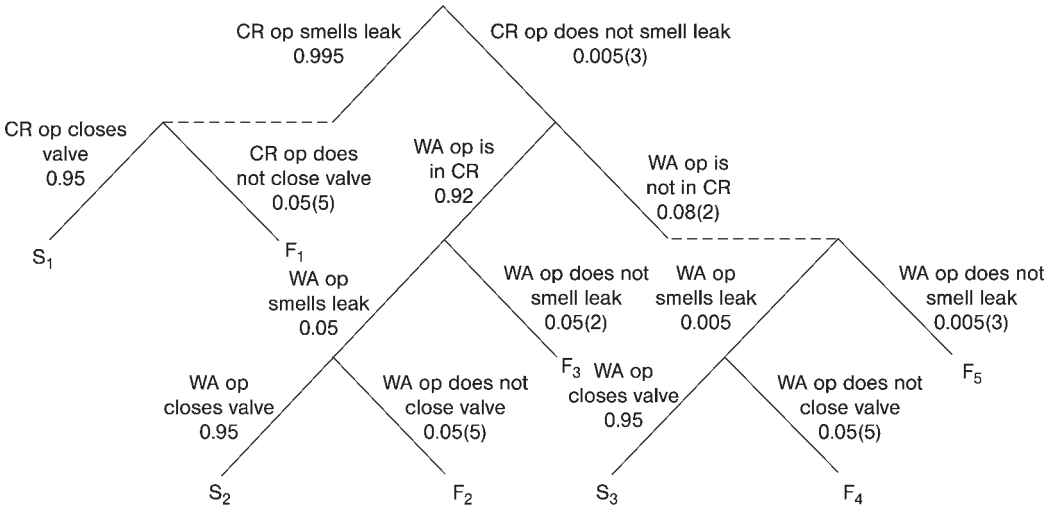

CR	control room
CR op	operator in control room
WA op	operator that does the inspection walk around
F_i	failure path ($i = 1$ .. 5)
S_i	success path ($i = 1$ .. 3)

The numbers given within parentheses are the error factors

Evaluation on the basis of mean values

$$F = F_1 + F_2 + F_3 + F_4 + F_5 = 0.9935 \cdot 0.08 + 0.065 \cdot 0.92 \cdot 0.45 \cdot 0.08 + 0.0065 \cdot 0.92 \cdot 0.55 + 0.0065 \cdot 0.08 \cdot 0\ .9935 \cdot 0.08 + 0.0065 \cdot 0.08 \cdot 0.0065 \approx 0.080$$

$$S = S_1 + S_2 + S_3 = 0.9935 \cdot 0.92 + 0.0065 \cdot 0.92 \cdot 0.45 \cdot 0.92 + 0.0065 \cdot 0.08 \cdot 0.9935 \cdot 0.92 \approx 0{,}920$$

$$F + S = 1$$

Figure 11. Event tree for assessing human error (primary event x_3 in the fault tree of Figure 9) and its numerical evaluation based on mean values.

The numerical evaluation of the fault tree of Figure 11 leads to:

Median:	5.4×10^{-2}
Expected value:	8.0×10^{-2}
5th centile:	1.3×10^{-3}
95th centile:	2.3×10^{-1}
Error factor K_{95}:	4.3

Expected Frequency of a Larger Release. Using the failure probabilities for the technical components and the probability of human error as well as the expected frequency of pipe rupture a total frequency for the leak not being closed off

Median:	4.3×10^{-4} a^{-1}
Expected value:	1.7×10^{-3} a^{-1}
5th centile:	2.8×10^{-5} a^{-1}
95th centile:	6.6×10^{-3} a^{-1}
Error factor K_{95}:	15.3

results.

In this particular case the contribution of human error amounts to approximately 97%, so that automating the closing of the valve might be considered.

1.7. Semiquantitative Methods

1.7.1. LOPA (Layer of Protection Analysis)

A more recent development in the sector of risk analysis for process plants is the layer of protection analysis (LOPA) [57]. It uses the

underlying idea of event tree analysis (Section 1.2.1). Generic failure rates are attached to the initiating events, for example, failure of a coolant pump. Likewise this is true for the unavailabilities of protective barriers which are meant to control the initiating event (e.g., limiting or SCRAM systems). These barriers must be independent from one another. To obtain an estimate for the risk the expected frequencies of undesired events, such as the release of hazardous materials, which occur after the barriers have failed are combined with categorized accident consequences. LOPA provides an order-of-magnitude estimate of risk and shall not replace a detailed analysis.

1.7.2. SQUAFTA (Semiquantitative Fault Tree Analysis)

An important obstacle to using fault tree analysis for process plants is the dearth of appropriate reliability data. This leads to time-consuming and error-prone searches. In any case the quality of the analysis suffers from the circumstance that non-plant-specific data cannot completely capture the specific situation (i.e., type of components, quality of maintenance, etc.) in the plant under investigation. This is why the program system SQUAFTA [58] uses generic ranges for reliability data (see Section 1.8). These ranges are intended to account for their uncertainties. The latter stem amongst others from the fact that data is transferred from the plant of origin to another plant with different conditions. The uncertainties are propagated through the numerical evaluation of the fault tree. Results are given for minimal cut sets and the entire tree in natural language. A numerical output supports the identification of design weaknesses. The program system is accompanied by a library containing reliability data for components deployed in process plants. These are selected to account for the relevant maintenance interval by indicating a cardinal number. An analogous procedure is provided for the expected frequencies of initiating events and human error probabilities.

The procedure provides the advantages of a fault tree analysis at lower work expenditure. Dependencies, which are often present in process plant safety barriers and should not be neglected in order to avoid nonconservative results, are accounted for.

1.8. Numerical Evaluation of a Fault Tree Including Reliability Data Comparisons

In what follows the fault tree of Figure 5 is evaluated numerically. The presentation follows [21]. The objective is not only to show the numerical results but also to address the potential impact of different sets of reliability data on the result. This is important because plant-specific reliability data are practically not available for process plants.

Reliability Data. The reliability data originally prepared for the analysis were taken from [59–63]. In some cases the influence of corrosive media was accounted for by multiplying the failure rates by factors of 2 or 4, depending on the judged degree of influence. They are denoted by "original". Human error probabilities were evaluated following [47] (cf. Section 1.6).

The data set marked "GRS" results from a systematic collection and evaluation in the company operating the plant, but for different productions, e.g., TNT and nitroglycol [34]; the data are site-specific in case of the hexogen plant and plant-specific for nitroglycol.

The data set "OREDA" stems from the offshore experience presented in [35].

By far the most comprehensive collection is the reliability data collection in the nuclear power plant Biblis B [33]. It refers to a different industry. Yet, it reflects approximately the time period of the construction of the plants.

Not all the components to be assessed were covered by each of the sources. In these cases the original data were used. Sometimes the delimitation of the components was doubtful; the corresponding failure rates may therefore not totally cover the components.

The aforementioned problems naturally do not occur if plant-specific data are used. Additionally, the working environment of the components and the quality of the housekeeping is then reflected in the failure rates. The data denoted by "GRS" come closest to this

requirement for the hexogen plant and hence for the system to be analyzed here.

All data sets, except for the original one, were evaluated on the basis of the number of failures and the accumulated time of operation by using a Bayesian approach with an uninformative prior density function and the Poisson likelihood function of Equation (15). The result is approximated by a log-normal distribution characterized by its median and the error factor K_{95}. The latter implies that the interval generated by dividing the median by K_{95} and multiplying it by K_{95} comprises 90% of the values of the corresponding failure rate.

The underlying idea in [58] (cf. Section 1.7.2) is that reliability data are always affected by uncertainties, which are enhanced by their transfer from other installations to the one under investigation. Accepting this fact they may as well be represented by ranges. The ones chosen are indicated in Table 6 as expected frequencies for initiating events, denoted by the failure rate λ of the corresponding component, and as probabilities for the unavailabilities of standby components u. The results of the calculations are stated in terms of their mean values and the associated standard deviations.

The frequency range containing the arithmetic mean of the 5th and 95th percentiles of the failure rate λ is assigned; furthermore, the probability range containing the arithmetic mean of the time-averaged unavailabilities calculated by using the 5th and 95th percentiles of the failure rate λ is chosen. The time-averaged unavailability is obtained from Equation (12).

The reliability data and class assignments used for the evaluation of the fault tree of Figure 5 are presented in Table 6.

Table 6. Assignment of the expected frequencies of initiating events and the unavailabilities of standby components to different classes

Class	Expected frequency range, a^{-1}	Probability range
1	$10.0 < \lambda \leq 1.0$	$0.1 < u \leq 0.8$
2	$1.0 < \lambda \leq 0.1$	$0.01 < u \leq 0.1$
3	$0.1 < \lambda \leq 0.01$	$0.001 < u \leq 0.01$
4	$0.01 < \lambda \leq 0.001$	$0.0001 < u \leq 0.001$
5	$0.001 < \lambda \leq 0.0001$	$0.00001 < u \leq 0.0001$
6	free choice	free choice

Minimal Cut Sets. The fault tree of Figure 5 has the following minimal cut sets, which are presented in relation with the initiating event to which they contribute:

Initiating event 1:

$$\kappa_7 = x_1 \cdot x_4 \cdot x_{10};\ \kappa_{11} = x_1 \cdot x_2 \cdot x_{10};\ \kappa_{15} = x_1 \cdot x_5 \cdot x_{10};\ \kappa_{16} = x_1 \cdot x_8 \cdot x_{10};$$

$$\kappa_{17} = x_1 \cdot x_3 \cdot x_{10}$$

$$\kappa_{18} = x_1 \cdot x_6 \cdot x_7 x_{10}$$

Initiating event 9:

$$\kappa_3 = x_9 \cdot x_{10}$$

Initiating event 11:

$$\kappa_1 = x_{11}$$

Initiating event 12:

$$\kappa_4 = x_{12} \cdot x_{16};\ \kappa_8 = x_{12} \cdot x_{13};\ \kappa_9 = x_{12} \cdot x_{17};\ \kappa_{12} = x_{12} \cdot x_1;$$

$$\kappa_{13} = x_{12} \cdot x_{15};\ \kappa_{14} = x_{12} \cdot x_{18} \cdot x_{19}$$

Initiating event 20:

$$\kappa_2 = x_{20} \cdot x_{22};\ \kappa_6 = x_{20} \cdot x_{23}$$

Initiating event 21:

$$\kappa_5 = x_{21} \cdot x_{22};\ \kappa_{10} = x_{21} \cdot x_{23}$$

To obtain the corresponding probability, the following theorems are used [23]:

The expected value of a sum is equal to the sum of the expected values:

$$E[x_1 + x_2 + \ldots x_I] = E\left[\sum_{i=1}^{I} x_i\right] = \sum_{i=1}^{I} E[x_i] \tag{28}$$

and, in case of mutual independence, which is always assumed (common cause events are introduced into the fault tree separately)

$$E[x_1 + x_2 + \ldots x_I] = E\left[\prod_{i=1}^{I} x_i\right] = \prod_{i=1}^{I} E[x_i] \tag{29}$$

And the expected value of the indicator variable x_i is equal to its unavailability.

$$E[x_i] = u_i \tag{30}$$

where $E[]$ denotes the expected value of the quantity in brackets.

Hence using the "rare event approximation", i.e., products of small quantities are neglected

$$U \approx \sum_{j=1}^{J} E[\kappa_j] \tag{31}$$

approximates the unavailability of the entire system. If initiating events are involved, the unavailability of the initiating event is set equal to 1 in a first step. The result thus obtained is then multiplied by the expected frequency of the event.

The procedure is shown for initiating event No. 21, which involves components 21, 22, and 23. From Table 6 (original data) we have:

21: Failure of thermostat for R1: $\lambda_{50} = 3.2 \times 10^{-6}\,h^{-1}$; error factor $K_{95} = 2.2$; mean value $\lambda = 3.6 \times 10^{-6}\,h^{-1} = 3.14 \times 10^{-2}\,a^{-1}$. The latter is the annual frequency for the initiating event No. 21.

22: Failure of TAH04: $\lambda_{50} = 3.2 \times 10^{-6}\ h^{-1}$; error factor $K_{95} = 2.2$; mean value $\lambda = 3.6 \times 10^{-6}\ h^{-1}$. Considering the time between functional tests of $\theta = 672$ h, Equation (12) gives $u = 1.208 \times 10^{-3}$. A calibration error with a median $u_{50} = 0.01$ and a dispersion factor $K = 5$, hence $u = 0.016$ is added to this value. This gives a total for event No. 22 of $u = 0.0173$.

23: No countermeasure on alarm TAH04: q_{50} 0.005; error factor $K_{95} = 10$; mean value $q = 0.00133$.

Applying Equations (29) and (30) and setting the unavailability of event No. 21 of $u = 1$ gives

$$E[\kappa_5] = 0.0173 \quad \text{and} \quad E[\kappa_{10}] = 0.00133$$

Using Equation (31) gives the unavailability of the barriers

$$U \approx 0.0187$$

Multiplying this value by the expected frequency of event No. 21 gives the expected frequency of the contribution of initiating event No. 21 to the undesired event as

$$5.87 \times 10^{-4}\,a^{-1}$$

This corresponds to result in Table 9 (last line of the column "original data").

Results. The fault tree of Figure 5 is evaluated by using the reliability data from Table 7. The initiating events are assessed by using the frequencies from the table directly, whilst all other components are treated on the basis of Equation (12) by using the times between inspections θ indicated in the footnote of Table 7.

Table 8 provides the corresponding numerical values. They were obtained by using straight Monte Carlo with 10^6 trials [64]. This large number ensures that even the tails of the distributions for the reliability data are well represented. Since the fault tree leads to just 18 minimal cut sets, this is possible with computing times below one minute.

It is evident that the differences are not excessive; the relative difference between the highest and the lowest mean value is 37% (excluding the range-based calculation). The range calculated covers the major part of any of the resulting probability density functions. It thus provides an appropriate assessment giving somewhat conservative values.

An analysis concerning the individual initiating events is presented in Table 9. Despite numerical differences it is evident that the unavailabilities of the barriers are virtually unaffected by the choice of the data set. When ranges are used, the absolute values are higher, but their order is not affected.

An overview of the components whose failure contributes most to the final result is provided in Table 10. It is obtained by setting the failure rate of the component indicated in the leftmost column to zero and calculating the reduction in system failure frequency. It is evident that the first eight components play an important role, although their ranking is not identical. No substantial differences in the identification of components with large impact on the result can be noted.

Conclusions. The calculations performed for the cooling system show that results using different data sets do not differ substantially; in particular, the comparison of the relative importance of different initiating events is virtually not affected. Thus, the same weak points of the design would be identified irrespective of the data set used. Even the gross method using ranges does not call for a substantial modification of this statement. These findings are supported by [65, 66].

However, the results do not prove that this is true in general. Therefore, one should strive to provide plant-specific reliability data that remove all doubt concerning their applicability. However, in the meantime the dearth of data available for probabilistic analyses of process

Table 7. Reliability data from different sources for describing the basic events of the fault tree of Figure 5

Component no. i	Description	Original		GRS		OREDA		Biblis		Ranges
		Median, 10^{-6} h^{-1}	Factor of dispersion K_{95}	Median, 10^{-6} h^{-1}	Factor of dispersion K_{95}	Median, 10^{-6} h^{-1}	Factor of dispersion K_{95}	Median, 10^{-6} h^{-1}	Factor of dispersion K_{95}	Class assignment
1	Operational failure pump P1A[b]	42	1.9	52.2	1.1	31.6	3.2	13.7	1.3	1
2	Alarm via flow meter FAL1 fails[a]	16	5.8	185	2.5	3.6	2.0	17.2	1.4	2
5	Reserve pump P1B does not start[c]	11	3.2	28	1.4	2.8	3.3	22.9	1.2	3
7	Check valve behind PA1 does not close[c,d]	0.28	6.0	8.3	2.5	0.17	8.4	0.19	2.5	5
8	Check valve behind PA2 does not open[c,d]	0.28	6.0	8.3	2.5	0.17	8.4	0.7	1.7	5
9	Supply to cold part of the tank too low because of a pipe leak[b,d]	1.4	6.0	1.4	6.0	1.4	6.0	1.4	6.0	3
11	Undetected leak behind pressure switch[b,e]	0.06	6.0	0.06	6.0	0.06	6.0	0.06	6.0	4
12	Operational failure pump PA2[b]	42	1.9	52.2	1.1	5.1	2.5	13.7	1.3	1
13	Failure PAL06[a]	6.5	4.2	0.93	8.4	2.8	2.0	7.5	1.2	4
16	Reserve pump P2B does not start[c]	11	3.2	28	1.4	2.8	3.3	22.9	1.2	3
17	Check valve behind P2B does not open[c,d]	0.28	6	8.3	2.5	0.17	8.4	0.7	1.7	5
18	Check valve behind P2A does not close[c,d]	0.28	6	8.3	2.5	0.17	8.4	0.19	2.5	5
20	Failure of refrigerating unit R1[b,d]	168	3.0	23.3	3.3	168	3.0	168	3.0	1
21	Failure of thermostat for R1[b]	3.2	2.2	33.1	2.5	4.8	2.2	3.0	1.3	3
22	Failure of TAH04[a]	3.2	2.2	60.4	1.5	4.8	2.2	3.0	1.3	3
	Human error probabilities in 10^{-6}									
3	No attention paid to flow alarm FAL1	500	10.0	500	10.0	500	10.0	500	10.0	3
4	No manual start reserve pump P1B	500	10.0	500	10.0	500	10.0	500	10.0	3
6	Hand valve before P1A not closed	10000	5.0	10000	5.0	10000	5.0	10000	5.0	2
10	Leak not detected	1000000	1.0	1000000	1.0	1000000	1.0	1000000	1.0	6
14	Pump P2B not started manually	500	10.0	500	10.0	500	10.0	500	10.0	3
15	No attention paid to pressure alarm PAL06	500	10.0	500	10.0	500	10.0	500	10.0	3
19	Hand valve before P2A not closed	500000	5.0	500000	5.0	500000	5.0	500000	5.0	1
23	No countermeasure on alarm TAH04	500	10.0	500	10.0	500	10.0	500	10.0	3

Usual time between inspections $\theta = 672$ h.

[a] A calibration error with a median $u_{50} = 0.01$ and a dispersion factor $K = 5$ is added in the calculations.

[b] Initiating event;

[c] $\theta = 168$ h.

[d] Estimated error factor.

[e] Estimate, numbers in boldface indicate that the value was taken from "original" due to a lack of a corresponding datum in the referred source.

Table 8. Characteristic parameters of the expected annual frequencies of cooling system failures (distribution parameters based on 10^6 Monte Carlo trials)

	5th centile	Median	Mean	95th centile	K_{95}
Original	0.019	0.061	0.078	0.20	3.2
GRS	0.046	0.091	0.100	0.18	2.0
OREDA	0.016	0.055	0.073	0.19	3.4
Biblis	0.012	0.045	0.063	0.17	3.8
Ranges			0.47±0.41		

plants should not be an impediment to their useful application in improving plant safety, especially when dominating initiators and accident sequences are to be identified. The latter only requires relative and not absolute statements.

2. Consequence Analysis

Causes for releases and the procedure for calculating their expected frequencies of occurrence were presented in Chapter 1. The following sections deal with the treatment of the consequences if the substances involved are flammable, explosible, or toxic or exhibit several of these properties at the same time, which means dealing with the right-hand side of Figure 1.

The models presented below are deterministic. However, their boundary conditions, represented by "characteristics" in Figure 1, are probabilistic in the strict sense. This is shown, for example, in Figure 12, where the expected frequencies of different leak sizes are presented. The deterministic approach implies on the contrary that a specified boundary or initial condition, e.g., a leak with a diameter of 10 mm^2, occurs with probability 1.

Hence, the main difficulty in assessing consequences does not lie so much in the adequacy and quality of the models, but in the correct formulation of the boundary and initial conditions. Another complication is the fact that the boundaries are mostly open, e.g., the atmosphere, and not fixed like the walls of a pipe. Potential accident paths are presented in Figure 13.

Accidents may occur inside the plant equipment, e.g., a runaway reaction inside a reactor or equipment or an internal fire with subsequent loss of containment, or follow releases due to causes stated in Figure 13. The state of aggregation of the substances involved is determined by their process and storage conditions, i.e., pressures and temperatures inside the containment. Additionally, their composition must be contemplated. Releases range from slow discharges through pinholes through rapid discharges from full bore holes to virtually instantaneous discharges (puff releases) after catastrophic failures of vessels, which last for a few milliseconds. Therefore the following discharge conditions are normally contemplated:

- Liquid
- Compressed gas
- Pressurized liquefied gas

both as puff releases or releases spread over time. During and after release the substances involved interact with the environment in a way which depends on their properties, those of the environment, and the physical conditions of their release. Accordingly, the released material may ignite immediately, form a pool, or disperse in the atmosphere.

The models used for calculating discharge presented in → Plant and Process Safety, 5. Engineered Safety Measures, Section 3.2 can be applied as well to the discharge from leaks by using an adequate discharge factor.

If the discharge is in gaseous form and no immediate ignition takes place the substances disperse in the atmosphere. If a liquid is released, pools are formed. The substance then evaporates. Pools grow with increasing released quantity and change their geometry. If there is a discharge into a bund the geometry is determined by that of the bund. The level then rises with an increasing spilt quantity.

By way of example the different possible outcomes from a release of a gas stored under pressure are shown in Figure 14. They are represented by an event tree (see Section 1.2.1). It is desirable to attach probabilities to the different paths of the event tree. However, this is a difficult and somewhat controversial task; values may be found, e.g., in [68–70].

Table 9. Expected frequencies of the initiating events, unavailabilities of the corresponding barriers, and expected frequencies of cooling system failures from the different initiating events

	Original data			GRS			OREDA		
Initiating event	Annual frequency of the initiating event	Unavailability of barriers	Annual frequency of the undesired event	Annual frequency of the initiating event	Unavailability of barriers	Annual frequency of the undesired event	Annual frequency of the initiating event	Unavailability of barriers	Annual frequency of the undesired event
1	0.40	2.94×10^{-2}	1.17×10^{-2}	0.46	9.41×10^{-2}	4.31×10^{-2}	0.36	2.04×10^{-2}	7.25×10^{-3}
9	2.22×10^{-2}	1	2.22×10^{-2}	2.22×10^{-2}	1	2.22×10^{-2}	2.22×10^{-2}	1	2.22×10^{-2}
11	9.51×10^{-4}	1	9.51×10^{-4}	9.51×10^{-4}	1	9.51×10^{-4}	9.51×10^{-4}	1	9.51×10^{-4}
12	0.40	2.32×10^{-2}	9.20×10^{-3}	0.46	2.33×10^{-2}	1.07×10^{-2}	0.36	2.01×10^{-2}	7.16×10^{-3}
20	1.84	1.87×10^{-2}	3.43×10^{-2}	0.27	3.83×10^{-2}	1.02×10^{-2}	1.84	1.93×10^{-2}	3.54×10^{-2}
21	3.14×10^{-2}	1.87×10^{-2}	5.87×10^{-4}	0.34	3.83×10^{-2}	1.30×10^{-2}	4.72×10^{-2}	1.93×10^{-2}	9.08×10^{-4}
Total			7.9×10^{-2}			1.0×10^{-1}			7.4×10^{-2}

	Biblis			Ranges		
Initiating event	Annual frequency of the initiating event	Unavailability of barriers	Annual frequency of the undesired event	Annual frequency of the initiating event	Unavailability of barriers	Annual frequency of the undesired event
1	0.12	2.66×10^{-2}	3.23×10^{-3}	5.5	6.1×10^{-2}	0.34
9	2.22×10^{-2}	1	2.22×10^{-2}	5.5×10^{-2}	1	5.5×10^{-2}
11	9.51×10^{-4}	1	9.51×10^{-4}	5.5×10^{-3}	1	5.5×10^{-3}
12	0.12	2.33×10^{-2}	2.83×10^{-3}	5.5	6.1×10^{-2}	3.4×10^{-1}
20	1.84	1.85×10^{-2}	3.40×10^{-2}	5.5	5.6×10^{-2}	3.1×10^{-1}
21	2.66×10^{-2}	1.85×10^{-2}	4.92×10^{-4}	5.5×10^{-2}	5.6×10^{-2}	3.1×10^{-3}
Total		6.4×10^{-2}		1.0		

Table 10. Reduced values of the frequency of system failure in % assuming that the specified component or human act does not fail in ascending order based on original data (without basic events 9, 11, and 20 and all events representing human error; cf. Table 7)

Component No. *i*	Original	GRS-A-1500	OREDA	Biblis	Ranges
1	29.8	21.5	49.2	37.7	16.2
2	38.1	25.8	60.4	53.6	24.0
12	70.8	94.9	58.0	64.1	84.6
13	79.1	99.2	69.2	80.0	92.4
16	92.3	97.4	90.8	84.8	92.4
5	92.3	97.6	90.8	84.8	92.8
21	99.4	83.6	92.8	98.2	99.2
22	99.4	83.6	92.8	98.2	99.2

2.1. Pool Formation and Vaporization from Pools

If a fluid is released, a pool is formed. Vaporization must then occur before a cloud is formed, which is dispersed in the atmosphere. The process of vaporization determines the rate at which the substance enters the cloud; it represents the source term. In [71] the following three situations are distinguished:

1. Spillage of a volatile liquid at atmospheric temperature and pressure, e.g., acetone spillage of a superheated liquid
   a. at ambient temperature and under pressure, e.g., butane
   b. at high temperature and under pressure, e.g., hot cyclohexane
2. Spillage of a refrigerated liquefied gas at low temperature but atmospheric pressure, e.g., cold methane

Releases both into bunds and directly onto the ground must be addressed. If the release is into a bund the geometry and area are given. If, on the other hand, a spillage on the ground must be modeled, a circular pool is generally assumed. According to [72] the following factors are crucial in determining the vaporization rate of the pool formed after spillage:

- Average liquid pool temperature governed by the heat balance for the pool
- Liquid pool surface area
- Mass transfer coefficient from the pool

There is a large variety of models addressing the problem of pool size and evaporation from the pool; an overview and evaluation is given in [73]. It appears that GASP [74] is one of the most advanced models despite missing details in pool formation and restriction to circular pools. A number of rule-of-thumb approaches may be found in [75, 76]. In [77] specific aspects of treating mixtures are addressed; [78, 79] provide an overview of experimental work done in the area.

In GASP the following system of differential equations is solved [72]

$$\frac{dr}{dt} = u$$

$$\frac{du}{dt} = \frac{4gh}{r} - C_F$$

$$\frac{dV}{dt} = \frac{q_s}{\rho_l} - \frac{u_{rA}}{A_{top}} - \frac{q_d}{\rho_l}$$

$$\frac{dT}{dt} = \frac{A_{top}(H - \rho_l u_{rA} L_v)}{c_{p,l}\rho_l V} + \frac{q_s(T_{qs} - T)}{\rho_l V}$$

$$\frac{dV_d}{dt} = \frac{q_s}{\rho_l}$$

$$\frac{dV_E}{dt} = u_{rA} A_{top}$$

r: radius of the pool, m;
u: spreading velocity of the pool, m/s;

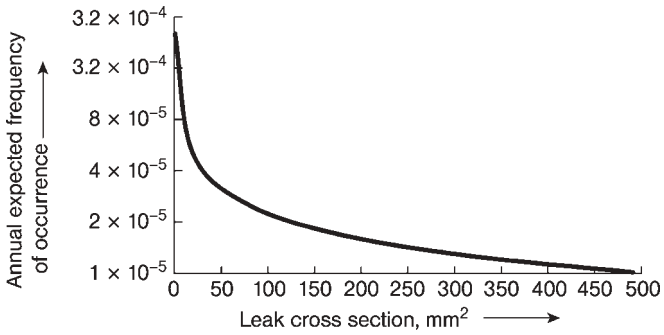

Figure 12. Expected annual frequencies for leaks of different sizes in a pipe with DN 25 (calculation based on [67])

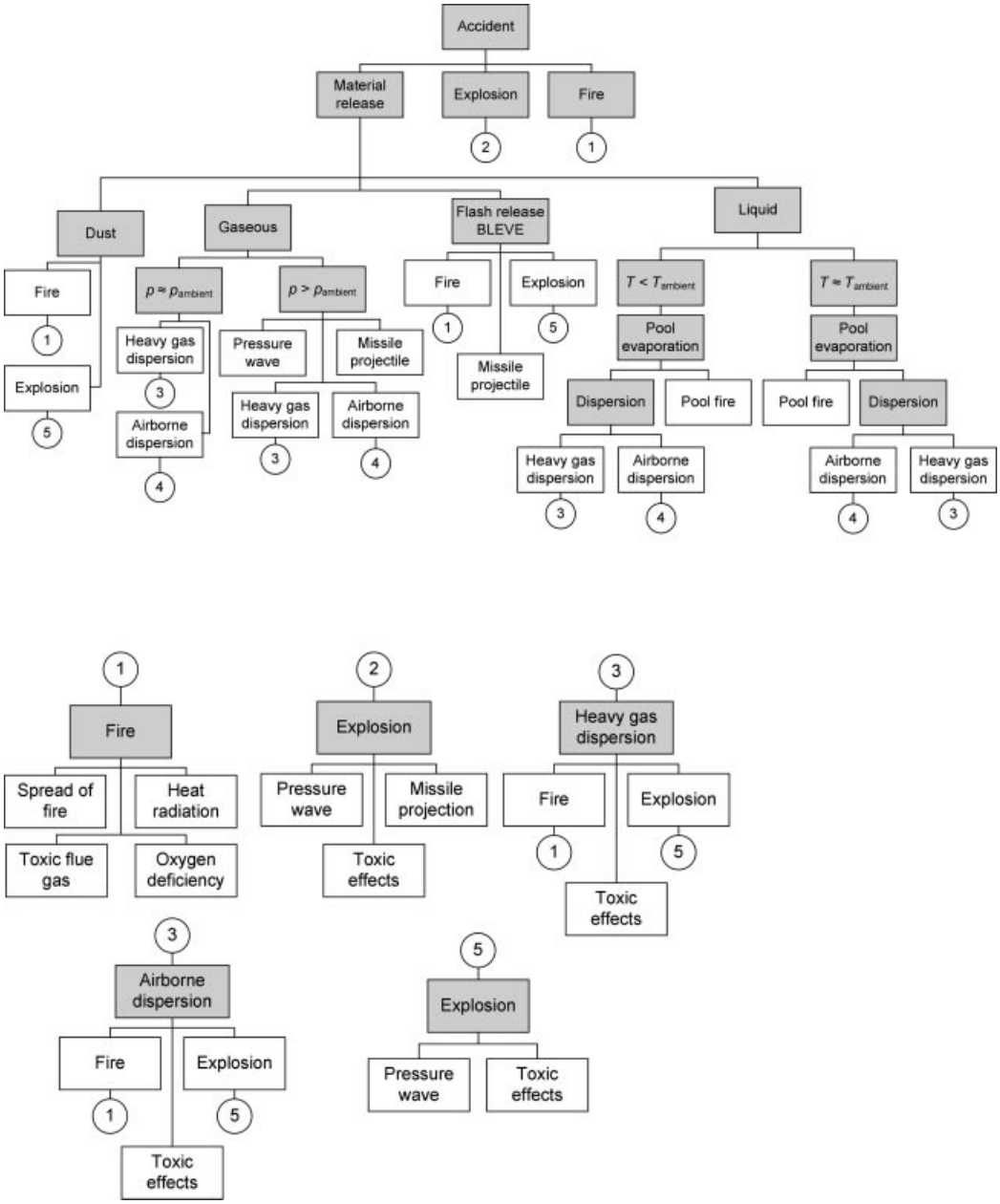

Figure 13. Potential types and characteristics of accidents in process plants

g: acceleration due to gravity, m/s^2;
h: height of the pool, m;
C_F: frictional resistance;
V: pool volume, m^3;
q_s: liquid supply rate to the pool, kg/s;
ρ_l: liquid density, k/m^3
u_{rA}: liquid surface regression rate, m/s;
A_{top}: pool surface area, m^2;
q_d: drainage rate, kg/s;
T: pool temperature, k;
H: heat flux density, W/m^2;
L_v: heat of vaporization of pool liquid, J/kg;
$c_{p,l}$: heat capacity of liquid, J kg^{-1}·K^{-1}
T_{qs}: liquid supply temperature, K;
V_d: volume of liquid discharged into the pool, m^3;
V_E: volume of liquid vaporized from the pool, m^3

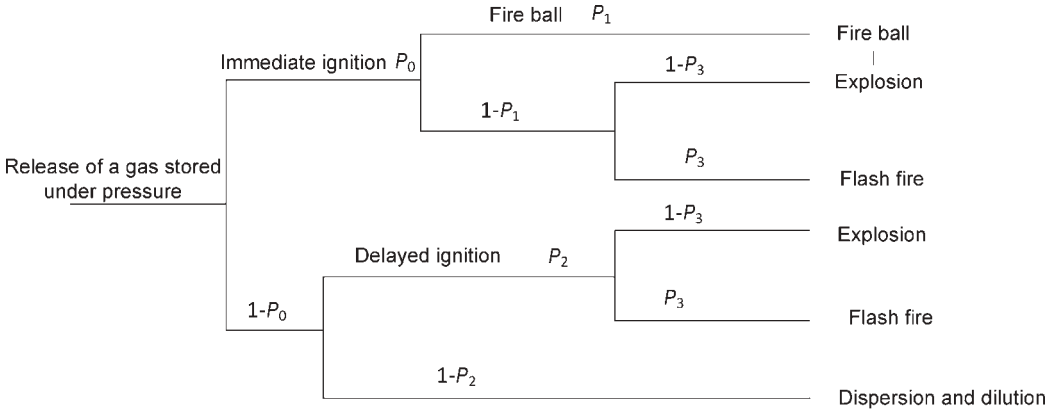

Figure 14. Event tree for the release of a gas stored under pressure (P_i, $i = 0,\ldots, 3$: conditional probabilities for the event to follow the path in question) [68]

According to [73] the following features are addressed in GASP, whose treatment may require slight modifications to be made to the above equations:

On land

- Spreading of liquid on land (either unconfined or confined by a bund)
- Instantaneous and continuous releases
- Smooth and rough ground
- Conduction from the ground, convection from the air and solar radiation

On water

- Spreading of liquid on water (either unconfined or confined)
- Instantaneous and continuous releases
- Heat transfer from contact with the water, film boiling heat transfer, convection from the air, solar radiation

LNG

- LNG treated as methane
- Vaporization of LNG pools on land and on water by
  - Boiling (vaporization at constant temperature driven by the heat flux to the pool)
  - Evaporation (vaporization driven by removal of vapor from above the pool surface
  - General heat balance allowing for changing temperature

Figure 15 shows the source term for atmospheric dispersion for the example of a spillage of cold chlorine given in [72]. It was calculated with GASP (cf. [74]) and the PHAST code [70], which is in widespread use for process plant risk assessments. Some explanations for the differences encountered, among them the wrong spreading law for the pool, i.e., $r(t) \sim t^{1/2}$ and

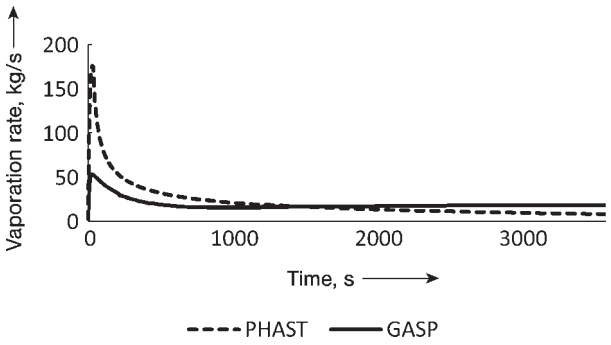

Figure 15. Evolution with time of the evaporation rate of the pool, comparison between GASP and PHAST

flaws in the relationship for the evaporation heat flow used in PHAST, are given in [80]. This shows that care must be exercised in assessing a source term from pool vaporization; this applies a fortiori if rule-of-thumb approaches are used [75, 76].

2.2. Vapor Cloud Dispersion

Industrial gases are transported, stored and used in steadily increasing amounts. Since many of these gases are either toxic flammable or both, there is heightened concern amongst the public and the regulatory bodies over the potential hazards in case of accidental releases.

The objective of this chapter is to explain the basics of vapor cloud dispersion. In particular the present German practice for obtaining estimates of the size of the area endangered by accidental spills is elucidated.

2.2.1. Formulation of the Problem

Accidental releases are characterized by

- Variable spill rates
- Variable gas properties
- Variable spill scenarios (instantaneous, continuous)
- Variable atmospheric conditions during the spill
- Variable obstacle configuration into which the gas is released

This results in a large number of possible parameter combinations which need to be separated into suitably defined sub-groups. The first distinction is usually made with respect to the density of the release.

Industrial gases are typically heavier than air, either due to their higher molar mass or since they are liquefied by pressure or stored and transported at very low temperatures. Once the gas is released a heavy gas cloud develops which forms a flat layer near the ground with a typical front vortex (gravity head) and a sharp density step at the upper edge. This heavy gas cloud is largely driven by gravity and develops a momentum of its own, initially quite independent of the atmospheric conditions. With increasing distance from the source more and more ambient air is entrained into the vapor cloud, thereby decreasing the density difference and adding momentum of the surrounding wind flow into the cloud. When the density of the cloud comes close to the density of the ambient air, the initial heavy gas dispersion phase is over. Atmospheric turbulence instead of internal cloud turbulence determines the mixing, and the diluted cloud disperses as if it were a neutrally dense gas and solely subject to atmospheric conditions (passive dispersion phase). Figure 16 gives a visual impression of the initial (gravity spreading) dispersion phase of a heavy gas cloud.

In terms of concentration the gravity spreading dispersion phase extends usually down to a few percent of the source concentration. This corresponds to the lower flammability limit of most flammable gases, i.e., for these gases a heavy gas dispersion model usually covers the whole area of interest.

In case of toxic gases which can still be harmful at concentrations of a few ppm or less

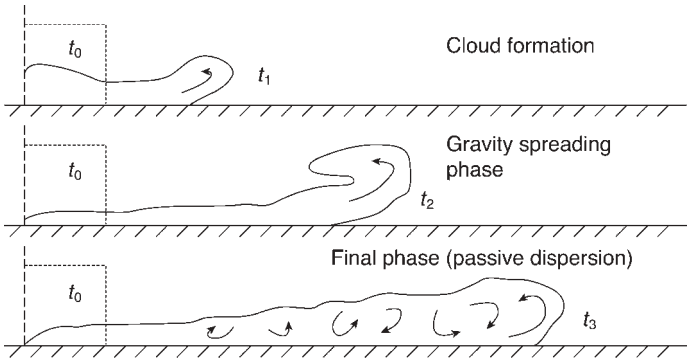

Figure 16. Sketch of the development of a heavy gas release with time t

it is necessary to extend the calculation over a much larger area. If the gas is heavier than air the heavy gas model needs to be coupled with a second model which uses the output of the heavy gas code as input and simulates the cloud dispersion in the subsequent passive phase. For neutrally dense or buoyant spills only the second phase model needs to be applied.

2.2.2. German Practice

Licensing procedures for potentially dangerous plants require a certain degree of uniformity which ensures that different plant operators are treated equally. In Germany the Engineering Society VDI releases guidelines for numerous purposes. For applications as discussed here the VDI-Guidelines 3783 Part 1 and Part 2 are relevant [81, 82]. They contain screening tools for accidental releases of neutrally dense and buoyant (Part 1) or heavy (Part 2) gases. These tools were already developed more than 20 years ago. However, they are still intensely used since their program codes run on simple PCs, come with user-friendly menus, and require only model inputs which can easily be provided.

Screening Tool for Neutrally Dense or Buoyant Vapor Clouds. The screening tool for neutrally dense or buoyant vapor clouds is based on the Gaussian dispersion formula for instantaneous point sources with reflection at the ground. For worst-case assessments reflection takes place also at an inversion layer above the cloud, thereby confining the vapor cloud within a narrow layer between the ground and the assumed inversion height. Sigma parameters according to [83] are used and an effective source height is calculated according to Guideline VDI 3782, Part 3 [84]. Line, area, and volume sources are code-internally generated through superimposition of multiple point sources, and time-varying or continuous spills through stringing together several release sequences.

Gaussian models are applicable to pollutant emissions into stationary and uniform atmospheric flows, for example, tall stack releases in flat, unobstructed terrain. For concentration predictions in complex structured industrial areas where flow conditions are usually far from uniform or stationary and where the vapor clouds are released near the ground into an industrially shaped landscape, this model type cannot properly be applied. Guideline VDI 3783, part 1, is therefore increasingly criticized, and VDI is looking for alternatives. However, finding a more reliable alternative is not an easy task, as is subsequently shown.

Tools which have the potential to accommodate obstacles in a reasonable way are microscale meteorological models of prognostic type. These models are based on the Navier-Stokes equation. Directly solving the equation in a turbulent flow requires a very fine grid to capture all the relevant scales, down to the so-called Kolmogorov scale (usually less than a millimeter). Furthermore, a time-dependent solution over sufficiently long periods is needed to yield stable time averages of the flow variables. This approach is called direct numerical simulation (DNS). As its computational demand is too high for the Reynolds numbers typically encountered in atmospheric boundary layers, DNS is not applicable here.

The computational demand can be substantially reduced when the time-dependent equations are solved on a grid that is fine enough (on the order of a meter in the case of a plant or city quarter) to resolve the obstacles and the larger atmospheric eddies. This approach is called large eddy simulation (LES). The small scales are formally removed from the flow variables by spatially filtering the Navier–Stokes equations. The influence of the small scales then appears as subfilter stresses in the momentum equation. Since the large eddies are always unsteady, LES models require input conditions which are time-dependent as well. Whilst less demanding than DNS, LES still requires significant computer resources, which go beyond the capabilities most users presently have.

In view of this the still most wide-spread method used for the computation of turbulent atmospheric flows is the Reynolds-averaged Navier–Stokes (RANS) approach. Within this approach the equations are averaged in time over all turbulent scales, to directly yield the statistically steady solution of the mean and turbulent flow variables. Like LES the averaging leads to additional terms in the momentum equation, known as Reynolds stresses. They represent the effects of the turbulent fluctuations

on the averaged flow and must be parameterized. This is the task of turbulence closure models. In most models presently in use the Reynolds stresses are assumed to depend linearly on the strain rate, as do the molecular stresses. The eddy viscosity appears as a proportionality factor that can be calculated by using additional differential equations for the various order moments. Many modelers regard the two-equation turbulence closure schemes, which solve differential equations for the turbulent kinetic energy k and the dissipation rate ε, to be a good compromise between universal validity and operating expense. In particular, the standard $k-\varepsilon$ model is widely used in engineering and micro-meteorological applications, despite the fact that it produces too much turbulent kinetic energy in regions of stagnant flow. Several modifications have been proposed which ease this problem, but mostly at the expense of the quality of other flow property predictions.

Another option is the use of standard turbulence models from the RANS approach in time-dependent simulations. Contrary to LES the averages are defined as ensemble or as time averages over small time intervals, although the latter definition leads to more additional terms in the momentum equation than in the case of ensemble averaging. This approach is also known as unsteady RANS (URANS). This type of model is used in standard meteorological meso- and macroscale applications (weather forecasts, etc.). URANS models are driven by time-dependent boundary conditions. They account, e.g., for different land uses with different radiation budgets and provide time-dependent predictions. In the context of urban applications, URANS models are under development. However, much more powerful computers than presently available and substantial research efforts will still be needed before the first reliable unsteady obstacle resolving predictions for urban-scale dispersion problems become available.

A further class of models which are still in use are diagnostic models. They do not use the Navier-Stokes equation and are based solely on mass conservation. The important influence of pressure gradients and forces on the flow development can only indirectly, i.e., empirically, be taken into account. These models start with a first guess of the three-dimensional flow field that is subsequently modified until the divergence of the flow falls below a chosen limit and mass conservation is assured. For a given obstacle array many different mass-conserving flow fields can be found, depending on the particular choice of the initial flow field and the "tuning of knobs" inside the model which, e.g., determine whether the fluid at a specific position moves over or goes around an obstacle. Although practitioners tend to ignore that, diagnostic models may be helpful in analyzing known cases, in particular when a good set of observational data is available for the area of interest. However, they cannot themselves be regarded as tools for the prediction of new and thus still unknown cases.

Lagrangian models, finally, are pure dispersion models, i.e., they follow individual plume parcels and model their paths on the basis of a random walk process. They need a complete mean and turbulent flow field as model input, which is usually delivered in form of 3D-gridded fields by either a diagnostic or prognostic model. Consequently, the quality of Lagrangian model predictions is closely linked to the quality of the model that was chosen to provide the flow field.

In view of these difficulties it is not yet clear what Germany's next-generation dispersion model for accidental releases of neutrally dense or buoyant gases will look like. There are tendencies to take the cheap way and to choose a diagnostic model for the flow field in combination with a Lagrangian model for the concentration field. There is evidence, however, that such a combination will not be able to provide reliable predictions.

Screening Tool for Vapor Clouds Heavier than Air. Modeling heavy-gas dispersion is much more difficult than modeling neutrally dense or buoyant plumes. Since chemical spills do not usually occur in flat and unobstructed terrain and heavy gases disperse near to the ground, obstacles play a much more dominant role than in case of buoyant releases, which can rise to higher elevations and for which shortly downwind from the source it is often possible to consider the buildings within the roughness parameterization only. For the gravity spreading phase of heavy gases, this would not be an

option. Truly obstacle-resolving prognostic numerical models are needed which are very demanding with respect to computer power. They are becoming available now but were out of reach in the 1980s when after the incidents in Bhopal and Seveso the authorities urgently demanded aid in decision making.

Therefore, when preparing the guideline for heavy-gas dispersion calculations (VDI 3783, Part 2), the VDI committee disapproved numerical models and opted instead for a guideline based on physical modeling, i.e., on results from wind-tunnel experiments. The wind-tunnel laboratory of Hamburg University was tasked to do the experiments [85]. To cope with the large amount of possible parameter combinations (see Section 2.2.1) it was necessary to structure the problem and to develop a good strategy for the generalization of the experimental results.

Certain similarity requirements must be fulfilled to transfer results from small-scale wind-tunnel experiments to prototype scale. These similarity laws are usually obtained by dimensional analysis, a method which makes use of the fact that physical equations must be dimensionally homogeneous and hence the parameters occurring therein can only appear in certain combinations.

The derivation of similarity laws is subsequently outlined at the example of an instantaneous heavy gas release as it was realized in the Thorney Island field tests [86]. Figure 17 shows the situation. A volume V_0 of heavy gas with density ρ_0 and viscosity μ_0 is released into an atmospheric boundary-layer flow characterized by a power-law wind profile with exponent n and a boundary layer thickness δ. The initial

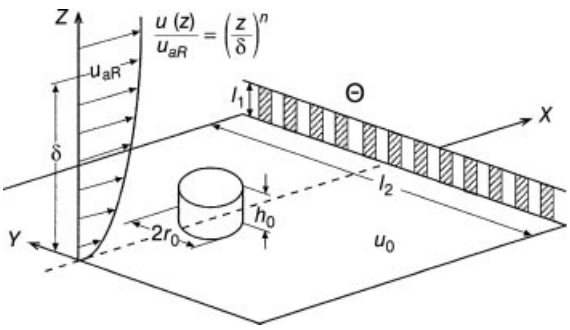

Figure 17. Instantaneous release of a volume of heavy gas into a shear flow disturbed by an obstacle. Definition sketch taken from [85].

shape of the cloud is unknown in reality. Hence, for simplicity a cylinder with height h_0 and radius r_0 is assumed. The properties of the surrounding air are described by ρ_a and μ_a, z_a characterizes the surface roughness, and $\bar{u}_{aR}$ the velocity in a given reference height. The spread of the cloud is affected by several obstacles. Their geometry is fully defined by the length scales $l_1, \ldots, l_n$ and the porosity Θ, symbolized by a simple fence in Figure 17.

We restrict ourselves to the gravity spreading Θ zone which is dominated by the (negative) buoyancy of the cloud and extends down to a few percent of the initial gas concentration. Within this zone, density differences between the cloud and its environment are much larger than those in the ambient flow. Therefore, the influence of ambient stratification on the spread of the cloud is small and can be neglected. With this restriction in mind, the local dilution $\chi = \Delta c/\Delta c_0$ (where Δc and Δc_0 are the local and initial concentration excess above ambient, respectively) depends on the following variables

$$\chi = f_1(t, x, y, z, g, \rho_0, \mu_0, V_0, r_0, z_R, \rho_a, \mu_a, \bar{u}_{aR}, \delta, l_1, \ldots, l_n, \Theta) \tag{32}$$

By applying dimensional considerations, a characteristic length scale, timescale, and velocity scale

$$L_{ci} = V_0^{1/3} \quad T_{ci} = \left(\frac{L_{ci}}{g'}\right)^{1/2} \quad U_{ci} = (L_{ci} g')^{1/2} \tag{33}$$

can be defined with $g' = g\Delta\rho_0/\rho_a$ the "effective" acceleration due to gravity and $\Delta\rho_0 = \rho_0 - \rho_a$.

The subscripts c and i indicate that these scales are characteristic variables for an instantaneous gas release. Nondimensionalization of Equation (32) results in

$$\chi = f_2\left(\frac{t}{T_{ci}}, \frac{x}{L_{ci}}, \frac{y}{L_{ci}}, \frac{z}{L_{ci}}, \frac{\Delta\rho_0}{\rho_a}, \frac{L_{ci}U_{ci}}{\mu_0/\rho_0}, \frac{L_{ci}\bar{u}_{aR}}{\mu_a/\rho_a}, \frac{r_0}{L_{ci}}, \frac{z_R}{L_{ci}}, \frac{\bar{u}_{aR}}{U_{ci}}, \frac{\delta}{L_{ci}}, \frac{l_1}{L_{ci}}, \ldots, \frac{l_n}{L_{ci}}, \Theta\right) \tag{34}$$

Equation (34) indicates that the local dilution χ as a function of the normalized time t/T_{ci} in both model and full-scale takes on identical values at locations determined by the coordinates x/L_{ci}, y/L_{ci}, and z/L_{ci}, provided that all the remaining dimensionless parameters on the

right-hand side of this equation can also be matched in the wind-tunnel experiment. These parameters are the density excess ratio of the initial cloud, a cloud Reynolds number and an ambient Reynolds number, the aspect ratio of the initial cloud r_0/L_{ci}, the roughness parameter z_R/L_{ci}, the velocity ratio $\bar{u}_{aR}/U_{ci}$, which has the quality of a Froude number (as can be seen when U_{ci} is replaced by Eq. 33), the nondimensionalized mixing height δ/L_{ci}, the dimensionless length scales, l_1/L_{ci} to l_n/L_{ci}, and the porosity Θ.

Both the dimensional analysis and the wind-tunnel experiments do not include those processes leading to the formation of the initial cloud (burst of a tank, evaporation of a liquefied gas). A possible ignition of the cloud if the gas were flammable is also excluded from the analysis. We assume that the source is fully described by an appropriately chosen initial density and initial volume and concentrate solely on cloud dispersion.

In the case of a continuous release, the initial volume V_0 is replaced by the initial volume flux $\dot{V}_0$. Since $\dot{V}_0$ contains the basic units length and time, dimensional analysis results in the characteristic scales

$$L_{cc} = \left(\frac{V_0^2}{g'}\right)^{1/5} \quad T_{cc} = \left(\frac{\dot{V}_0}{g'^3}\right)^{1/5} \quad U_{cc} = (\dot{V}_o g'^2)^{1/5} \tag{35}$$

and in the nondimensionalized variables

$$\chi = f_3\left(\frac{t}{T_{cc}}, \frac{x}{L_{cc}}, \frac{y}{L_{cc}}, \frac{z}{L_{cc}}, \frac{\Delta\rho_0}{\rho_a}, \frac{L_{cc}U_{cc}}{\mu_0/\rho_0}, \frac{L_{cc}\bar{u}_{aR}}{\mu_a/\rho_a}, \frac{r_o}{L_{cc}}, \frac{z_R}{L_{cc}}, \frac{\bar{u}_{aR}}{U_{cc}}, \frac{\delta}{L_{cc}}, \frac{l_1}{L_{cc}}, \ldots, \frac{l_n}{L_{cc}}, \Theta\right) \tag{36}$$

The subscript cc identifies a characteristic variable in the case of a continuous release.

Note that the VDI definition of similarity parameters differs from that proposed in [87], in which main difference lies in the fact that the ambient wind speed employed to form the characteristic scales. Since the zero ambient wind case is excluded from the analysis thereby, this approach was not adopted.

In a small-scale model it is neither possible nor necessary to match all the similarity numbers listed in Equations (34) and (36) to prototype values. The t/T_c terms disappear when the analysis is restricted to ensemble mean values of excess concentration maxima (instantaneous release) or to suitably defined time mean values (steady continuous release). In general, the Reynolds numbers (terms 6 and 7 on the right-hand side of the equations) are significantly smaller in a physical model than in the field. This has, however, only marginal implications as long as the Reynolds numbers are kept above a certain critical value. For the cloud Reynolds number $L_{ci}U_{ci}/(\mu_0/\rho_0)$ this value is about 400 according to [88]. For continuous spills the critical value of the Reynolds number depends on the specific release conditions. For low-momentum ground releases which are considered here, $L_{cc}U_{cc}/(\mu_0/\rho_0)$ is, according to experience, a peripheral variable.

Since obstacles are represented directly in a scale model and do not need to be included in the roughness parameterization, z_R is usually small. With $z_R/L_c \ll 1$ in both model and prototype, the roughness criterion is at least approximately fulfilled as long as the profile exponent n (see Fig. 17) is matched. Similar arguments hold for the boundary layer thickness δ/L_c which is much larger than unity in both cases (index c alone indicates characteristic values for both instantaneous and continuous releases).

With the exception of extreme values which are not considered here, the aspect ratio r_0/L_c should affect the cloud development only in the vicinity of the source. Further downstream details of the initial cloud shape are expected to become progressively less relevant. For the determination of lower flammability distances (LFD), defined as the distance from the source within which ignitable gas concentrations occur, it seems to be sufficient to characterize the cloud by its initial volume (or volume flux) alone.

With the provisions concerning the Reynolds number in mind, approximate similarity is to be expected by using an undistorted wind-tunnel model and matching the density excess ratio and the velocity ratio.

The dispersion experiments in the wind tunnel were carried out in a carefully designed boundary layer which matched the mean and turbulent characteristics of a natural boundary layer under neutral stratification [89, 90]. The heavy gas clouds were modeled through releases of sulfur hexafluoride/air mixtures. Instantaneous spills have been performed utilizing a cylindrical container with a volume of 450 cm^3 as sketched in Figure 17. At the time

of release, the side wall of the container was abruptly retracted into the wind tunnel floor. Continuous releases were realized through an orifice mounted flash into the tunnel floor. Volume fluxes of 100 to 500 L/h were emitted. The vertical momentum of the discharge was small.

To cover the heavy gas dispersion problem in its full complexity would have led to a huge and highly intractable experimental program. To reduce the number of experiments to a minimum, some of the similarity parameters in Equations (34) and (36) were varied in a systematic way in order to quantify their importance for the dispersion process.

The similarity requirement to keep both the excess density ratio $\Delta\rho_0/\Delta\rho_a$ and the densimetric Froude number (identical with the velocity ratio $\bar{u}_{aR}/U_c$) the same in model and prototype has the consequence of inconveniently and sometimes even impractically low wind velocities in the small-scale experiment. To match both parameters in a physical model corresponds to the application of a mathematical model utilizing the full, non-Boussinesq-approximated equations. On the other hand, relaxing the excess density ratio requirement and using the Froude number as the sole scaling parameter for buoyancy effects would correspond to a Boussinesq-approximated mathematical model. Since the introduction of the Boussinesq approximation is a common tool in mathematical simulations, it was appealing to check its consequences also in a physical model by distorting the density ratio.

Controversy still surrounds the use of distorted density scaling. Whereas concentration versus time traces reported in [91] show lower peak concentrations but extended time durations of cloud passage, pertinent experiments carried out in [92] and [93] indicate only differences within normal experimental scatter. On the other hand, in simulations of the China Lake field trials in a density distorted model, the heavy gas clouds were found to be moving generally too slowly in the wind tunnel [94].

The results of the experiments carried out for the VDI-group in the boundary layer wind tunnel of Hamburg University [85] showed exactly the same trend as was reported [94] (see Fig. 18 for instantaneous releases). When a certain experiment was repeated by varying the density excess ratio but keeping the densimetric Froude number the same, a cloud speed reduction in proportion to the density distortion was clearly noticed. Local peak concentrations, however, seemed to be only marginally effected. Since a shift in cloud arrival and departure times does not change the lower flammability distances and thus the area within which the gas–air mixture is hazardous, the subsequent experiments with instantaneous spills could be carried out with the Froude number as the essential scaling parameter, the density ratio remaining as a free parameter.

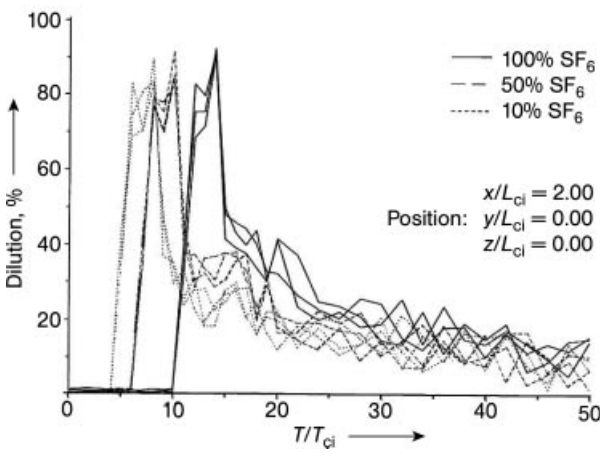

Figure 18. Concentration versus time traces for instantaneously released heavy gas clouds at a fixed position for different initial densities [flat terrain, $\bar{u}_{aR}(L_{ci}) = U_{ci}$]

Results from experiments with continuous spills exhibited a similar feature. Changing the density excess ratio $\Delta\rho_0/\Delta\rho_a$ by a factor up to ten had only marginal implications on ground level concentration decay. Especially in the range of lower flammability concentrations, the differences were well within normal experimental scatter. In conclusion, Froude number modeling appeared to be appropriate in case of continuous releases as well. The requirement of identical density excess ratios could be relaxed.

Risk prevention strategies are usually based on worst case assessments. In order to discover unfavorable conditions, the wind velocity ratio $\bar{u}_{aR}/U_{ci}$ was systematically varied and the concentration field at ground level monitored. Figure 19 shows the functional dependence of local maximum ground level concentrations (ensemble means) c_M, normalized with the maximum of all concentration maxima at this particular location c_{uM}, for varying distances from the source x/L_{ci}, and varying velocity ratios, $\bar{u}_{aR}/U_{ci}$. The results were obtained from instantaneous releases into a boundary layer unobstructed by obstacles.

As was to be expected, the concentrations were comparatively small for low wind velocities, since the cloud spreads horizontally in all directions. The concentration ratio was small again for large wind velocities due to the intense dilution of the cloud by ambient turbulence. Between these two extreme situations a maximum appeared. It occurred at about $\bar{u}_{aR}(L_{ci})/U_{ci} = 1$, which means that the lower flammability distances are largest when the front velocity of the heavy gas cloud (proportional to U_{ci} under stagnant ambient conditions) is of about the same magnitude as the advection velocity $\bar{u}_{aR}$ (taken at reference height L_{ci}). Comparable results were obtained for continuous releases. Also here, the largest lower flammability distances were obtained for velocity ratios of about 1. Since unfavorable ambient conditions are of predominant interest in risk assessment studies, the experimental program was focused on the worst-case wind velocity. This had the additional benefit of diminishing the Reynolds number problem since $\bar{u}_{aR}(L_{ci}) = U_{ci}$ is usually a moderate to high wind velocity.

In case of an accidental release the quantification of the source term is usually a difficult task. A cloud forms which often consists of a mixture of evaporated gas and ambient air. If the gas was pressurized, droplets of liquid gas may also be contained in the mixture (vapor flash). The density of the mixture is not exactly known. Fortunately, however, the density excess ratio itself is only of secondary importance. It enters the problem indirectly through the similarity parameters, but here only with powers of 1/2 or less. Therefore, in most cases, it should not lead to large errors when the initial density of the initial cloud is taken to be simply the density of the gas at boiling temperature.

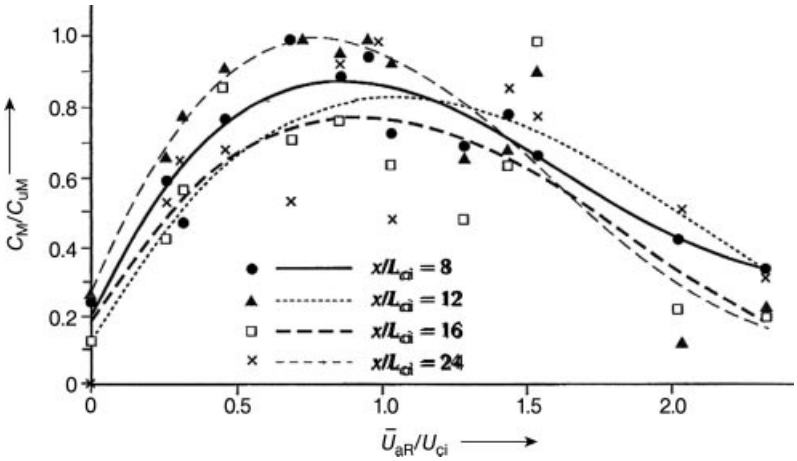

Figure 19. Normalized concentration maxima c_M/c_{uM} as a function of wind velocity ratio $\bar{u}_{aR}/U_{ci}$ at several ground-level positions for instantaneously released heavy gas clouds

Another uncertainty exists concerning the volume or volume flux of the cloud. Although the released mass flow of the gas can be regarded as being known, the dispersing cloud warms up, thereby expanding to a larger volume than it had initially. In the wind-tunnel experiments only isothermal clouds were modeled. For compensation, the initial volume V_0 (or volume flux $\dot{V}_0$) was increased to the value it takes on when warmed up to ambient temperature.

To determine the sensitivity of lower flammability distances (LFD) to these source parameters, some tests with varying mass fluxes of pressurized propane released continuously in unobstructed, flat terrain were carried out. In the first case, the density was set to $\rho_0 = 1.87$ kg/m^3, thereby assuming that the heavy gas warms up to ambient temperature immediately after the spill, with a corresponding increase in $\dot{V}_0$. In the second scenario the density of propane at boiling point temperature $\rho_0 = 2.36$ kg/m^3 was used, and the increase in volume neglected. Figure 20 shows the lower flammability distances (based on mean values of the lower flammability limit for propane, i.e., 2.1 vol%) for the two cases as a function of the spill rate for unfavorable wind conditions $(u_{aR}(L_{cc}) = U_{cc})$. Although extreme situations were assumed the LFDs differ by only about 20% which is not much in the context of a safety analysis. At first glance it is surprising that the lower flammability distance decreases when the gas density increases. The reason is that the lateral spread is more intense for the heavier cloud with the consequence of a reduced LFD value. Since, on the other hand, the neutrally dense cloud does not give the largest flammability distance, there must be a worst-case density ratio. According to experience it is in the range between $0 \leq \Delta\rho_0/\rho_a \leq 0.5$, i.e., most heavy gases of practical interest have density ratios above that range.

Another unknown quantity in the formulation of the source term is the amount of air mixed into the cloud during cloud formation. For risk analysis applications it seems to be appropriate to neglect mixing processes at the source. The release of a (then smaller) volume of pure gas, in comparison with the mixture containing an identical mass of heavy gas, should always lead to the larger flammability distance and therefore to a conservative estimate. This assumption has been also confirmed experimentally.

Wind-tunnel validation experiments were carried out by using field data from continuous release tests with methane (Burro and Maplin Sands experiments) and propane (TÜV Hamburg and Maplin Sands experiments). The field data covered different source conditions from nearly momentum-free spills of deep-cooled liquefied propane and methane over flash releases to jetlike discharges of pressurized propane. The spill rates varied over a wide range. The experiments were carried out both

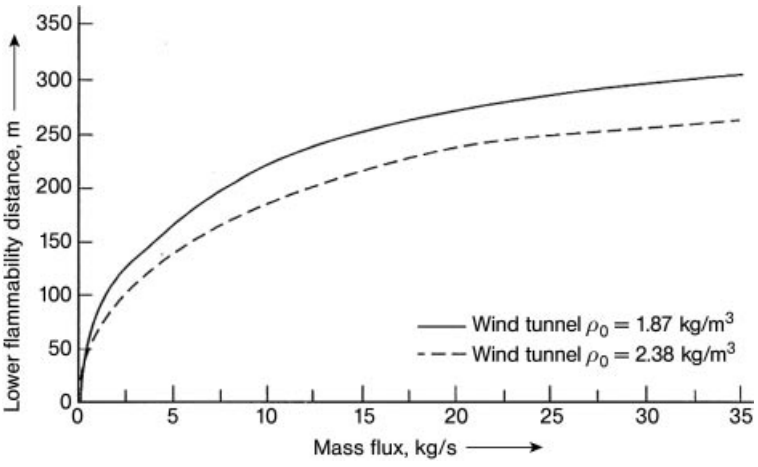

Figure 20. Sensitivity of lower flammability distances for fixed mass fluxes but different release scenarios (see text)

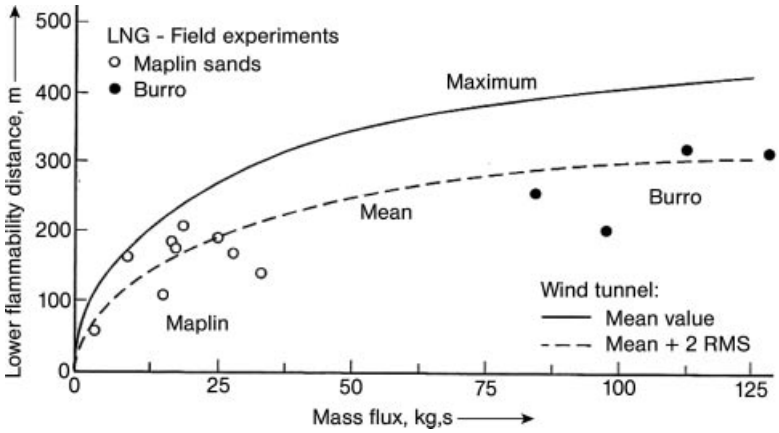

Figure 21. Comparison of data obtained in the Maplin Sands and Burro field trials with results from the wind tunnel experiments

over land and over water at varying ambient wind and stratification conditions. For details see [95–98].

In Figure 21 the lower flammability distances monitored in the Burro and Maplin LNG field trials are presented as a function of spill rate (symbols). They are compared with those from the wind-tunnel tests (curves), which were carried out with pure SF_6 and at an ambient wind speed of $u_{aR}(L_{cc}) = U_{cc}$. As in the field, the test area was flat and unobstructed. For the comparison, the initial density in the large-scale experiments was assumed to be the gas density at boiling temperature, the initial volume flux $\dot{V}_0$ was increased to the value it takes on at ambient temperature, and, finally, entrainment of ambient air into the cloud during cloud formation was neglected. Due to concentration fluctuations within the cloud, lower flammability distances based on ground-level mean concentration values (dashed line) and maximum concentration values (continuous line) were determined. According to theory the maximum curve (defined as mean + 2 RMS) should envelop all field data which were similarly based on concentration maxima but not necessarily taken under unfavorable ambient wind conditions. As can be seen, fair agreement was obtained, and this was the case as well for the propane experiments.

Small-scale/full-scale comparisons with instantaneously released heavy gases were carried out by using field data obtained in the HSE heavy gas dispersion field trials at Thorney Island, UK, during 1982/83 [86]. By using a foldaway tent, 2000 m^3 of denser-than-air gas was instantaneously released in each experiment. The experimental setup corresponded to that sketched in Figure 17. The field trials were mainly carried out in unobstructed terrain, with the exception of a few cases in which the mitigating effect of a 5 m-high, semicircular fence was tested. All experiments were repeated in the wind tunnel by using a model on the scale 1:165 and matching all relevant similarity parameters. The agreement was again satisfactory. Figure 22 shows this for the example of trial No. 20, which was done in the presence of a fence.

The data were taken at a position behind the fence. The figure contains several concentration versus time traces. Due to the turbulence within and outside of the cloud, there is a high degree of naturally occurring repeat variability in the measurements. Although only "one-shot" data were available from the full-scale trials, model experiments were repeated five times to get some idea of the degree of variability. Also included in Figure 22 are the results from wind-tunnel experiments carried out under identical conditions but without the fence. As the comparison shows, the protection provided by the fence is remarkable and leads here to a decrease in the concentration maximum by nearly one order of magnitude.

To meet the demand of authorities and industry for an easily applicable method for the determination of flammability distances in

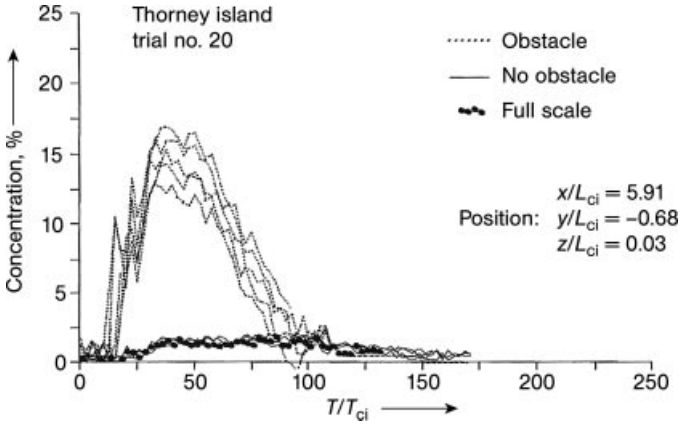

Figure 22. Small-scale/full-scale comparison of Thorney Island experiment No. 20. The potential concentration versus time traces in the absence of the fence are also included in the figure.

urban or industrial landscapes, systematic wind-tunnel experiments with a variety of obstacle configurations were carried out. These obstacle configurations included street canyons with different orientation towards the wind, street crossings, downslopes, ditches, mitigating walls, and cube arrays. Some of these obstacles led to a significant increase, others to a significant reduction, of the extent of the area within which hazardous gas concentrations can occur. The obstacle configurations were chosen such that both extremes were covered in the experiments, in order to obtain quantitative information to which degree obstacle effects can modify the dispersion of a heavy-gas cloud.

Subsequently, as an example for an unfavorable obstacle configuration, the results from a street canyon oriented parallel to the wind direction are presented. The canyon was infinitely long, its width was $2L_{ci}$ ($14L_{cc}$) and the height of the bordering buildings was L_{ci} ($7L_{cc}$). Flow visualization indicated that the height of the buildings was already sufficient to trap the heavy gas cloud completely. Instantaneous and continuous releases were realized. The wind velocity $\bar{u}_{aR}$ measured at height L_c was chosen to be the characteristic wind speed U_c. Ground-level concentration versus time traces were recorded at eight locations downstream from the source. Mean and maximum (mean + 2 RMS) values of the local concentrations $\Delta c/\Delta c_0$ were determined by time-averaging the concentration versus time traces (steady continuous releases) or ensemble-averaging the excess concentration maxima obtained in 10 repeats of the same experiment (instantaneous releases).

The results obtained were transformed into graphs, as presented in Figure 23. They allow direct determination of worst-case lower flammability distances as a function of the lower flammability concentration for all major flammable gases. Assuming, e.g., the instantaneous release of 2000 kg of pressurized propane, the density of the gas at boiling temperature ($-42.1°C$) is $\rho_0 = 2.38$ kg/m^3 and supposing that the propane evaporates completely, the initial volume of the cloud is $V_0 = 1050$ m^3 (taking into account the expansion of the cloud due to temperature increase to ambient temperature during dispersion). According to Equation (33), the characteristic length of the spill is $L_{ci} = 10.16$ m. Assuming the release of pure propane and considering that the lower flammability concentration (LFC) is 2.1%, Figure 23 provides the lower flammability distances based on mean and maximum ground-level concentrations, i.e., $\mathrm{LFD}_{mean} = 37L_{ci}$ 376 m and $\mathrm{LFD}_{max} = 41L_{ci} = 417$ m, respectively. If the same spill were to occur in flat, unobstructed terrain, the corresponding LFD values would be 234 m and 305 m. In the case of a semicircular wall of $0.4L_{ci}$ height located $4L_{ci}$ downwind from the source, the pair of lower flammability values would decrease to 42 and 66 m, respectively.

The street canyon described above represents one of the most unfavorable obstacle

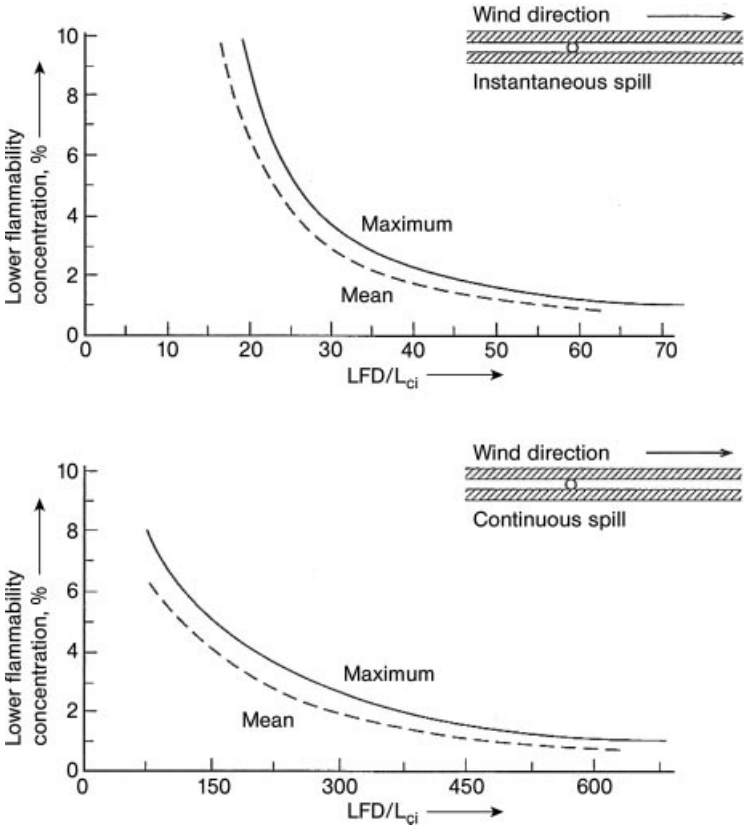

Figure 23. Lower flammability distances for instantaneously (top) and continuously (bottom) released heavy gas for varying lower flammability concentrations

configurations, whereas the semicircular wall proved to be one of the most effective mitigating structures. The range within which lower flammability distances change due to obstacle effects is therefore known. Obstacle arrays of practical interest are likely to be between these two extremes. A first estimate of LFD values can therefore be obtained also for those obstacle configurations which were not covered in the investigation.

Altogether 25 obstacle configurations were realized in the wind tunnel experiments [89, 90]. From the results, graphs according to Figure 23 were deduced. As demonstrated, these graphs can easily be used to determine the lower flammability distances for all major flammable gases heavier than air. Due to the dimensionless presentation of the results, the graphs are applicable to any spill rate.

To extend the range of applicability of the results to toxic heavy gases, additional measurements were carried out to determine the size of the cloud at the end of the gravity spreading phase (which was somewhat arbitrarily assumed to coincide with the 1% concentration level). The data obtained can be used as input data for a numerical model which calculates concentrations and dosage values for locations in the far-field of the cloud.

The experimental data were summarized in a data bank. A menu-guided program was written which enables the user to use the results quite easily on personal or main frame computers.

Determining heavy-gas dispersion presents challenging modeling requirements. Complex geometry areas and unsteady, negatively buoyant flows drive current computing capabilities to its limits. Numerical models which are principally capable to do the job are necessarily of LES type. Such models are presently under development but research tools rather than state of application. In contrast to Guideline part 1

which is based on a Gaussian model, Guideline part 2 with its physical modeling backbone will probably remain the standard German screening model for a couple of years to come.

2.3. Pool Fires and Spill Fires

The discipline of combustion and flames makes an important contribution to loss prevention in process plants. When a flammable liquid, gas, or solid is released accidentally and is ignited an industrial fire occurs. These fires are frequently intense emitters of thermal radiation and pollutants such as smoke and other combustion products. The thermal radiation is the primary mechanism for damage, e.g., to adjacent objects and injury of plant personnel and potentially people beyond the boundaries of the plant [99–102]. In some cases, the development of large smoke plumes (e.g., Buncefield event [103] or 700 Kuwaiti oil fires during the Second Gulf War in 1990) endangers people and the environment or air traffic. It is important for the combustion behavior of flames [104–109] to consider both the causes and the effect of fires and explosions in process plants. Flames inside the plant include flames in vessels, pipes, and cool flames [99].

The treatment here is restricted to flames in the open, i.e., pool fires, spill fires, unconfined fires, (storage) tank fires, slot fires occurring after ignition of fuel releases caused by an accident in process plants. Such pool fires are a part of several possible burning regimes [110, 111]. A *vapor cloud fire* (*flash fire*) occurs if the released liquid fuel can be volatized to form a cloud of combustible fuel–air mixture, with a subsequent gas-phase ignition. If the burning region then moves back towards the spilt fuel a *pool fire* is established. Alternatively if the spill is relatively small and the fuel release happens in the presence of ignition sources a *jet flame* occurs. If the release in the presence of ignition sources is very large, a *fireball* develops. The behavior and the modeling of jet flames, vapor cloud fires (flash fires), and flares are summarized in [99, 101, 102] and in Section 2.5.

A typical event tree for the accidental release of a flammable material, showing the different pathways that lead to various types of open fires is given in [110, 112].

In many process plant fires the thermal radiation is the dominant mode of *heat transfer*. About this rather complex topic only an outline treatment is given in the present context. Selected standard texts on radiant heat transfer are [111–121].

2.3.1. Zones and Measurable Quantities

When a flammable liquid accidentally spills onto the ground or water and is ignited, often a pool fire occurs. Pool fires are non-premixed, buoyancy-driven flames established over horizontal liquid or solid fuel surfaces other important types. There is a considerable literature about experimental studies and modeling of pool fires, summarized in [99, 101, 102, 122]. A practical way to describe the complex phenomena in a pool fire are the concepts of a number of fairly well-defined zones and of measurable quantities, although both concepts have no direct correspondence to the fundamental physical parameters controlling the combustion and different transport processes. The following zones can be distinguished in most pool fires (Fig. 24):

1. Especially in deep pools there may be significant convective flows within the liquid fuel and interactions between the fuel and the vessel. Both phenomena influence the (external) characteristics and the burning behavior of the fire.
2. Above the fuel surface there is a constant-shaped conical zone, including unburned fuel vapor or fuel parcels and vapors of pyrolysis products.
3. The conical vapor zone is surrounded by a luminous clear flame zone, also with an approximately constant shape.
4. Above the zone in (3) there is a further combustion zone (pulsation zone) including intermittency and turbulence phenomena.
5. Finally there is a generally turbulent, mainly nonreacting buoyant plume, which is characterized by axial and lateral profiles with decreasing temperature and velocity.

Each zone is described in detail and different physical characteristics are formulated which control the behavior of these zones and their

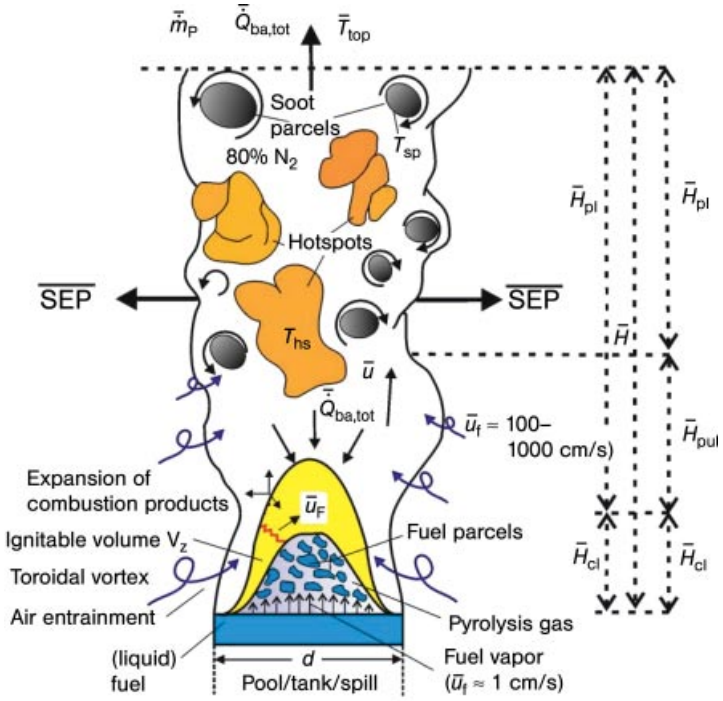

Figure 24. Characteristic flame in adiabatic unconfined pool and tank fires [112]
$\bar{H}_{cl}$ mean height of the clear flame zone; $\bar{H}_{pul}$ mean height of the pulsation zone; $\bar{H}_{pl}$ mean height of the plume zone; $\bar{m}_P$ mean mass flow rate of the combustion products; T_{top} mean temperature at the flame tip; $\dot{Q}_{op,tot}$ mean total heat flow rate at the flame tip; $\bar{u}$ mean flow velocity; $\bar{u}_F$ mean flame velocity, $\bar{u}_f$ mean fuel vapor velocity.

interactions [123]. A pool fire is then quantified by the following main measurable quantities [99, 101, 102, 124]:

1. Mass burning rate $\dot{m}''_f$ in kg fuel s^{-1} m^{-2}) or liquid burning velocity v_a in mm/min. The quantities $\dot{m}''_f(d)$ or $v_a(d)$ generally depend on the pool diameter d. With increasing d the flow regime of a pool fire changes from laminar to turbulent. Early experiments [125] show that there are two basic burning regimes (limiting cases [126]) for pool fires:
   a. Radiatively dominated burning for relatively large diameters $d \geq 1$ m,
   b. Convectively dominated burning for very small diameters $d < 0.2$ m.

   The most important parameter is the maximum mass burning rate $\dot{m}''_{f,max}$ theoretically occurring at infinite diameter $d \to \infty$. In more recent experiments [127] the limit diameter d', beyond which $\dot{m}''_f(d)$ becomes independent of d or may decrease slightly is not $d' \leq 2$–5 m but $d' \leq 20$ m, e.g., for crude oil. The maximum rate $\dot{m}''_{f,max}(d')$ is related to the radiatively dominated burning regime where the fire is effectively optically thick. For the experimental indication of a slight decrease of $\dot{m}''_f(d)$ at very large diameters $d \geq 10$ m there are not enough reliable data. A review of equations to estimate $\dot{m}''_f$ as a function of d, fuel, t, $-\Delta h_c/\Delta h_v$, u_w, and pool rim effects is given in [99, 101, 112, 123]:

$$\dot{m}''_f(d) = \dot{m}''_{f,max}(1 - e^{-k\beta d}) \tag{37}$$

   where t (s) is the time, u_w (m/s) the wind velocity, k (m^{-1}) an absorption-extinction coefficient and β (−) is a mean beam length corrector, which cannot be derived [128, 129].
2. Total heat release rate $\dot{Q}$ (kW):

$$\dot{Q} = \dot{m}''_{f,max}(-\Delta h_c) A_P \eta_c \tag{38}$$

   where η_c is the efficiency of combustion
3. Flame height or flame length H (m). Generally, H is taken to be either the maximum

visible height H_{max} or the time-averaged visible height $\bar{H}$. The experimental determination of H_{max} and $\bar{H}$ is the intermittency criterion [130]. A review of equations to estimate H_{max}/d and $\bar{H}/d$ as a function of the fuel Froude number $Fr_f \equiv \dot{m}''_f/\rho_a\sqrt{gd}$ and the dimensionless wind velocity $u^*_w = u_w/u_c$ is given in [99, 101, 102, 112]:

$$\frac{H}{d} = a \cdot Fr_f^b \cdot u_w^c \tag{39a}$$

with

$$u_c = \left(\frac{g\dot{m}''_f d}{\rho_a}\right)^{\frac{1}{3}} \tag{39b}$$

where u_c (m/s) is a characteristic velocity, ρ_a (kg/m^3) is the density of the ambient air and a, b, c are empirical fuel-dependent parameters, summarized in [112]. There is also a low-level Froude number Fr_v.

4. Flame temperature T (K). Generally, in a fire there are axial and radial distributions of temperatures depending on the diameter d and fuel, which are not well known. The measurements and predictions of temperatures in fires are very difficult [131, 132]. For example, in a single JP-4 pool fire ($d = 16$ m) the following temperature regions exist [103, 112]: 873 K $< T_{hs} <$ 1653 K, 573 K $< T_{sp} <$ 973 K, where T_{hs}, T_{sp} are flame temperatures referring to hot spots and soot parcels.
5. Soot and smoke production rates $\dot{V}_s$ (m^3/s) or $\dot{m}_s$ (kg/s). The measurements and predictions, especially in large fires, of $\dot{V}_s$ or $\dot{m}_s$ are difficult. The behavior and modeling of large-scale sooting fires is a highly complex subject and remains a challenge and relevant problem [122, 133, 134].
6. Thermal radiation, described either as the surface emissive power (SEP) in kW/m^2 or as the fraction of the combustion energy radiated f_{rad} (−), is the dominant mode of heat transfer [103, 112, 135].

2.3.2. Physical Characteristics

In the following a summary of physical characteristics or principal factors influencing the measurable quantities (see above) associated with a pool fire is given [112, 123, 128, 131–134], i.e., pool geometry (d, liquid depth, substrate), fuel type and composition, ventilation conditions (e.g., wind), surrounding geometry (e.g., open air, height of compartment, proximity to walls), and nature of the bounding materials (e.g., edge effects due to the "lip" of a pan).

Fuel Type. The dependence of the above mentioned six measurable quantities on the type or composition of the fuel is very complex; it is predictable only in some special cases. Mostly only a qualitative understanding is possible. For example, the burning behavior of alcohol pool flames is different from most other hydrocarbon fires, essentially because the small variation of its $\dot{m}''_f$ on diameter d. The reason for this effect, $\dot{m}''_f \approx \dot{m}''_{f,max}$, is that alcohol pool flames produce only small amounts of soot particles, i.e., they burn very cleanly. Another characteristic effect is the decrease of the SEP for aromatic or hydrocarbon fires with long-chain fuels.

Bounding Materials of Pool Fires and Lip-Height Effects. In pool fires, mostly discussed in the literature, the liquid fuel is contained within a confinement, e.g., a vessel with walls of definite height or a bund, which allows the fuel to exist as a layer of sufficient thickness. The burning behavior of such pan fires or tray fires is different from that of spill fires (see Section 2.3.3). For reasonably small pools [136] the burning behavior depends clearly on the material of the vessel, primarily caused by differences in heat losses.

Several edge effects exist due to the lip of a pan above the fuel surface to confine the liquid. These effects include greater turbulence near the flame base (leading to a higher convective heat transfer), decreased flame height H, increased gas emissivity ε_g, increased gas-phase temperature near the fuel surface [137], and hence increased $\dot{m}''_f$ [138]. However, there is insufficient data on lip height effects.

Wind and Other Ventilation Effects. The effects of wind or ventilation on pool fires are very complex. For example, the wind velocity has the following effects on a pool fire:

1. Enhancement of convective flows

2. Improvement of mixing processes and combustion efficiency leading to increased flame temperatures [136]
3. A decrease in flame height [99, 101, 112, 129, 139]
4. Development of flame tilt and flame drag [99, 101, 112, 139, 140]
5. Significant changes to the thermal radiation profiles [141]
6. A significant increase in fuel vaporization and mass burning rate in large open-air pool fires
7. A great increase in the mass burning rate in the case of confined pool fires e.g., tunnel fires or fires within a compartment or corridor; these fires, in particular large pool fires (see Section 2.3.6), are significantly underventilated in natural ventilation conditions [142–145].

Nonsteady or Transient Effects. Most analyses of pool fire behavior address steady-state burning. There are several nonsteady effects caused by heat transfer to the sides and the base of the pan (especially in shallow pools) and heating of the fuel itself. These effects lead to a steady increase of the mass burning rate. A further transient effect within the steady-state burning phase is caused by the increase in the lip height as the fuel level drops. As the fuel is consumed the fuel layer becomes thinner. Hence, the heat transfer to the substrate increases greatly so that the mass burning rates diminish. Completely nonsteady burning occurs with many fuels, such as crude oils, whose composition varies strongly during the burning time.

Boilover. Some fuels do not show steady-state burning behavior; they rapidly boil on attaining a certain temperature, combined with an overflow of the pan and an expanding of the fuel surface. Especially hydrocarbons with moisture content tend to boilover phenomena [146–148].

Pulsation. Pool fires exhibit a pulsating behavior, as reviewed in [123, 149, 150]. The oscillation frequency f is in general correlated by a Strouhal–Froude number relationship $f(d) = Sr\,Fr_f\sqrt{g/d} \propto d^{-0.5}$, where $Sr = f\,d/u_f$ is the Strouhal number, $u_f \equiv v_a$ the velocity u_f or the regression rate v_a of the liquid fuel, and $Fr_f \equiv v_a/\sqrt{g\,d}$ is the fuel Froude number. A modified correlation, derived in [151] is $f(d) \propto d^{-0.63}$, validated for n-hexane, methanol, JP-4, and diesel/premium gasoline/pentane pool flames for $0.03 < d < 8$ m. These pulsations significantly influence the air entrainment in pool fires and thus the completeness of combustion and the soot production (see below).

2.3.3. Spill Fires and Fuel Layer Thickness Effects

An important variant of the pool-fire problem is the liquid spill, which leads to a spill fire in shallow pans or generally without confinement of the fuel. The fuel-layer thickness (fuel depth) is typically in the range of 0.7–4 mm and may not be sufficient to achieve steady-state burning.

The overall heat release rate $\dot{Q}$ (see Eq. 24) of spill fires depends on $\dot{m}''_f$ and the potential size of the spill, i.e., the surface area A_P of the fuel. The fuel surface area is of great importance but is difficult to predict, as it depends on the initial momentum of the spilled fluid, the fluid surface tension, and the porosity and roughness of the substrate materials [152]. Any uncertainty in the fuel depth leads directly to a change in the fuel surface and hence the fire size. The size and conditions in a spill fire depend on whether the spill is continuous or instantaneous [112]. The fuel depth can decrease after ignition, owing to the change in fuel properties, combined with a potential increase in the fuel surface of about 50 %.Unconfined spill fires show a strong reduction in convective heat flows within the fuel and an increase in heat losses to the substrate. As a result the reduced mass burning rate $\dot{m}''_{f,spi}$ of a spill fire is $\dot{m}''_{f,spi} \approx 0.2 \cdot \dot{m}_{f,p}$, where $\dot{m}''_{f,p}$ is the mass burning rate of a pool fire [154].

The effects of fuel layer, weathering, and emulsification of the fuel on flame spread rates [152, 155, 157] above a water substrate is given in [155].

2.3.4. Soot Production

Soot consists of carbon particles with diameters d_s in the nanometer range which are produced in a fire, oxidized, and glow, often in yellow and/or

orange. The visibility of a fire is caused by the continuous emission of radiation in the visible spectrum by the burning soot. Carbon particles agglomerate to form long-chain carbon molecules or black smoke when the carbon produced by pyrolysis is only partially oxidized or is not oxidized at all because of the lower local temperature.

There are many soot formation studies [153, 156, 158, 159]. It can be concluded that soot production in pool fire (plumes) is a highly complex subject for the following reasons:

1. The formation and oxidation processes vary spatially
2. There are strong temperature- and fuel-dependent effects
3. The influence of turbulent fluctuations is important
4. Pulsation of pool fires has a significant effect on soot production.

Nevertheless it is possible with a simplified analysis [160, 161] to establish generalized state relationships for major gas species and soot [160, 162, 163]. Some fundamental results are:

1. In overfire (fuel-lean) regions of the plume the soot amount varies with fuel type but is approximately independent the position in the plume. Beyond a certain flame residence time the soot yield reaches an asymptotic value and depends thereafter only on mixing levels.
2. In underfire (fuel-rich) regions are exist strong correlations between the soot volume fraction $f_{s,v}$ and temperature; the soot exists in nearly constant temperature layers, i.e., is largely confined to a narrow region of mixture fraction and temperature.
3. To predict soot yields some global kinetic models are used (cf. [164, 165]) despite the difficulty in correlating soot yields to mixture fractions. These global kinetic multistep models include nucleation, coagulation, and surface growth processes by using flamelet representations of each. This approach overcomes limitations which are present in correlations to mean mixture fraction. However, some problems with modeling the turbulent interaction remain. In particular, it is shown in [163] that spectral radiation intensities might be increased by 40–100% from estimates typically based on mean properties.

There are several models to relate the emissivity ε_F and/or the extinction coefficient k of the fire gases to the soot concentration c_s. Gray-gas models are proposed and/or used in pool fires [101, 135, 139, 166–168]. More advanced models, which include spectral resolution in a finite number of bands, i.e., weighted sum of gray-gas models and narrow-band models are reviewed in [169, 170]. The absorptivity of agglomerating carbon particles depends only weakly on fuel and flame types [171].

In [172] the classical principle of smoke point is used to relate soot production to material properties [173]; a numerical methodology is proposed to obtain soot volume fractions.

Very little work has been done on the measurement of smoke production rates in large turbulent fires. From measured smoke production in crude oil fires ($0.085\ \text{m} < d < 17.2\ \text{m}$) the mass fraction smoke yield $\frac{m_{sm}}{m_c} \cdot m_f = Y_{sm}\,(\%)$ can be correlated as [174]:

$$Y_{sm}(d) = 2.758 \cdot log\, d + 9.412 \tag{40}$$

where the constants depend very critically on the fuel chemical composition and pyrolysis properties.

The following two physical phenomena may contribute to the production of smoke in large-diameter fires, even in "clean-burning" fuels, such as methane or LNG and ethanol:

1. The first phenomenon is caused by the lack of oxygen in the fuel rich vapor core near the flame axis above the fuel surface. Within this core there is not enough oxygen to burn the carbon particles produced by the pyrolysis processes of fuel vapor. In this zone not only are carbon particles produced but also a decrease of the overall heat release rate $\dot{Q}$ occurs, and hence a decrease of the temperature, which results in increased smoke production.
2. The second phenomenon is a decrease of the effective concentration of fuel and fuel vapor in the core zone caused by recirculation of burnt gases by a toroidal vortex existing in most large fires. Part of this fuel-concentration decrease contributes to the formation of

carbon particles. The following two reverse effects of smoke exist, where the domination of the two effects depends on the chemical properties of the fuel, chemistry of combustion, the physical dimensions and the hydrodynamic of the gas flow within the fire. The first effect (smoke-blockage effect [110, 175]) is the absorption (shielding) of the emitted thermal radiation resulting in a significant reduction of the thermal radiation hazard distances Δy_{cr} [166]. However, this is true only under the assumption that the whole fire including the lower clear flame zone (see Fig. 24) is obscured by a sufficiently thick layer of black smoke. This obscuration leads also to a strong decrease of f_{rad}. The second effect of smoke is an increase of the temperature of the flame gases caused by the decrease of the radiant emission. No model exists that includes all mentioned phenomena and effects. Additionally there is a lack of experimental data, in particular due to the height H_{cl} (d, fuel) of the clear flame zone as a function of d and fuel type.

2.3.5. Heat Transfer

In liquid pool flames with $d < 0.3$ m the thermal radiation can be neglected and the convective heat transfer dominates [176, 177]. However, in most practical fire scenarios with liquid fuels, thermal radiation is the dominant mode of heat transfer [101, 123, 178, 179]. The thermal radiation hazard from a pool fire depends mainly on the fire size (i.e., d) and the fuel type (i.e., flame height H, liquid properties) [140]. More specifically, thermal radiation (radiative heat loss) is caused by the major combustion products (CO_2, H_2O, CO) and carbon particles (soot and smoke) in the flame and plume. In large pool fires the absorption coefficient x_s is mainly due to soot and it is shown that the main fraction ($> 90\%$) of the radiation in fire plumes is emitted from the visible region of the flame, where carbon particles radiate heat [180]. In moderate-sized liquid pool fires the radiated heat flux near the plume depends strongly on fuel-dependent rates of soot and the production of combustion products [181]. For large hydrocarbon fires ($d >$ 3 m) the fire gases become optically thick [112], i.e., the effective emissivity $\varepsilon_F = 1-\tau_s \approx 1-0.01 \approx 0.99$ and the surface emissive power SEP saturates [101, 182–185]. Pool fires with smaller diameters $d \ll 3$ m can also be optically thick if strongly sooting fuels burn. In sooty fires of still larger diameters $d \gg 3$ m, the SEP is essentially reduced by a factor of up to 6 [101, 183, 184]. This is called the smoke blockage effect (see above). This issue is complicated by the occurrence of strong intermittency in the appearance of hotter luminous zones on the external surface of the fire, including the phenomenon of turbulent mixing. Hence, averaging approaches are no longer valid (cf. Section 2.3.6).

2.3.6. Large Pool Fires

Initially small pool fires are convectively dominated and large pool fires are radiatively dominated. However, the term "large pool fire" refers also to diameters of $10\text{ m} < d < 100$ m. In the following large fires are optically thick, i.e., often for $d \gtrsim 3$ m.

Several phenomena, which are exhibited by large pool fires, were mentioned above. However, in this section these issues and other key features of large pool fires are discussed.

Fire Tests. For a further fundamental understanding of the different processes in large pool fires, experimental and modeling studies are necessary. Most of the large-scale experiments of interest for obtaining radiation validation data are reviewed in [179]. Work on detailed measurements to identify soot production, flow fields, and heat-transfer mechanisms in large-scale liquid pool fires is being done at Sandia National Laboratories in Albuquerque, New Mexico [186–188]. Several sets of fire tests were carried out within oil-spill mitigation programs in the USA and Japan [189–191]. The experiments were the basis for the development of important aspects of the fire dynamic simulator (FDS) [192–194]. Detailed large-scale experiments on pool fires of different liquid fuels were carried out to identify the thermal radiation (SEP), dissipative structures, probability distributions of temperature of hot spots and soot parcels, oscillation phenomena, wind influences, and flow fields at the Universities Stuttgart [131, 132, 151, 195] and Duisburg-Essen [112, 133, 134]. These experiments led to

the completely new model OSRAMO II [103, 196] and started the development of CFD simulation of large pool fires in Germany [112, 133, 134, 197–203].

In addition—also for a better understanding of large-scale pool fires—an experimental program with small-scale liquid pool fires was carried out to identify mass density fields, thermal boundary layers, density sources and sinks, temperature fields, periodic and quasiperiodic phenomena, flow velocity fields, and concentration fields of stable species [151, 195, 199, 204–207].

Low-Level Froude Number and Low Reynolds Number Flow. A fundamental aspect of the fluid flow in large-scale pool fires is the very low fuel vapor Froude number:

$$Fr_v(d) \equiv \frac{u_v}{\sqrt{gd}} \tag{41a}$$

with

$$u_v = \frac{\rho_f}{\frac{M_f}{T_{f,bp}}\frac{273}{22.4}} v_{a,max} \tag{41b}$$

where M_f (kg/kmol) is the molar mass of the liquid fuel, $T_{f,bp}$(K) the boiling point of the liquid fuel, and u_v the initial velocity of the vaporized fuel on the order of 0.75 cm/s $\lesssim u_v \lesssim$1 cm/s [208, 209]. The values of these low-level Froude numbers are in the range $Fr_v \approx 3.2 \times 10^{-3}$ ($d = 1$ m) and $Fr_v \approx 3.2 \times 10^{-4}$ ($d = 100$ m). The reason for the very low Froude numbers Fr_v is the roughly constant u_v if the mass burning rates $\dot{m}''_f$ are approximately constant at large diameters 1 m $\leq d \leq$ 20 m (dependent on fuel type [140]) whereby the source length scale d continues to increase. The velocity is a key feature of large-scale pool fires. This low u_v in combination with buoyancy effects and the low Reynolds number flow leads to several theoretical and experimental difficulties [123]. These difficulties concern the interaction between fuel and oxidizer, the soot production in the fire, and the heat feedback rate $\dot{Q}_{ba}$ to the fuel surface. The knowledge of the structure of such flows is essential, since the vertical entrainment in the near flow field is the dominant entrainment mechanism. For scaling the near-field entrainment data phenomenological models of entrainment based on large-scale vortex dynamics are needed; for this purpose LES codes are important [123]. Furthermore, the pulsation phenomenon in fire plumes is related to the behavior in the near field. A Rayleigh–Taylor instability due to the density stratification in the region where the flow necks above the fuel surface leads to periodic and quasiperiodic [151] oscillations. A strong acceleration of the flow along the plume axis within one d is shown experimentally and by modeling. At a height of around $d/2$, i.e., at the point where the streamwise velocity reaches zero, the formation of the toroidal vortex structure occurs (see Fig. 24), which controls the eddy shedding. There are Strouhal–Froude number correlations [150, 210] but the mechanism involved in the instability is not yet completely understood [40].

Soot Production. Recent research on large pool fires [211, 212] confirms that the increased production of soot in large-scale fires is a key factor which controls the behavior of these fires. Unlike in smaller fires, where relatively clean burning flames occur with soot emergence only at the flame tip, large fires show a great amount of soot production in the lower part of the fire plume [123]. The soot formation leads to the existence of two different sections in a large pool fire:

1. A clear flame zone (a luminous band) just above the fuel surface (fuel source)
2. Obscuration of the fire by dark smoke in the upper parts of the plume

With increasing d the soot yields increase, reaching approximately constant values of soot mass fractions $f_{m,s}$ ($d >$ 2–3 m) $\approx$ 0.15 [213]. For a prediction of reliable smoke concentrations in large pool fires, it is necessary to do more theoretical and experimental investigations on soot processes [123].

Radiative Heat Transfer and Energy-Blockage Phenomena. The radiative heat transfer in large pool fires ($d \gtrsim$1 m) has been studied extensively [110, 123, 132–134, 197]. It is clear that the mass burning rate $\dot{m}''_f$ is dominated by the radiative feedback to the pool surface, dependent on the fuel type and diameter d. This feedback shows significant structural differences between low-sooting (e.g.,

alcohol) flames compared to large hydrocarbon fires. An estimation of $\dot{m}''_f$ for free-burning fires is given in [128]. The phenomenon of radiative energy blockage by a large attenuation of the radiative feedback exists in the fuel-rich region near the pool surface [123].

A similar blockage phenomenon exists to the external radiation with a significant decrease of the SEP and thus a decrease in f_{rad}, whereby the value can fall as low as $f_{rad} \approx 0.03$ at $d > 30$ m [123]. More reliable methods are still required for predicting radiative heat rate loss, including the effects of radiative blockage.

The blockage phenomenon to the outside of the fire occurs in large pool fires with a ratio C/H > 0.3, where a large portion of the external surface of the fire is obscured by an envelope of thick black smoke due to formation of soot parcels. However, this smoke shield is not complete and it opens up randomly, according to the turbulent nature of the flow. As a consequence the fuel is transported in the radial direction where it can be combusted more efficiently, to release pulses of great radiation intensity by formation of hot spots (cf. Section 2.3.7). The intermittency of the hot spots and soot parcels leads to problems with the prediction of the radiation field, although equivalent surface area approaches have been mostly used [101].

2.3.7. Modeling of Pool Fires

Recent Pool Fire Models. Fire models range from very simple relations for specific tasks to extremely complex simulation tools including many submodels to predict different aspects of fire behavior. Which fire model is used in any specific scenario depends on (1) the scenario itself, (2) the required outputs, and (3) the desired accuracy of the prediction.

With current models it is possible, in principle, to include the calculations of

1. Plume characteristics
2. Dispersion of combustion products
3. Heat transfer to adjacent objects

which are often required output for risk analysis [123, 214].

Although computer technology has reached a very high level in recent years, a compromise is generally required between the desired complexity (e.g., model resolution, number, and type of submodels) and the CPU time required for simulations. Modern models are able to simulate pool fires with a certain accuracy, but they still have some limitations. This is due to a lack of detailed knowledge, e.g., on soot formation and hence on thermal radiation, as well as on the chemistry/radiation–turbulence interactions. Some recent pool fire models (cf. [99]) are discussed below.

The ISIS-3D model [215] accounts for the fuel evaporation rate and radiation heat transfer and is able to estimate the total heat transfer from larger fires to objects engulfed in the flame or nearby. It is possible to describe the general characteristics of the object temperatures within a fairly short computer time. Validations are carried out by comparing the model outputs with data from large pool fire experiments.

The fire dynamic simulator [194, 216] uses simplified Navier–Stokes equations [217], also called the low Mach number combustion equations, which describe the low-speed motion of gas driven by buoyancy forces and chemical heat release. For the prediction of large-scale fire und plume behavior that includes plume characteristics, combustion product dispersion, and heat effects to adjacent objects, the large-eddy simulation (LES) is used. The code FDS was developed by NIST, and the model has been validated also against many pool fires [216, 218].

For a practical numerical simulation it is necessary to introduce simplifications in the Navier–Stokes equations. Thus, useful numerical codes were developed, known as computational fluid dynamics (CFD).

For modeling pool fires the CSAFE group in Utah/USA [219] has developed state-of-the-art methods on massive parallel computers. As an archetypal fire a heptane pool fire ($d = 20$ m) was used to demonstrate the integration of multiscale phenomena. A detailed soot mechanism is incorporated in a LES fire simulation by using the intrinsic lower dimensional manifolds (ILDM) method. The sensitivity of the radiant heat transfer to the soot formation mechanism has also been studied. The simulation tool can predict global characteristics of large-scale pool fires, including the puffing frequency and the velocity profiles close to the base of the pool fire.

However, there are several quantities associated with radiative heat transfer and species generation that cannot be predicted. Although LES modeling appears as the most promising technique, it has still many limitations when applied to large pool fires [220]. Hence, work on modeling pool fires continues [221–224].

Another promising model of large pool fires on parallel computers is used by the research group at the Department for Chemical Engineering I, University Duisburg-Essen, Germany. With the corresponding computer code pool, fires of different diameters in the rage 1 m $\leq d \leq$ 25 m and different fuels like *n*-pentane, gasoline, diesel, JP-4, LNG, and organic peroxides (e.g., DTBP, di-*tert*-butyl peroxide) were investigated. Based on LES for turbulence modeling transient simulations are performed that take into account the detailed behavior of the fire plume [133, 134, 197–199, 206, 225]. A promising method is the use of an assumed-PDF approach with laminar flamelets depending on the mixture fraction approach for combustion modeling. With this method the CPU time can be reduced although nonequilibrium chemistry is considered. For soot modeling the Magnussen, Tesner, or Moss–Brokes models are used, while an efficient soot flamelet model is under development. The soot models play an important role to obtain the effective absorption coefficients for solving the radiative transfer equation (RTE). Both a weighted sum of gray-gas model (WSGGM) and a new special step function based on the behavior of dissipative structures in pool fires leads to effective absorption coefficients as a function of temperature of the fluid dynamic structure. The discrete-ordinates model has been shown to be a good way to model the thermal radiation of large pool fires [134, 197]. Many results are presented and discussed on workshops at ICES (Institute for Combustion & Energy Studies) University of Utah, Salt Lake City, USA and SANDIA National Laboratories, Albuquerque, USA [196, 198–203, 206, 207, 226].

In summary, the CFD simulation is a promising method to predict the following transient quantities in large pool fires: flow velocity fields, flame temperature fields, surface emissive power (SEP), radiative loss fraction, irradiance E, critical thermal distances and species concentrations, without and with wind influence. The CFD predicted SEP(x,y,t) on an instantaneous isosurface with temperature T 400 K is shown in Figure 25. A clear, hot flame zone above the fuel surface with a surface

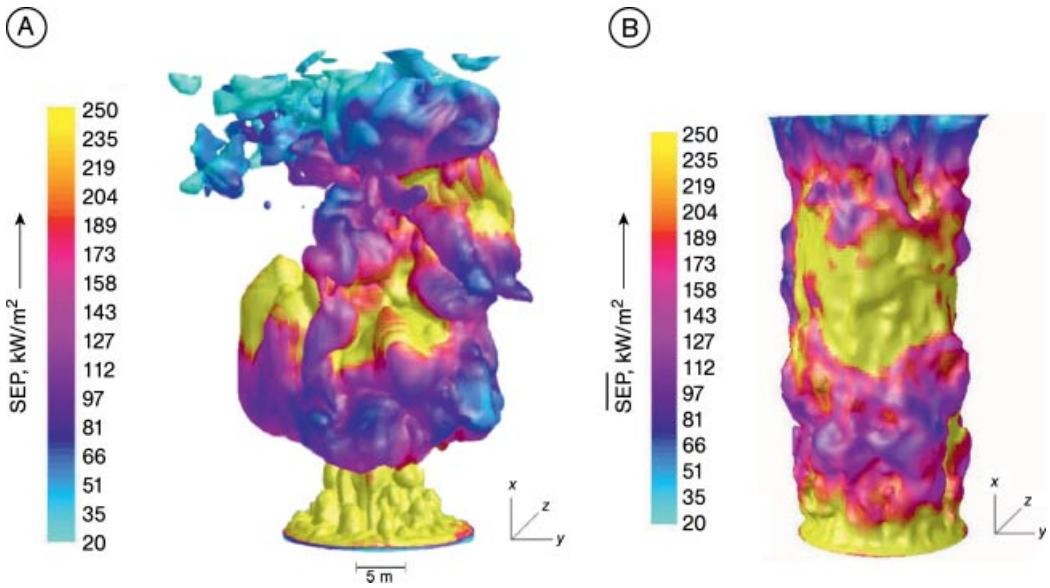

Figure 25. CFD predicted surface emissive power fields on an isosurface with $T = 400$ K of a JP-4 pool fire ($d = 16$ m) A) Instantaneous SEP(x,y,t) field; B) Time-averaged $\overline{\text{SEP}}$(x,y) field

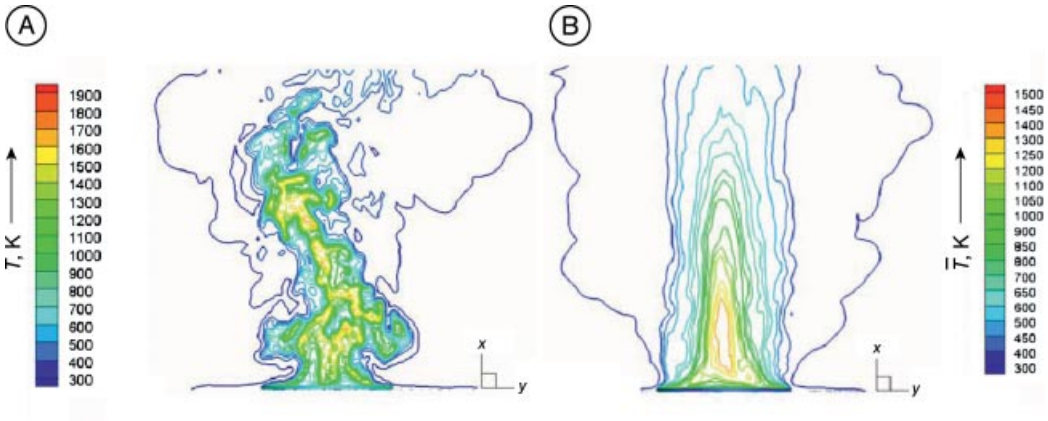

Figure 26. CFD predicted temperature fields in a JP-4 pool fire ($d = 16$ m) in the plane $z = 0$
A) Instantaneous isotherms $T(x,y,0,t) = \text{const.}$; B) Time-averaged isotherms $T(x,y,0) = \text{const.}$

emissive power SEP $= 250$ kW/m^2 can be recognized. Further very strong inhomogeneities of SEP(x,y,t) (Fig. 25A) and $\overline{\text{SEP}}$ (x,y) (Fig. 25B) are observed. From CFD simulation very strong inhomogeneities of the temperature fields $T(x,y,z,t)$ and the temperature fields $\bar{T}(x, y,z)$ are predicted (Fig. 26).

The predictions of the time-averaged $\overline{\text{SEP}}(d,$ JP-4) dependence with OSRAMO II and CFD simulation as well as the measurement points for different fuels as a function of pool diameter d are presented in Figure 27. For kerosene, JP4, and other smoky pool fires in the range 0.1 m $\lesssim d \lesssim$ 100 m a very good agreement

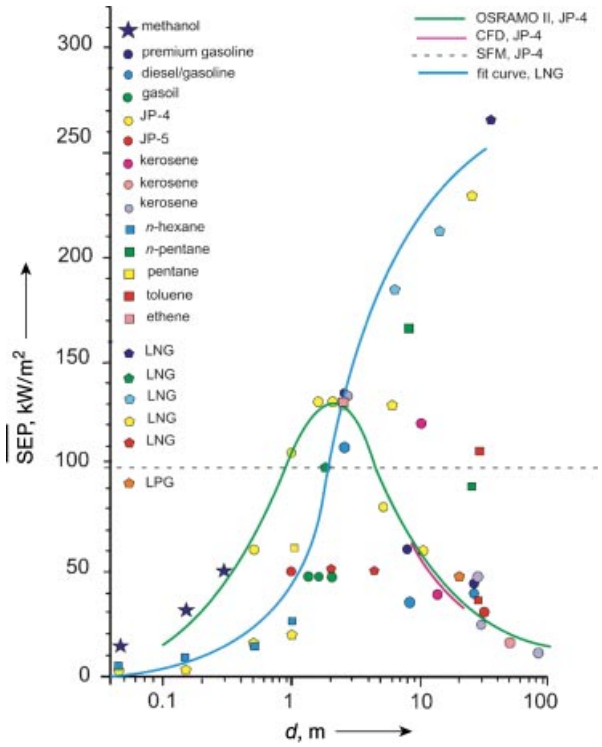

Figure 27. OSRAMO II- and CFD predictions of the time-averaged $\overline{\text{SEP}}(d,$ JP-4); dependence as well as measurement points for different fuel as a function of d

between predictions and measurements exists. Hence, OSRAMO II is validated for these fuels. For other fuels and in particular for LNG there are, at present, partially still larger deviations between prediction and measurements.

An important result is that for most fuels $\overline{\mathrm{SEP}}(\mathrm{d})$ decreases at $d \gtrsim 2$ m with increasing d. However, for LNG the decrease of $\overline{\mathrm{SEP}}(d)$ can probably be expected at $d > 35$ m. Note that the deviations are also caused by the uncertainty of measured $\overline{\mathrm{SEP}}$ values. Values depend on the size of the flame surface A_F, which is very difficult to predict [166].

The Radiation Model OSRAMO II. The model OSRAMO II (Organized Structures RAdiation MOdel) was developed to predict heat transfer to adjacent objects. OSRAMO II, which represents a reasonable compromise between the complex CFD simulation tools with many submodels and the simplified models such as the solid flame radiation models, is summarized in [112]. The validated model OSRAMO II has the advantage of a significantly reduced calculation time compared with CFD models. In the following a short summarized description of the recent large pool fire radiation model OSRAMO II is given [103, 112].

Organized Fluid Dynamic Structures. A detailed analysis of the instantaneous VIS and IR radiance structures of large-scale pool fires has shown that in a real pool fire the following organized (dissipative or coherent) fluid dynamic structures [151, 195] exist:

1. Effective reaction zones (re)
2. Hot spots (hs)
3. Soot parcels (sp)
4. Fuel vapor parcels (fp)

The model OSRAMO II accounts for the existence of these organized structures including the modeling of the effective absorption coefficient $x_{\mathrm{eff},i}$ (i = re, hs, sp, and fp) of the organized structures to describe the smoke blockage effect caused by the formation of carbon particles. The following approximations for these fluid dynamic structures are assumed:

1. The organized structures i are homogeneous flame gas mixtures (i = re, hs, fp) or carbon-particle soot clouds (i = sp) with a characteristic length scale l_i
2. All organized structures are gray bodies which are absorptive, emittive, and transmissive, whilst scattering is neglected
3. Each organized structure has a separate constant, time-averaged temperature $\bar{T}_\mathrm{re} \neq \bar{T}_\mathrm{hs} \neq \bar{T}_\mathrm{sp} \neq \bar{T}_\mathrm{fp}$
4. Each organized structure has a separate constant, time-averaged modified effective absorption coefficient $\bar{\hat{x}}_{\mathrm{eff,re}} \neq \bar{\hat{x}}_{\mathrm{eff,hs}} \neq \bar{\hat{x}}_{\mathrm{eff,sp}} \neq \bar{\hat{x}}_{\mathrm{eff,fp}}$
5. The hot spots and soot parcels appear stochastically distributed on the flame surface with the area fractions $\bar{a}_\mathrm{sp}(d) = 1 - \bar{a}_\mathrm{hs}(d)$ of hot spots and soot parcels

Calculation of Actual Surface Emissive Power. With OSRAMO II the time-averaged, actual surface emissive power $\overline{\mathrm{SEP}}^{\mathrm{II}}_{\mathrm{act}}(d)$ of a pool fire, partly obscured by smoke is given by the following equations [112, 227]:

$$\overline{\mathrm{SEP}}^{\mathrm{II}}_{\mathrm{act}}(d) = \bar{a}_\mathrm{hs}(d)\overline{\mathrm{SEP}}^{\mathrm{ma}}_{\mathrm{hs}}(d) + \bar{a}_\mathrm{sp}(d)\overline{\mathrm{SEP}}_{\mathrm{sp}}(d) \tag{42a}$$

with the surface emissive power $\overline{\mathrm{SEP}}_i(d)$ in $\mathrm{kW/m^2}$ from the organized structures (i = hs, sp):

$$\overline{\mathrm{SEP}}_i(d) = [1-\bar{\bar{\tau}}_i(d)]\sigma(\bar{T}_i^4 - \bar{T}_\mathrm{a}^4) + \bar{\bar{\tau}}_i(d)[1-\bar{\bar{\tau}}_\mathrm{re}(d)]\sigma(\bar{T}_\mathrm{re}^4 - \bar{T}_\mathrm{a}^4) \tag{42b}$$

where $\bar{T}_i$ (K) are temperatures for i = hs, sp; $\bar{T}_\mathrm{a}$ (K) is the ambient temperature; and $\bar{\bar{\tau}}_i$ the modified, effective transmissivities of the organized structures with i = re, hs, sp:

$$1-\bar{\bar{\tau}}_i(d) = \bar{\bar{\varepsilon}}_{\mathrm{eff},i}(d) = 1-\exp(-\bar{\hat{x}}_{\mathrm{eff,i}}\mathrm{d}) \tag{42c}$$

where $\bar{\bar{\varepsilon}}_{\mathrm{eff},i}$ (−) are the modified effective emissivities and $\bar{\hat{x}}_{\mathrm{eff},i}$ ($\mathrm{m^{-1}}$) the modified, effective absorption coefficients of the organized structures with i = re, hs, sp:

$$\bar{\bar{x}}_{\mathrm{eff},i}(T_i) \equiv \bar{x}_{\mathrm{eff},i}(T_i)b_i = 1.81 \times 10^3 \bar{f}_\mathrm{v} b_i \bar{T}_i \approx 1.12 \times 10^{-3} b_i \bar{T}_i \tag{42d}$$

where $\bar{f}_\mathrm{v}$ (isooctane) $\approx 6.2 \times 10^{-7}$ is the soot volume fraction [228] and b_i [−] a ratio, defined in Equation (42e); the characteristic length scales $l_i(d)$ (m) of the organized structures with i = re, hs, sp:

$$l_i(d) = \frac{\bar{\bar{x}}_{\mathrm{eff},i}}{\bar{x}_{\mathrm{eff},i}} d \equiv b_i d \tag{42e}$$

and the area fractions $\bar{a}_i$ (−) of the organized structures with i = hs, sp:

$$\bar{a}_{hs}(d) = 1 - \bar{a}_{sp}(d) = 1 - \exp\left[-\left(\frac{d_0}{d}\right)\right]^{a_1} \quad (42f)$$

where d_0 (m) and a_1 (−) are empirical parameters.

A multiple, nonlinear regression referring to the empirical $\overline{SEP}_{exp}(d)$ curve for the fuel JP-4 leads to the following temperatures $\bar{T}_i$, absorption coefficients $\bar{\hat{x}}_i$ of the organized structures with i = re, hs, sp and parameters d_0, a_1 [229]:

$$\bar{T}_{re} = 1413\,K(1140°C) \quad \bar{\hat{x}}_{eff,re} = 0.380\,m^{-1} \quad d_0 = 3.260\,m$$
$$\bar{T}_{hs} = 1329\,K(1056°C) \quad \bar{\hat{x}}_{eff,hs} = 0.404\,m^{-1} \quad a_1 = 1.104$$
$$\bar{T}_{sp} = 632\,K(359°C) \quad \bar{\hat{x}}_{eff,sp} = 1.035\,m^{-1} \quad (42g)$$

The $\overline{SEP}_{hs}(d)$ and $\overline{SEP}_{sp}(d)$ curves for hot-spots and soot parcels have maxima and reach constant values of $\overline{SEP}_{hs}(d \gtrsim 6\ m) \approx 177$ kW/m^2 and $\overline{SEP}_{sp}(d \gtrsim 1\ m) \approx 9$ kW/m^2. The curves show that the ratio $\overline{SEP}_{hs,max}/\overline{SEP}_{sp,max} = 6$ is valid. The decrease of the $\overline{SEP}^{II}_{act}(d)$ curve for the total flame for $d \gtrsim 2$ m is caused by the area fractions $a_{sp}(d)$ of the soot parcels, which increase strongly with d. The increase of all $\overline{SEP}(d)$ curves up to a maximum is caused by an increase of the emissivities $\bar{\hat{\varepsilon}}_{eff,i}(d)$ according to Equation (42c) and very small values of $\bar{a}_{sp}(d)$ according to Equation (42f). It is important to compare the $\overline{SEP}^{II}_{act}(d)$ curve from the validated OSRAMO II according to Equation (42a) with the $\overline{SEP}(d)$ curves from other models used till now (Fig. 28). All of the other models cannot describe the measurements (see Fig. 27) at $d \lesssim 4$ m and $d \gtrsim 30$ m.

Based on detailed measurements from thermograms [134] the time-averaged $\overline{SEP}$ for a pool fire at a certain diameter d in the radiation model OSRAMO III [103] does not have a constant value, but a probability density function (PDF) $g(\overline{SEP},d)$, as shown in Figure 29. This PDF represents the stochastic behavior of the hot spots (hs) and soot parcels (sp) in smoky single-pool fires (d = 16 m) in the following $\overline{SEP}_{hs}$ and $\overline{SEP}_{sp}$ ranges [103, 112]: 33 kW/m^2 $\lesssim \overline{SEP}_{hs} \lesssim$ 430 kW/m^2 and 6 kW/m^2 $\lesssim \overline{SEP}_{sp} \lesssim$ 50 kW/m^2.

Calculation of Critical Thermal Distances. CFD simulation is also a helpful tool to determine the irradiance $\bar{E}_{CFD}(\Delta y/d)$ by virtual radiometers that are defined at several positions in the computational domain at different relative distances $\Delta y/d$ in horizontal direction from the pool rim [112]:

$$\bar{E}_{CFD}\left(\frac{\Delta y}{d}\right) = \tau_{at}\alpha_{ta}\varphi_{E,F}\left(\frac{\Delta y}{d}\right)\overline{SEP}_{CFD} \quad (43)$$

where α_{ta} (−) is the absorptivity of the receiver element and $\varphi_{E,F}(\Delta y/d)$ the view factor function for a vertical, cylindrical-shaped fire [101, 112]. Relative critical thermal distances $\Delta y_{cr}/d$ from a large pool fire can be determined from Equation (43) by using a limit value E_{cr} = 1.6 kW/m^2 for harmful effects (see Fig. 30) [230]. For JP-4 fires $\Delta y_{cr}/d$ values decrease for organic peroxides like DTBP fires the $\Delta y_{cr}/d$ values increase with increasing d. The relative critical

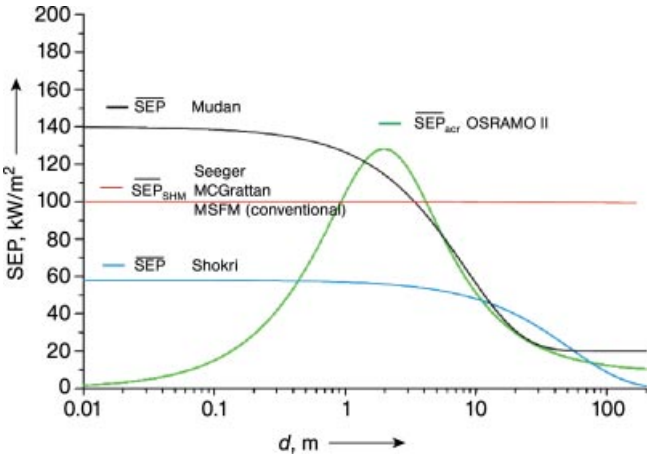

Figure 28. $\overline{SEP}_{act}(d)$ curves predicted with the validated model OSRAMO II in comparison with till now used models [103]

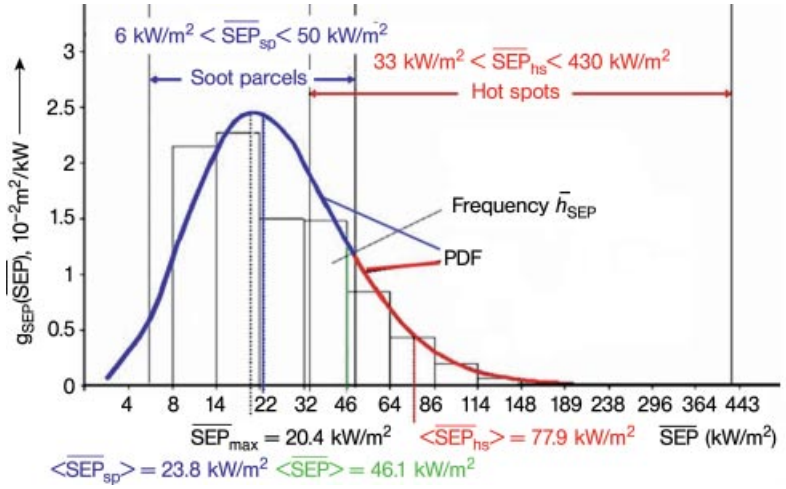

Figure 29. Log-normal PDF $g(\overline{\mathrm{SEP}})$ and experimental histogram $h_{\overline{\mathrm{SEP}}}$ of a JP-4 pool fire ($d = 16$ m) in the radiation model OSRAMO III [103]

thermal distances of DTBP pool fires are larger than those of JP-4 pool fires by a maximum factor of about 2.7.

2.3.8. Conclusions and Outlook

The phenomenology of large-scale pool fires has been qualitatively characterized for several decades. Many of the specific processes have been described extensively. In order to classify pool fires in a quantitative manner, some well-defined parameters have been established. At present, quantitative predictions, especially of temperatures, air entrainment, and species concentrations, can be carried out, but their reliability is still unclear, in particular for more complex scenarios.

Despite enormous work on large-scale pool fires significant uncertainties in predicting the behavior of these fires exist. As clearly formulated in [122], there is "a critical need for more well instrumented experimental studies as well as further development of numerical models".

Many uncertainties exist in the area of spill fires [122]. Attempts at modeling large-scale

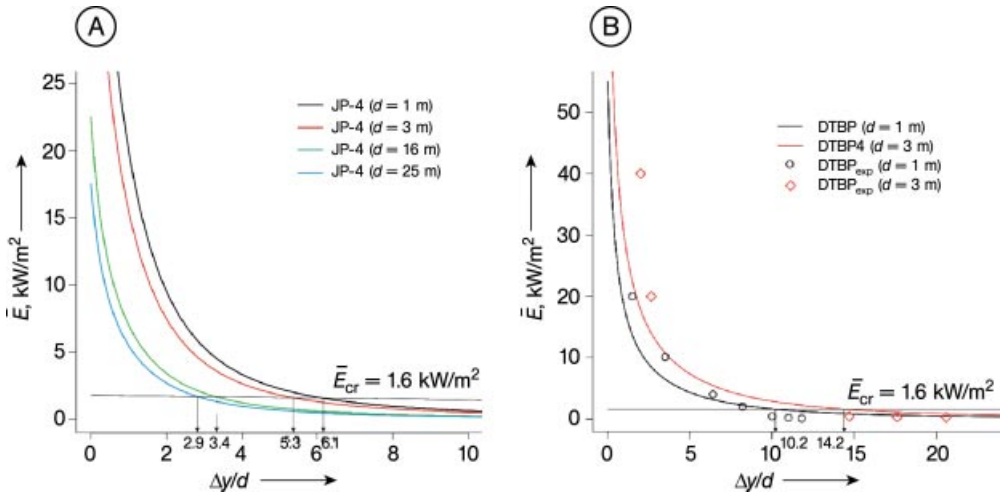

Figure 30. CFD predicted relative critical thermal distances $\Delta y_{cr}/d$ of A) JP-4 pool fires and B) DTBP pool fires

pool fires are very difficult or are hindered because of the following problems

1. Finding a mathematical closed-form solution of the governing equations (conservation of overall mass, species mass, momentum and energy).
2. Finding models describing the physics and chemistry of pool-fire behavior which lead to filtered equations and closure of the governing equations. These equations should include the range of length and time scales which can be resolved numerically.

A simulation science based analysis of large-scale pool fires using a massively parallel computing exists. However, such analyses are very time consuming, and uncertainties remain. With the presented new simplified models the calculation time can be reduced significantly, but the accuracy of the outputs is generally decreased.

It is important to note that large-scale pool fires are turbulent, which leads to the existence of dynamic vortical structures or organized structures. Thermal radiation is the dominant mode of heat transfer in larger pool fires, which is strongly affected by the presence of soot and smoke. Therefore, fire chemistry must include reaction mechanisms for soot formation, growth, and oxidation. To understand or model the behavior of larger pool fires all these coupled aspects must be considered.

A challenging and relevant problem remains the modeling of heat transfer from large-scale pool fires to adjacent objects. The inclusion of radiative and convective heat transfer leads to important unknowns and hence to new uncertainties.

2.4. Flash Fires, Fireballs, and Jet fires

If there is a release of a flammable vapor and sufficient time before ignition for a cloud to be formed, either a flash fire or a fire ball may result (see Fig. 14). This is supported by the experimental evidence presented in [231]. At least six out of ten vapor cloud experiments resulted in a fireball. An explosion is possible as well if one or several of the following conditions are met [232]

- Partial confinement and/or obstruction
- Jet release
- Explosively dispersed cloud
- High-energy ignition

Consequently no explosion is expected if none of these conditions are satisfied. Additionally, Figure 14 shows that another possible outcome is simply dispersion.

2.4.1. Flash Fires

A flash or vapor cloud fire is defined in [232] as "The combustion of a flammable gas or vapor and air mixture in which the flame propagates through that mixture in a manner such that negligible or no damaging overpressure is generated".

There are relatively few models for treating vapor cloud fires. Their objective is to determine the heat radiation levels as a function of distance from the cloud surface. While it may be assumed that anyone inside the burning cloud would suffer fatal injury, the degree of harm to persons outside depends on factors such as the SEP of the cloud and their distance from the cloud center. Hence, the consequence assessment chiefly consists of a dispersion calculation assessing the dimensions of the cloud (cf. Section 2.2).

In [233] three models are mentioned. It is stated there that their application is limited to low momentum sources, that there is little or no validation, and that there are areas of disagreement in calculating flame height and flame speed.

In what follows the semi-empirical procedure of Raj and Emmons is presented on the basis of [232, 234]. The model takes into account the speed of the flame as it moves through the cloud. It is assumed that during combustion there is a turbulent flame front propagating into the unburned cloud at a constant velocity which is roughly proportional to the wind speed, and that at high gas concentrations there is a tall flame plume at the edge of the unburned cloud. Then the flame height is calculated from

$$H = 20d\left[\frac{S^2}{dg}\left(\frac{\rho_0}{\rho_a}\right)\frac{wr^2}{(1-w)^3}\right]^{1/3} \tag{44}$$

where the flame speed S is obtained from

$$S = 2.3 \cdot U_w \tag{45}$$

where U_w is the wind speed in m/s. The ratio of the density of fuel and air is given by

$$\left(\frac{\rho_0}{\rho_a}\right)^2 = \left[\frac{(1-\phi)M_{air}+\phi M_{fuel}}{M_{air}}\right] \tag{46}$$

The stoichiometric air/fuel mass ratio r is calculated from the stoichiometric mixture composition ϕ_{st} and the molecular weights of air M_{air} and fuel M_{fuel}.

Finally, w is obtained from the actual mixture composition ϕ_{st}, the stoichiometric mixture composition ϕ_{st}, and the expansion ratio for stoichiometric combustion α

$$w = \frac{\phi-\phi_{st}}{\alpha(1-\phi_{st})} \quad \text{for} \quad \phi > \phi_{st}$$

$$w = 0 \quad \text{for} \quad \phi \le \phi_{st} \tag{47}$$

The expansion ratio α is typically equal to 8 for hydrocarbons.

To assess the impact on the surroundings a surface emissive power (SEP) must be assumed. According to [232] $E = 173$ kW/m^2 is appropriate in this case.

The duration of the fire is taken to be

$$t_d = \frac{D}{S} \tag{48}$$

where D is the cloud diameter in m and S the flame speed according to Equation (45). The size of the cloud and the part that lies within the limits of flammability may be assessed on the basis of atmospheric dispersion calculations (cf. Section 2.2)

If the flame is assumed to be a flat plane, as is done in [232], the variation of flame width W with time is given by

$$W = 2 \cdot \sqrt{R^2-(R-S \cdot t)^2} \tag{49}$$

During the time t_D W increases from 0 to R and drops back to 0 again.

The foregoing model is still widely used; more recently a CFD gas dispersion and flash fire model, namely, the Kameleon FireEx model, has been developed [235]. The importance of correctly assessing the cloud shape is illustrated by the large impact of the cloud height on the result, as illustrated by Figure 31.

2.4.2. Fireballs

Fireballs are defined as "a burning fuel–air cloud whose energy is emitted primarily in the form of radiant heat. The inner core of the cloud consists almost completely of fuel, whereas the outer layer (where ignition first occurs) consists of a flammable fuel–air mixture. As the buoyancy forces of hot gases increase, the burning cloud tends to rise, expand, and assume a spherical shape." [232]. According to [234] there are several situations in which they may occur, i.e.

- Bursting of a vessel under fire conditions
- Bursting of a vessel without a fire
- Ignition of a release from a pipeline for liquefied gas

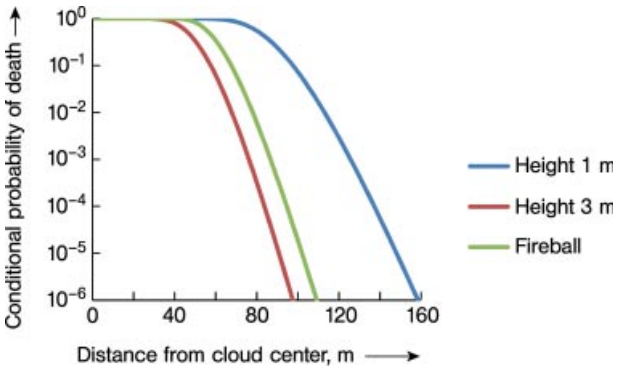

Figure 31. Flash fire from a release of 1500 kg of propane forming a cylindrical cloud with 10 vol% fuel concentration for two different heights and a wind speed of 2 m/s and the same release modeled as a fireball (using probit equation no. 9 from Table 20 in Chap. 3)

- Eruption of hot oil giving rise to a release of burning vapor

Often a fireball accompanies a BLEVE (boiling liquid vapor cloud explosion, see Section 2.5.3) which may result from the rupture of a vessel containing a liquefied gas.

An important parameter for assessing the damage from a fireball is its surface emissive power unless the object to be protected is within the fireball itself and therefore directly exposed. The model presented here is the frequently used solid flame model. According to [233] the results substantially depend on how the SEP is defined and measured. In [234] a low value of 141 kW/m^2 and a maximum value of 450 kW/m^2 are quoted. In [232] a range from 320 to 350 kW/m^2 is indicated; on this basis a SEP of 350 kW/m^2 is recommended there.

The majority of models for treating fireballs is based on correlations for diameter and duration (cf. [232, 234]). More fundamental models are discussed, for example, in [234]; the application of CFD to fireballs is described, e.g., in [236].

The correlation for the fireball diameter reads as follows

$$D = k_1 M^{n_1} \tag{50}$$

where D is the diameter of the cloud in m, k_1 a constant, n_1 an index, and M the mass of fuel in the fireball in kg.

The duration of the fireball t_d (s) is calculated according to

$$t_d = k_2 M^{n_2} \tag{51}$$

Several sets of values for the constants in Equations (50) and (51) are quoted in [234]. Some of them are given in Table 11.

Table 11. Coefficients for Equations (1) and (2) (according to [234])

Model no.	k_1	n_1	k_2	n_2	Substance
1	5.55	0.333	–	–	propane
2	6.36	0.325	2.57	0.167	hydrocarbons
3	5.25	0.314	1.07	0.181	*n*-pentane
4	5.80	0.333	0.45	0.333	hydrocarbons
5	5.88	0.333	1.09	0.167	propane
6	5.72	0.333	0.45	0.333	butane
7	5.33	0.327	0.923	0.303	hydrocarbons
8	6.48	0.325	0.852	0.26	LPG
9	5.50	0.333	0.38	0.333	hydrocarbons

Investigations presented in [237] came to the conclusion that the coefficients proposed in [232] furnish conservative results. These are no. 4 from Table 11 for the diameter D of the fireball and for its duration t_D:

- $M \leq 30000$ kg (coefficients of no. 4 from Table 11)
- $M > 30000$ kg (coefficients of no. 2 from Table 11)

In [238] the limiting value of the above inequalities for M is given as 37 000 kg based on investigations of HSE.

Whether the outcome of a fireball is assessed to be more severe than that of a flash fire depends on the parameter values, as is illustrated by Figure 31.

2.4.3. Jet Fires

Jet fires may arise in cases of releases from apertures either planned (e.g., flare) or unforeseen (e.g., leak or rupture). In [239] a jet fire is defined as a "turbulent diffusion flame resulting from the combustion of a fuel continuously released with some significant momentum in a particular range of directions". Among them the horizontal direction is often the most dangerous, because the flame may impinge on adjacent objects. Depending on the fluid released a jet fire may result from one-phase or two-phase flow. Although CFD was applied to jet fires already a long time ago [240] semi-empirical models are still commonly used [241, 242]. Hence, empirical correlations for characteristic parameters of jet flames are given below following and shortening the presentation in [239].

Flame Length for Vertical Releases. The flame length is the distance from the release point to the defined end of the flame; the latter is usually defined as the envelope of the visible flame, because the dark end with soot radiates comparatively little heat. This is true for some hydrocarbons but does not apply to sonic natural gas flames, which are almost invisible close to the release point. According to API R521 the following correlation may be applied for vertical subsonic flares of gaseous

fuels in still air

$$L = 2.76 \cdot Q^{0.452} \tag{52}$$

where L is the length in m and Q the heat released in combustion in MW. An alternative due to WERTENBACH is

$$L = 18.5 \cdot \dot{m}^{0.41} \tag{53}$$

where $\dot{m}$ is the mass flow rate in kg/s.

MCCAFFREY derived the following correlation for vertical flame lengths based on subsonic and sonic vertical releases of natural gas from 30–102 mm orifices and a heat release up to 470 MW

$$L = B + 200 \cdot D_e \tag{54}$$

where B is the flame liftoff distance (between the origin and the visible flame) in m and D_e is the effective hole diameter in m (the actual hole diameter for subsonic releases; for sonic releases the diameter to which the jet has expanded when reaching atmospheric pressure).

The best founded correlation for vertical releases in still air is due to BECKER et al., which after incorporating ideas by HAWTHORNE et al. is given below with KAGHATGI's extension

$$\left(\frac{2.85 \cdot D_e}{L_0}\right)^{2/3} = 0.2 + 0.024 \left(\frac{g}{D_e^2 u_e^2}\right)^{1/3} L_0 \tag{55}$$

where L_0 is the flame length in still air in m, W is the mass fraction of fuel in a stoichiometric mixture with air, g the acceleration due to gravity, and u_e the expanded jet velocity in m/s.

The implicit Equation (12) forms the basis of the conical frustum jet flame shape derived by CHAMBERLAIN [234].

Effect of Cross-wind for Vertical Releases. In a cross-wind situation the flame length shortens considerably due to enhanced entrainment and mixing. This effect may be represented by

$$L = L_0 [0.51 \exp(0.4 \cdot v) + 0.49] \tag{56}$$

where L is the wind-affected flame length in m and v the wind speed in m/s (L_0 as above).

Flame Liftoff. MCCAFFREY and EVANS using data from sonic and subsonic 20–470 MW methane flames determined that

$$\frac{B}{u_e} = 2.5 - 5 \text{ ms} \tag{57}$$

where B is the lift-off distance in m and u_e as above.

Flame Shapes for Nonvertical Releases. There is little data from large-scale jet flames for which the release direction forms an angle with the vertical axis. COOK et al. derived a center-line trajectory model for inclined natural gas flares based on data from 3.5–25 kg/s releases at an angle of 45° to the vertical, pointing into the wind, cross-wind, or downwind. The curvilinear flame length is given by

$$L = 1.555 \cdot Q^{0.467} \tag{58}$$

where L and Q are as above.

Surface Emissive Power. There is considerable confusion about SEPs for jet fires; "spot" and "average" values must be distinguished.

The assessment of the effects of jet fires depends largely on the type of model used, e.g., semi-empirical, integral, or field (CFD) model. The use of the SEP concept is debatable. If in a model an average SEP is required for a surface emitter flame shape it can be derived from correlations for the F factor (cf. [239]). Hence, the concept presented here should be used with caution and merely for screening.

In an account on experimental work a maximum SEP of 250 kW/m^2 is quoted in [234]; however, the variation along the flame is emphasized there. In [241] a range from 200 kW/m^2 to 400 kW/m^2 is indicated. HSE [243] gives an acceptable value for calculations of 200 kW/m^2. In [244] a value of 170.67 kW/m^2 is given for a methane jet flame.

2.4.4. Thermal Radiation Impacts at a Distance from the Source

To assess the effects of heat radiation on a target using the procedures of Section 2.7, the heat flux density must be calculated as a function of distance from the flame surface. In doing this two effects must be accounted for:

1. The reduction of the heat flux density owing to the geometries of the emitting and receiving bodies. This is described by the view factor $f_{ab}(x)$, which represents the ratio of the received to the emitted power.
2. The atmospheric transmissivity for radiation, which depends on distance and on the

humidity of the atmosphere; it is described by the transmissivity factor $\tau(x)$.

Hence, we obtain the heat flux density at distance x from the source

$$q''(x) = \mathrm{SEP}\cdot f_{\mathrm{ab}}(x)\cdot\tau(x) \tag{59}$$

While the view factor depends on the geometry and hence is flame-specific, the transmissivity applies for all cases; according to [232] it may be represented by

$$\tau(x) = 0.4343\cdot\ln[1.41\cdot\varphi^{-0.108}\cdot(\mathrm{x}-\mathrm{r})^{-0.13}] \tag{60}$$

where φ is the relative humidity of the atmosphere in %, and x the distance between the center line of the flame, which has radius r, and the receiver (both in m). The equation applies to relative humidities $\geq$20%. Higher humidities increase the absorption. HSE [243] accepts humidities $\leq$ 60% for fireballs and jet fires.

View Factor for Pool Fires. Pool fires are normally represented by the geometry of a tilted cylinder [244, 245]. With cylinder (flame) length L and radius r, both in m, and the tilt angle θ between the vertical line and the center line of the flame we have the following view factor for the flux incident on a plane at a distance of x m from the center of the pool (cf. [245])

$$\begin{aligned}\pi F_{\mathrm{v}} = {} & \left(\frac{a\cos\theta}{b-a\sin\theta}\right)\left[\frac{a^2+(b+1)^2-2b(1+a\sin\theta)}{\sqrt{AB}}\right] \\ & \left[\tan^{-1}\left(\sqrt{\frac{A}{B}}\sqrt{\frac{b-1}{b+1}}\right)\right]+\left(\frac{\cos\theta}{\sqrt{C}}\right)\left[\tan^{-1}\left\{\frac{ab-(b^2-1)\sin\theta}{\sqrt{b^2-1}\sqrt{C}}\right\}\right. \\ & \left.+\tan^{-1}\left\{\frac{(b^2-1)\sin\theta}{\sqrt{b^2-1}\sqrt{C}}\right\}\right]-\left(\frac{a\cos\theta}{b-a\sin\theta}\right)\left[\tan^{-1}\left(\sqrt{\frac{b-1}{b+1}}\right)\right] \\ \pi F_{\mathrm{h}} = {} & \tan^{-1}\left(\sqrt{\frac{b-1}{b+1}}\right)-\left[\frac{a^2+(b+1)^2-2(b+1+ab\sin\theta)}{\sqrt{AB}}\right] \\ & \left[\tan^{-1}\left(\sqrt{\frac{A}{B}}\sqrt{\frac{b-1}{b+1}}\right)\right]+\left(\frac{\sin\theta}{\sqrt{C}}\right)\left[\tan^{-1}\left\{\frac{ab-(b^2-1)\sin\theta}{\sqrt{b^2-1}\sqrt{C}}\right\}\right. \\ & \left.+\tan^{-1}\left\{\frac{\sqrt{b^2-1}\sin\theta}{\sqrt{C}}\right\}\right]\end{aligned} \tag{61}$$

where $a = \frac{L}{r}$, $b = \frac{x}{r}$, $A = a^2+(b+1)^2-2a(b+1)\sin\theta$, $B = a^2+(b-1)^2-2a(b-1)\sin\theta$, and

$$C = 1+(b^2-1)(\cos\theta)^2$$

F_{h} is the view factor for a horizontally placed object, and F_{v} that for vertical placement. Usually the squared average of both is used

$$f_{\mathrm{ab}} = \sqrt{F_{\mathrm{v}}^2+F_{\mathrm{h}}^2} \tag{62}$$

View Factor for Flash Fires. In the model described above the vapor cloud is considered to be a cylinder; the fire is modeled as a plane fire front moving with velocity S towards the target. That implies that the distance between the fire and the target is a function of time

$$x = l+\frac{D}{2}-S\cdot t \tag{63}$$

where l is the distance between the cloud center on the ground and the target, and D the cloud diameter, both in m.

For calculating the view factor we need h, the height of the cloud, which ideally stems from calculations of atmospheric dispersion and the flame width. The latter is divided by two, i.e., $b = W/2$, to determine contributions from either side of the normal on the flame surface [232]. This gives the view factors

$$F_{\mathrm{h}} = \frac{1}{2\pi}\left[\tan^{-1}\frac{1}{x_{\mathrm{r}}}-A\cdot x_{\mathrm{r}}\cdot\tan^{-1}A\right] \tag{64}$$

$$F_{\mathrm{v}} = \frac{1}{2\pi}\left[A\cdot h_{\mathrm{r}}\cdot\tan^{-1}A+\left(\frac{B}{h_{\mathrm{r}}}\right)\cdot\tan^{-1}B\right] \tag{65}$$

where

$$h_{\mathrm{r}} = \frac{h}{b}$$

$$x_{\mathrm{r}} = \frac{x}{b}$$

Hence we obtain

$$f_{\mathrm{hv}} = \sqrt{F_{\mathrm{v}}^2+F_{\mathrm{h}}^2} \tag{66}$$

To account for the contribution from both sides of the flame (see above)

$$f_{\mathrm{ab}} = 2f_{\mathrm{hv}} \tag{67}$$

is finally used.

View Factor for Fireballs. Fireballs are modeled as spheres radiating on a plane receiver; if we assume that the ball has not yet risen above the ground the following view factors are obtained

$$F_{\mathrm{h}} = \frac{(D/2)}{[x^2+(D/2)^2]^{3/2}} \tag{68}$$

$$F_v = \frac{x(D/2)^2}{[x^2+(D/2)^2]^{3/2}} \quad (69)$$

$$f_{ab} = \sqrt{F_v^2+F_h^2} \quad (70)$$

View Factor for Jet Fires. There is virtually no indication of view factors for jet fires. In the context of the presentation of the Craven model in [234], where the flame is modeled as a vertical cone, the following approximate view factor for a target at right angle with the flame axis is given

$$f_{ab} = \frac{rL}{\pi x^2} \quad (71)$$

where $\approx 10D_{max}$ (D_{max} is the maximum cone diameter in m) and x the horizontal distance between the axis of the flame and the target in m.

2.5. Explosions

Explosions are important mechanisms of damage to humans, the environment, or property which may arise from the operation of process plants. An explosion results from a rapid release of energy, which causes a blast wave. The pressure measured at right angles to the blast wave is known as side-on overpressure (sometimes called free-field overpressure). If the pressure transducer is placed in the middle of wall facing the blast front, the reflected overpressure is obtained. The dynamic pressure is defined as $\rho u^2/2$ where ρ is gas density and u gas velocity. A time plot of the pressure wave from an explosion of a vapor cloud is shown in Figure 32 [246]. A positive-overpressure phase is followed by a negative one, whose damaging potential should also be considered.

The following cases of explosions may be distinguished

- Release of stored compression energy (e.g., compressed gas)
- Release of a liquefied gas (e.g., flash release)
- Release of stored chemical energy (e.g., explosives, flammable gases, decomposition)
- Energy release due to a fast surface reaction (e.g., dust explosion, steam explosion, aerosols)
- Thermal explosion (e.g., runaway reaction)
- Condensed-phase explosions (e.g., an explosive)

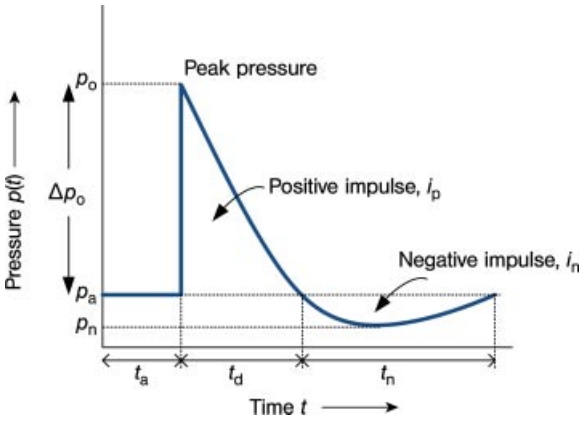

Figure 32. Time plot of the explosion side-on overpressure of a vapor cloud explosion

The cause may be physical, chemical, or both. Properties of materials and conditions which may give rise to explosions are treated in → Plant and Process Safety, 2. Hazardous Materials and Process Conditions; runaway reactions are dealt with as well.

Explosions may be confined or unconfined, with intermediate situations being possible. Confined explosions give rise to higher pressure increases than unconfined ones.

Consequences of explosions may be

- Generation of missiles (Section 2.6)
- Blast effects
- Thermal radiation
- Formation of craters
- Terrestrial shock waves

The treatment given below mainly deals with unconfined explosions. For treating explosions several models are available [247, 248]:

- *Empirical models* are also referred to as quasi-theoretical and are based on limited experimental data; they can be considered as the most simplified methods for treating blast effects from vapor cloud explosions. Well-known models belonging to this category are the TNT model [234], the TNO multi-energy model [244] and the Baker–Strehlow Model [250].
- *Phenomenological models* are simplified physical models which only represent essential aspects of the physics of explosion. This

category includes SCOPE (Shell Code for Over-pressure Prediction in gas Explosions) [251] and CLICHÉ (confined linked chamber explosion) [252, 253].
- *CFD models* solve the partial differential equations governing the explosion process. Probably, the best known model of this category is FLACS (flame acceleration simulator) [254].

According to [247] empirical models are suited for screening, phenomenological methods represent a good substitute for CFD, and CFD allows a detailed representation of real scenarios.

However, insufficient knowledge of phenomena, uncertainties, and limitations of any of the methods became evident in the investigations carried out in the aftermath of the Buncefield accident. In [255] the following phenomena were investigated in order to explain the unexpectedly high pressure peaks ($>$ 200 kPa) encountered

- Mist explosion
- Multiple detonation
- Strong ignition
- Multiple ignitions
- Stratified explosion
- Flame acceleration due to dust particles
- Unsteady deflagration accelerated by forward radiation from the flame front
- Unsteady deflagration without radiative effects
- Cellular flames
- Chemistry effects
- Pancake-shaped cloud
- Inhomogeneous fuel concentration
- Internal tank explosion
- Localized high overpressure
- Precursor event

The investigations are still continuing.

In what follows two of the empirical models are presented, the TNT model and the Baker–Strehlow–Tang (BST) model.

2.5.1. TNT Equivalency Method

To compare the consequences of energy releases, for example following depressurization of a gas stored under pressure or the explosion of an explosible substance, they must be referred to a common denominator. Knowledge about the effects of explosives serves as a basis in this case. Many of the correlations used are related to the blast effects of TNT (trinitrotoluene).

The important difference between the explosion of an explosive and that of a flammable gas is brisance. That is reflected by a very short pressure wave in the case of TNT as compared with that produced by explosions of flammable gases. Despite this difference and other limitations, discussed in detail, e.g., in [248], the TNT model is still the most widely used procedure for assessing explosion effects. Its basic idea is to convert the explosion energy to be treated into the corresponding quantity of TNT (TNT equivalent). For this equivalent values between 4190 and 4650 kJ/kg are indicated in [244]; in [234] a value of 4681 kJ/kg is proposed.

An important parameter for characterizing the explosion effect is the peak side-on overpressure. This may be determined according to the following relationship, which stems from [255] and was renormalized to agree with the Marshall curve [244]

$$p_s = 159.5077 \cdot \frac{808\left[1+\left(\frac{r'}{4.5}\right)\right]}{\sqrt{\left[1+\left(\frac{r'}{0.048}\right)\right]\left[1+\left(\frac{r'}{0.32}\right)\right]\left[1+\left(\frac{r'}{1.35}\right)\right]}} \tag{72}$$

where p_s is the side-on overpressure in kPa from an explosion at atmospheric pressure, r' the scaled distance, which is calculated according to $r' = r/W_{TNT}^{1/3}$; W_{TNT} is obtained by dividing the energy released in an explosion by the TNT equivalent, e.g., 4650 kJ/kg. Figure 33 shows a representation of Equation (72).

2.5.2. Vapor Cloud Explosions (VCE)

TNT Equivalency Method. The calculation of the equivalent mass of TNT for vapor cloud explosions is realized according to

$$W_{TNT} = \alpha \cdot \frac{W \Delta H_c}{E_{TNT}} \tag{73}$$

In Equation (73) W is the mass of reacting fuel in kg, ΔH_c its enthalpy of reaction in kJ/kg, and E_{TNT} the energy released in the explosion of 1 kg of TNT; α is the efficiency, which in the case of high explosives is taken to be equal

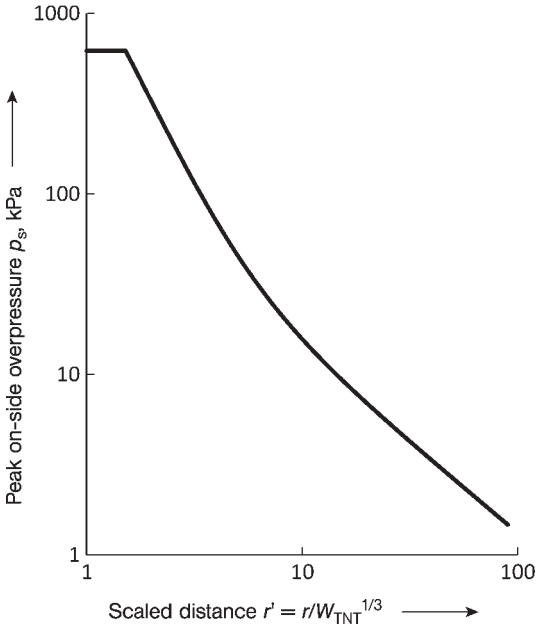

Figure 33. Peak on-side overpressure p_s as a function of scaled distance (so-called Marshall curve) in kPa for an initial (atmospheric) pressure of 10^5 kPa (Note: since the curve is not defined for pressures above 620 kPa, the pressure was fixed to 620 kPa in the corresponding range because it makes no difference concerning the probability of death (see Chap. 3), which is practically equal to 1 for 620 kPa and above)

to 1 [256]. Its value for vapor cloud explosions is discussed below.

There are quite a number of largely different values for the factor α, which reflects the efficiency of the explosion. Table 12 gives an overview. The differences highlight the fact that the quantity strongly depends on the boundary conditions.

According to [232] the energy $E = W \cdot \Delta H_c$ should be multiplied by the following factors in order to account for specific situations

- Explosion close to the ground: 2
- Spherical vessel slightly above ground for $r' > 1$: 1.1
- Cylindrical vessel slightly above ground: 1.6 if $1.6 < r' < 3.5$ and 1.4, if $r' > 3.5$

Baker–Strehlow–Tang Method. The Baker–Strehlow method [249] was developed to provide estimates of blast pressures from vapor cloud explosions. The model experienced various extensions [257, 258] and is now called the Baker–Strehlow–Tang (BST) method. It comprises a number of steps assessing flame speed, fuel reactivity, confinement, etc. [248]

- Walk through plant identifying potential explosion sites
- Decide on the dimensionality of the confined areas to work out flame speed
- Calculate burning velocity for fuel mixtures

The blast pressure and impulse are read from a series of graphs based on experimental experience.

The drawbacks of the TNT method, reflected by the spread of the yield factor (see Table 12), can be explained only in part by uncertainties concerning the amount of fuel released. A significant proportion of it is attributed to differences in the combustion mode of the vapor

Table 12. Efficiency α of vapor cloud explosions (based on [234, 244])

Authors	Efficiency
Brasie und Simpson (1968), Brasie (1976)	0.02 near-field and 0.05 far-field together with a method for assessing the released mass of fuel
Eichler und Napadensky (1977)	0.2 for 6.9 kPa overpressure
Health and Safety Executive (1979 and 1986)	0.03 for a gas with low reactivity (methane), 0.06 in case of medium reactivity (propylene oxide), 0.1 for high reactivity (ethylene oxide) together with a method for assessing the released mass of fuel
Exxon (CCPS 1994)	0.03 for open terrain and 0.1 for partial confinement together with a method for assessing the released mass of fuel
Industrial Risk Insurers (1990)	0.02
Factory Mutual Research (1990)	0.05 (low reactivity), 0.1 (medium reactivity), 0.15 (high reactivity)
CPR-14 E (1988)	0.1
British Gas (Harris and Wickens, 1989)	0.2 (for nondetonating clouds of natural gas, mostly methane)
Direction des Études et Recherches, France, (van den Berg and Lannoy, 1993)	0.0002–0.159 with a mean value of 0.03

cloud. A wide spectrum of flame speeds may result from flame accelerations under various confinement and congestion conditions in industrial environments. These are represented by a family of curves corresponding to various cloud combustion modes instead of a single one as for the TNT method. This family of curves provides positive pressure, negative pressure, and impulse as a function of distance [259] (Fig. 32).The main features of the procedure are presented here following [259, 260].

Based on a review of the literature the objective is to determine the flame speed of the explosion via the Mach number $M_{w,}$ which then serves for selecting the appropriate curve.

In order to obtain the peak side-on overpressure p_s, and impulse I, the following relations are used

$$r' = r\left(\frac{p_a}{E}\right)^{1/3} \tag{74}$$

$$\bar{p}_s = \frac{p_s}{p_a} \tag{75}$$

$$\bar{I}_s = I \cdot \frac{a_0}{E^{1/3} p_a^{2/3}} \tag{76}$$

where r' is the scaled distance, r the distance between the center of ignition and the target in m, E the total combustion energy of the fuel–air mixture under stoichiometric conditions in J, $\bar{p}_s$ the scaled overpressure, I the positive blast impulse in Pa·s, $\bar{I}_s$ the scaled impulse, and a_0 the speed of sound under ambient conditions in m/s; p_a is the initial pressure (mostly atmospheric, but other pressures are possible).

Flame speed is represented by the Mach number; here two representations are distinguished

- M_f: Flame speed measured in experiments relative to a fixed observer (Eulerian coordinate system)
- M_w: Flame speed in a moving system (Lagrangian coordinate system)

For low flame velocities the two are related as follows

$$M_f = \left(\frac{\rho_u}{\rho_b}\right)^{1/3} M_w \tag{77}$$

Table 13. Choice of the Mach number M_w

2-dimensional flame expansion (cylindrical flame)			
Fuel reactivity	Obstacle density		
	High	Medium	Low
High	DDT*	DDT	0.59
Medium	1.66	0.66	0.47
Low	0.66	0.47	0.079
2.5-dimensional flame expansion			
Fuel reactivity	Obstacle density		
	High	Medium	Low
High	DDT	DDT	0.47
Medium	1.0	0.55	0.29
Low	0.5	0.35	0.053
3-dimensional flame expansion (spherical or hemispherical flame)			
Fuel reactivity	Obstacle density		
	High	Medium	Low
High	DDT	DDT	0.36
Medium	0.50	0.44	0.11
Low	0.34	0.23	0.26

*DDT: deflagration–detonation transition.

This relation is invalid when M_f approaches unity. For supersonic flames

$$M_w = M_f \tag{78}$$

applies. For near-sonic flames

$$\frac{p_{max} - p_a}{p_a} = 2.4 \cdot \frac{M_f^2}{1 + M_f} \tag{79}$$

is used.

In Tables 13 to 15 the relevant quantities for the use of the above equations are given.

The foregoing tables enable one to determine the scaled distance (curve abscissa) and the Mach number corresponding to the problem under investigation. The scaled overpressure (both positive and negative) and impulse may then be read from the corresponding family of curves (on the ordinate of the diagrams) [259],

Table 14. Reactivity classification for flammable substances (after [232])

Fuel	Reactivity
Hydrogen, acetylene, ethylene oxide	high
Ethane, ethylene, propane, propylene, butane, isobutane	medium
Ammonia, methane, natural gas	low

Table 15. Mach numbers and p_{max} for Equation (79)

M_w	M_f	p_{max}	M_w	M_f	p_{max}
0.037	0.07	0.010	0.50	0.70	0.68
0.074	0.12	0.028	0.75	1.00	1.24
0.125	0.19	0.070	1.00	1.40	2.00
0.250	0.35	0.218			

where the Mach number is used to identify that curve from the family of curves which proceeds for the case at hand.

A comparison between the TNO multi-energy model and Baker–Strehlow–Tang method can be found in [261].

Figures 34 and 35 show some results of the application of the foregoing methods. Figure 34 focuses on a comparison; Figure 35 shows the impact of an explosion and a fireball. Since either would occur with a certain probability, the combination based on evaluating the probability of each from the event tree of Figure 14 is included as well.

2.5.3. Boiling-Liquid Expanding-Vapor Explosion (BLEVE)

In [232] a BLEVE (boiling-liquid expanding-vapor explosion) is described as "the explosively rapid vaporization and corresponding release of energy of a liquid, flammable or otherwise, upon its sudden release from containment under greater-than-atmospheric pressure at a temperature above its atmospheric boiling point. A BLEVE is often accompanied by a fireball if the suddenly depressurized liquid is flammable and its release results from vessel failure caused by an external fire. The energy released during flashing vaporization may contribute to a shock wave." Apart from pressure vessel failures due to an exposure to fire spontaneous (catastrophic) failures are also to be considered.

Hence, we are dealing with a physical and possibly, in addition, a chemical explosion. The treatment of the physical explosion is given below; the chemical explosion, if it proceeds, leads to a fireball. If 36% or more of the liquid is evaporated (see below) all released fuel is assumed to contribute to the BLEVE and eventually to the fireball. For hazard prediction purposes the amount of gas contained in a BLEVE can be assumed to be three times the amount of flash evaporation up to 100% of the available fuel [232].

It is generally claimed that for a BLEVE to occur a sudden pressure drop must take the liquid to the superheat limit spinodal [232, 234]. However, recent investigations cast some doubt on this [259].

The procedure outlined in [232, 244] is adopted here for the treatment of the expansion process. It is based on thermodynamically assessing the difference in internal energies between the original and expanded states. Additionally, the question is considered of whether, given the initial pressure, temperature, and type of substance, flashing of the liquid phase makes a contribution to explosion energy or not. An analogous procedure should be adopted if a gas does not behave as ideal, for example, due to very high pressures.

The energy content is determined by the internal energy $u(T,v)$ in kJ/kg. The

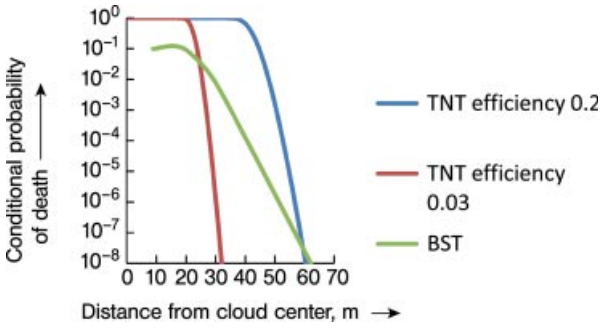

Figure 34. Conditional probability of death following the explosion of 1500 kg of propane calculated with the TNT and BST models ($M_f = 1$, 2-dimensional flame, obstacles: slightly above medium)

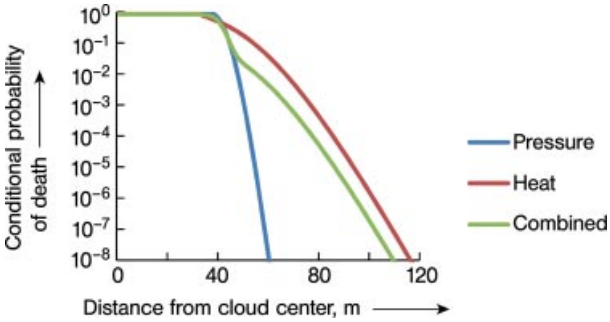

Figure 35. Conditional probability of death following the explosion (TNT model; efficiency 0.2) or fireball from 1500 kg of propane as well as the combination of both with probabilities calculated on the basis of Figure 14 with $P_1 = 0.7, P_3 = 0.6$, i.e., 0.7 for fireball and 0.12 for explosion

corresponding values must be read from tables. These mostly contain enthalpies $h(T,v)$ in kJ/kg, so that the following relationship must be applied

$$u(T,v) = h(T,v) - pv \tag{80}$$

where T is the absolute temperature, v the specific volume, and p the pressure. For a mixture of substances the thermodynamic properties are generally not known. The sum of the internal energies of the individual substances may then serve as a coarse approximation [244].

A gas and a liquid phase are always present inside the vessel. The energy converted during the expansion process is usually calculated by assuming an isentropic (adiabatically reversible) expansion. Of course, the real process is irreversible. However, the assumption of the process being adiabatic is almost true because we are dealing with fast processes which do not take sufficiently long for a substantial energy exchange with the surroundings. For example, a catastrophic vessel failure takes just a few hundred milliseconds.

The assumption of an isentropic change of state connects the gas content before expansion (1) with that afterwards (2), namely:

$$s_{1,g} = x_g s_{2,g} + (1-x_g) s_{2,l} \quad \text{so that} \quad x_g = \frac{s_{1,g} - s_{2,l}}{s_{2,g} - s_{2,l}} \tag{81}$$

where s denotes the specific entropy in kJ/kg and x the vapor ratio subscript "g" denotes gas phase and subscripts "l" liquid phase. The vaporization of the liquid phase during expansion is described by

$$s_{1,l} = x_l s_{2,l} + (1-x_l) s_{2,l} \quad \text{so that} \quad x_l = \frac{s_{1,l} - s_{2,l}}{s_{2,g} - s_{2,l}} \tag{82}$$

The energy E in kJ liberated during expansion is obtained as follows:

$$E = u_{1,g}\phi + u_{1,l}\varphi - [u_{2,g}x_g + (1-x_g)u_{2,l}]\phi - [u_{2,g}x_l + (1-x_l)u_{2,l}]\varphi \tag{83}$$

where ϕ is the mass of gas in the vessel and φ that of liquid before expansion in kg, i.e.

$$\phi = \frac{V}{v_{1,g}}\theta \quad \text{and} \quad \varphi = \frac{V}{v_{1,l}}(1-\theta) \tag{84}$$

where V is the vessel volume in m^3; the maximum volumetric fraction of vapor in vessels θ is usually not less than 0.1.

The foregoing considerations give the basis for assessing the physical effects of a BLEVE, that is, shock wave and missile flight (see Section 2.6).

The experimental and theoretical work of [262] suggests that the shock wave observed in a BLEVE is driven by vapor energy, whilst the process of rapid liquid flashing following tank failure is too slow to produce a shock wave.

According to [263] the overpressure as a function of distance in the far field (scaled distance > 2) can be calculated by the TNT equivalence method (Section 2.5.1). To the near field the following relationship should be applied (cf. [232])

$$\frac{p_1}{p_a} = \frac{p_{so}}{p_a}\left[1 - \frac{(\kappa_1 - 1)\frac{a_0}{a_1}\left(\frac{p_{so}}{p_a} - 1\right)}{\sqrt{2\kappa_0}[2\kappa_0 + (\kappa_0 + 1)]\left(\frac{p_{so}}{p_a} - 1\right)}\right]^{-2\kappa_1/\kappa_1 - 1} \tag{85}$$

where p_1 is the pressure inside the vessel in kPa, p_a the ambient pressure (101.3 kPa), p_{so} the absolute peak side-on pressure, a_1 the speed of sound in the vapor inside the vessel in m/s, a_0 the

Table 16. Ratio of specific heats (from [263])

Substance	Acrolein	Acrylonitrile	Ammonia	*n*-Butane	CO	Chlorine	Ethene	Benzene	Hydrogen	Dry air
$\kappa = c_p/c_v$	1.151	1.152	1.301	1.095	1.4	1.331	1.238	1.075	1.405	1.4

speed of sound in ambient air (340 m/s), κ_1 the ratio of specific heats of the vapor of the vessel contents (cf. Table 16), and κ_0 that of ambient air ($\kappa_0 = 1.4$). The above equation is implicit and must be solved iteratively.

The recommendation in [262] is to assess the shock wave for vapor and liquid energies separately (Eqs. 82 and 83), respectively] and combine them, this procedure being conservative. The experimental work of [262] suggests that the vapor energy alone is responsible for the shock wave. However, the possibility that at larger scales liquid flashing contributes to the shock wave is not discarded there. Figure 36 shows a comparison of both approaches.

Table 17 gives the near-field range according to Equation (74) with $r' = 2$, where according to Equation (85) a peak on-side overpressure of 1.64 bar results; using probit equation no. 4 from Appendix A (Table A1) a conditional probability of death of 0.8 is found to correspond to this overpressure.

Figure 37 shows the impacts of the physical (BLEVE) and the chemical (fireball) explosions as well as the combined effect of both. It is evident that harm is mainly due to the chemical explosion, a circumstance which makes the impact from the fireball and the combined impact practically coincide.

Table 17. Near-field ranges for the problem illustrated in Figure 36

Case	Near-field range, m
10% gas energy from liquid and gas	15.24
10% gas energy from gas only	3.60
40% gas energy from liquid and gas	15.41
40% gas energy from gas only	6.50

2.5.4. Dust Explosions

"The hazard of a dust explosion or a fire exists wherever flammable materials are handled. Generally, a dust explosion occurs only if the dust is dispersed in air, but transition from a fire to an explosion can occur, or vice versa" [234]. The conditions for a dust explosion are explained in → Plant and Process Safety, 2. Hazardous Materials and Process Conditions, Section 4.3.

According to [234] the following scenario is often encountered in industry: a primary explosion occurs in an item of a plant. Due to insufficient explosion protection or destruction by the primary explosion a flame arises. The air disturbance disperses the dust in the work room and causes a secondary explosion often involving a larger quantity of dust and hence more energy release than the primary explosion. The

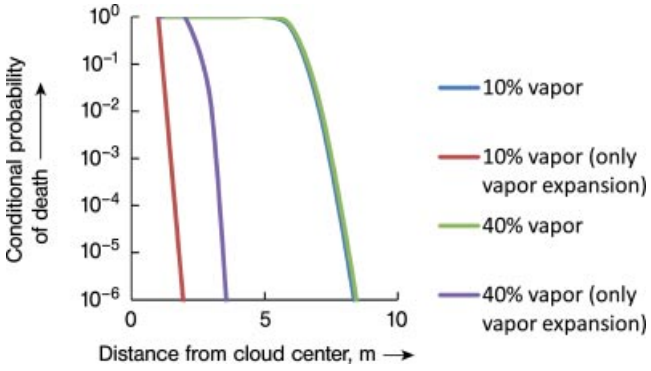

Figure 36. Conditional probabilities of death following the blast wave from a BLEVE of 1500 kg of saturated propane with different volume fractions of gas (energy from liquid and vapor as well as from vapor alone; TNT model)

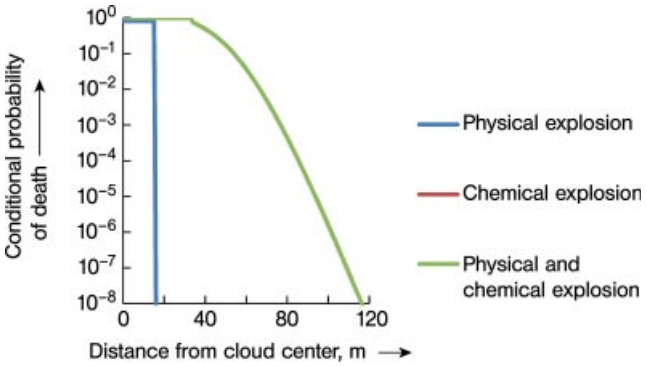

Figure 37. Conditional probabilities of death following the blast wave from a BLEVE of 1500 kg of saturated propane (energy from liquid and vapor; 10% vapor) and those produced by the ensuing fireball (20% atmospheric humidity) as well those from the combination of both (the curves for chemical explosion and for physical plus chemical explosion are virtually identical)

possibility of a dust detonation, however, is considered as being remote.

In what follows the spreading of the blast wave originating from a dust explosion is treated; [264, 265] give the following relationship for dusts of class St 1 (see → Plant and Process Safety, 2. Hazardous Materials and Process Conditions, Section 4.3)

$$p_r = p_{max,A}\left(\frac{R_s}{r}\right)^{3/2} \tag{86}$$

where

$$p_{max,A} = 0.2 \cdot p_{red} A^{0.1} V^{0.18} \tag{87}$$

$$R_s = 8SV^{0.3} \tag{88}$$

where R_s is the distance in m from the vent where the maximum pressure occurs ($S = 0.25$ for vertical and $S = 0.2$ for horizontal discharge), V the vessel volume in m^3, and A the vent area in m^2, $8V^{0.3}$ the maximum length of the flame of a homogeneous air–dust mixture in m, and p_{red} the maximum overpressure in the vented enclosure in bar.

Additional limitations are

- Pressure of vented enclosure $p_{red} < 2$ barg, vent opening pressure < 0.1 barg
- $0.1\ m^3 < V < 1000\ m^3$

In [265] the following simplified equation for blast overpressure at a distance r from the cloud center p_r is given along with a more refined approach.

$$p_r = p_a\left[1 + \frac{\kappa_0\left\{\frac{(\kappa_0+1)p_{red}}{\rho_a a_0^2}\right\}^{1/2}}{(\kappa_0+1)(logr)^{1/2}r}\right] \tag{89}$$

where κ_0 is the heat ratio of air (1.4) and the other quantities are defined as above.

Reference [266] provides a detailed account of dust explosions and [267] gives an overview of the numerous pending problems in the investigation of such explosions.

2.6. Vessel Fragmentation and Missile Flight

Pipes and vessels containing high-pressure gases or superheated liquids are closed systems. An explosion in such a system may produce fragmentation of the containment and thus generate missiles. These may directly cause injuries to people or damage structures. Furthermore, they may enhance accident effects by destroying or disabling surrounding process equipment and initiating accidents there. The latter phenomenon is known as the domino effect; it is of increasing concern in safety assessments [268, 269].

The presentation of vessel fragmentation given here closely follows [270, 271]. An account of accidents involving bursts and fragmentation is given in [272] and [273, 274].

The pressure of failure and hence the explosion energy in a vessel depend on the failure scenario. Causes of a vessel burst may be

- Overpressure (e.g., overfilling, warming up in combination with the failure of pressure relief)
- Mechanical failure (e.g., due to defects or boundary weakening, caused by embrittlement, corrosion, etc.)
- Engulfment in a fire

In the case of overpressure failure, the failure pressure of the vessel, i.e., its maximum working pressure times a safety factor (4 in case of carbon-steel vessels) should be used. Mechanical failures should be dealt with by applying the normal operating pressure and, in case of fire engulfment, a value of 1.21 times the starting relief pressure is recommended in [275]. Fractures of vessels may be either brittle or ductile, the latter being more likely.

The trajectory of the missile is calculated in two dimensions while accounting for the resistance of air proportional to the square of its velocity. This applies to the so-called ballistic range which lies between very low velocities, where resistance is proportional to velocity, and supersonic velocities, where resistance is a complex function. Fragments from vessel bursts are usually encountered in this range. We then have the equations of motion [272].

$$\frac{d^2x}{dt^2} + \frac{\rho \cdot C_D \cdot A_D}{2 \cdot m} \cdot \left(\frac{dx}{dt}\right)^2 = 0 \tag{90}$$

$$\frac{d^2y}{dt^2} \pm \frac{\rho \cdot (C_D \cdot A_D \mp C_L \cdot A_L)}{2 \cdot m} \cdot \left(\frac{dy}{dt}\right)^2 + g = 0 \tag{91}$$

where:

- x: horizontal direction in m
- y: vertical direction in m
- m: fragment mass in kg
- C_D: drag coefficient
- A_D: drag area (projected area) in m^2
- C_L: lift coefficient
- A_L: lift area (projected area) in m^2
- ρ: density of air in kg/m^3
- g: acceleration due to gravity in m/s^2.

Since the drag force is opposed to the direction of motion, in Equation (90) the direction of motion is always the same, while in Equation (91) it differs between the ascending (+) and descending (−) parts of the trajectory. For this reason the drag force is aligned with the force of gravity during ascent and opposed to it during descent. This leads to different solution functions for the two phases of flight, which can be obtained analytically [269]. Several input quantities are required for applying Equations (90) and (91) to practical cases:

- Pressure at the time of release
- Energy content of the vessel on rupture
- Degree of filling of the vessel at the initiation of the accident in the case of superheated storage
- Percentage of initial energy imparted to the fragments on the whole
- Number of fragments
- Shape and mass of fragments
- Percentage of initial energy imparted to the individual fragments
- Orientation of trajectory (azimuthal and polar angles of departure)
- Drag coefficient
- Wind direction and speed during the accident

All of them are either stochastic or uncertain. Both stochastic and uncertain quantities should be treated as random variables. They are represented by probability distributions and propagated through the calculations using the Monte-Carlo method [269–271]. There is not much observed evidence for generating the required probability distributions. Some indications are given here.

In [276] the following numbers of fragments originating from the rupture of spheres observed in accidents are given: 3, 4, 5, 5, 6, 16, and 19. From [273, 276] 46 relevant events for the rupture of cylindrical vessels were identified giving a mean number of 2.7 fragments. For cylinders a distinction must be made between bullets and end caps. However, there is no empirical indication as to their ratio. An important factor of influence still untreated in this context is the amount of leakage between fragments at the launch stage, which influences the energy imparted to the fragments. A detailed discussion of this phase of the accident for horizontal cylindrical vessels is given in [277].

The orientation of the fragment trajectory is characterized by the polar and azimuthal angles. No indication for preferential directions of the

polar angle of the flight trajectory has been found. In [276] the azimuthal angle is divided into 12 sectors, for which different probabilities have been identified. Hence, a preferred flight direction is indicated.

The drag coefficient C_D depends on factors such as geometry, surface roughness, and orientation with respect to direction of the flow. A blunt, sharp-edged shape with negligible Reynolds number dependence is assumed. A reasonable range for fragments from spheres is $C_D = 0.8–1.4$ which applies to shells for differing angles of attack. For end caps of cylindrical vessels $C_D = 0.8–1.1$ and for bullets C_D 1.1–1.8 applying to flat disks is deemed appropriate. Fragments tend to be chunky. Then the possibility of lift, an effect popularly known as "frisbying", need not be considered, in contrast with flat fragments.

The fill condition at the time of the accident, which is important for the calculation of the total energy imparted to the fragments in case of superheated storage, is practically never known for real accidents. It may be assumed to lie between 0.1 and 0.9.

Direction and speed of wind at the moment of the accident may have an impact on the flight trajectory of the fragments. They are stochastic variables but are normally neglected.

In case of lacking empirical evidence plausible assumptions for the probability distributions of the variable in question are made in [270, 271].

The initial velocity of a fragment is obtained from

$$v_0 = \left(\frac{2E_k}{m}\right)^{\frac{1}{2}} \tag{92}$$

where E_k is the kinetic energy imparted to the fragment, m its mass, and v_0 its initial velocity. The determination of E_k requires the energy content of the vessel to be calculated in the first place. In doing this one must differentiate between the storage of a gas and that of a superheated liquid. Several equations are in use for treating the expansion of an ideal gas. Among them are [275]

Brode's equation

$$E = \frac{p_1 - p_0}{\gamma - 1} \cdot V \tag{93}$$

Baker's equation

$$E = \left[1 - \left(\frac{p_0}{p_1}\right)^{(\gamma-1)/\gamma}\right] \frac{p_1}{\gamma - 1} \cdot V \tag{94}$$

Baum's equation

$$E = \left[1 - \frac{p_0}{p_1}\right]^{(\kappa-1)/\kappa} + (\kappa - 1)\frac{p_0}{p_1}\left\{1 - \left(\frac{p_0}{p_1}\right)^{-1/\kappa}\right\} \frac{p_1}{\kappa - 1} V \tag{95}$$

where:

- E: energy of explosion of the vessel in kJ
- V: volume of the vessel in m^3
- p_1: failure pressure of the vessel in kPa
- p_0: atmospheric pressure in kPa
- γ: ratio of specific heats

A detailed discussion of the merits and drawbacks of Equations (93)–(95) is given in [275]. In conclusion it is stated there that no consensus exists on how to assess the energy of an explosion of a pressure vessel. A pragmatic and conservative approach is to use the one of the three equations resulting in the highest energy.

In case of a superheated liquid a boiling liquid expanding explosion (BLEVE) occurs. The calculation of the physical energy released in such a case is presented in Section 2.5.3.

The energy thus calculated caters for vessel expansion, rupture, blast, and fragments. Hence, only a fraction of the energy of explosion appears as kinetic energy of the fragments. In order to arrive at this energy E_k, E must be multiplied by a factor which ranges between 0.2 and 0.5, with 0.2 being the recommended value [275].

The computer codes developed on this basis were validated by comparisons with experimental values and observations after accidents [270, 271]. In what follows only the comparison with findings after the accident in Mexico City is presented.

In the boiling-liquid expanding-vapor explosion (BLEVE) which occurred in the Mexico City disaster probably two out of three spherical vessels with characteristics given in Table 18 failed [274].

Table 18. Characteristics of the vessels from [274]

Parameter	
Vessel mass	146 259 kg
Vessel volume	1600 m^3

They contained superheated propane, butane, or a mixture of both. The failure pressure was assessed to be 1.34 MPa. For propane, which is assumed to be the vessel contents for being the predominant substance on the site, this corresponds to a saturation temperature of 310.9 K. From the graph provided in [275] an expansion work of 2 MJ/m^3 may be read (this is an alternative to the procedure outlined in Section 2.5.3). It refers to the vapor fraction in the vessel, since at this temperature flashing of the liquid fraction is unlikely to occur. The uncertainty surrounding this quantity is described by a constant pdf; the interval [1.8, 2.2] MJ/m^3 was chosen to represent it. The empirical findings on fragment ranges given in [274] are well represented by a truncated normal distribution, as done in Figure 38.

The average energy of a fragment hitting the ground after completing its flight is 28.2 MJ; the energy loss due to the drag force amounts to 37.0 MJ. The average velocity on touching ground is 54.1 m/s, a quantity larger than that required to penetrate a vessel. According to [274] the latter lies in the range 4–12 m/s.

Details on the explosion and missile generation of cased explosives may be found in [272].

2.7. Threshold Values, Probits, Damage

To assess the impact of an injury factor, e.g., pressure wave impact or toxic concentration, two methods are in use. One is the comparison with threshold values (see Table 19), which provides damage types for discrete steps of intensity of the injuring factor. The other one is the application of the probit (probability unit) concept, which allows for a continuous transition expressed in terms of probabilities of harm related to differing intensities of the injuring factor. This is an adequate way to provide knowledge from other areas, e.g., medicine and toxicology, in such a way that it can readily used by the engineer in analyzing risks.

Experience shows that the injuring or causative factors for harm from process plants may be represented by log-normal distributions [272]:

$$Y = k_1 + k_2 \ln x \qquad (96)$$

Table 19. Threshold values for fire and pressure loads (from [272])

Dose limit, kJ/m^2	Impact
375	third degree burns
250	second degree burns
125	first degree burns
65	threshold value for pain, no irritation or blisters on skin
Overpressure, bar	**Type of damage**
0.01	typical pressure for breaking glass
0.07	partial destruction of building; buildings become uninhabitable
0.34–0.48	virtually total destruction of building
0.69	major damage and shifting of heavy machinery (3000 kg) from its location

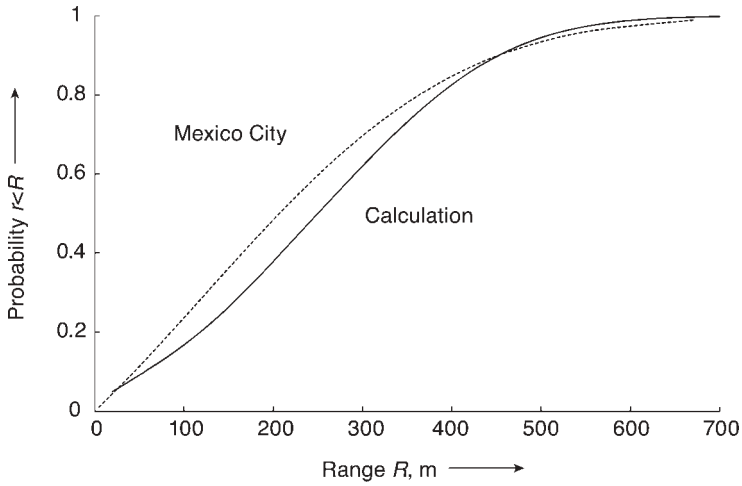

Figure 38. Comparison of fragment ranges observed after a BLEVE of stored liquefied propane in Mexico City [274] with calculation results [270]

where x is the causative factor, e.g., a peak pressure of a pressure wave. To obtain the probability corresponding to a certain intensity of x, the following relationship is used

$$p = \phi(Y-5) \tag{97}$$

where ϕ denotes the standard normal distribution [278]. The choice of the argument of the standard normal distribution is made such that $Y = 5$ corresponds to a probability of 0.5, i.e., the 50% value.

Appendix A provides an overview of probit equations for toxicity, pressure waves, and heat radiation.

3. Appendix A: Probit equations

In what follows a number of probit equations are compiled.

Probit equations for lethal toxic loads [279, 281]

Acrolein

1. $Y = -9.931+2.049\ln(C\cdot t)$

Acrylonitrile

1. $Y = -29.42+3.008\ln(C^{1.43}\cdot t)$

Ammonia

1. $Y = -30.75+2.049\ln(\int_0^\infty C(t)^{2.75}\cdot dt)$
2. $Y = -28.33+2.27\ln(\int_0^\infty C(t)^{1.36}\cdot dt)$
3. $Y = -35.9+1.85\ln(C^2\cdot t)$

Benzene

1. $Y = -109.78+5.3\ln(C^2\cdot t)$

Hydrocyanic acid

1. $Y = -29.42+3.008\ln(C^{1.43}\cdot t)$

Bromine

1. $Y = -9.04+0.92\ln(C^2\cdot t)$

Chlorine

1. $Y = -17.1+1.69\ln(\int_0^\infty C(t)^{2.75}\cdot dt)$
2. $Y = -36.45+3.13\ln(\int_0^\infty C(t)^{2.64}\cdot dt)$
3. $Y = -11.4+0.82\ln(\int_0^\infty C(t)^{2.75}\cdot dt)$
4. $Y = -5.04+0.5\ln(\int_0^\infty C(t)^{2.75}\cdot dt)$

Hydrogen chloride

1. $Y = -16.85+2.0\ln(C\cdot t)$

Ethylene oxide

1. $Y = -6.8+\ln(C\cdot t)^*$

Hydrogen fluoride

1. $Y = -48.33+4.853\ln(C\cdot t)$

Table 20. Probit equations for loads from different forms of energy [279, 280]

No.	Type of damage	Probit equation
1	Structural damage to frame structures	$Y = -23.8+2.92\ln p^0$
2	Eardrum rupture	$Y = -15.6+1.93\ln p^0$
3		$Y = -12.6+1.524\ln p^0$
4	Death due to lung injury	$Y = -77.1+6.91\ln p_0$
5	Death due to impact (whole-body displacement)	$Y = -46.1+4.82\ln J$
6	Serious injury due to body translation by impulse	$Y = -39.1+4.45\ln J$
7	Injury from missiles, particularly glass	$Y = -27.1+4.26\ln J$
9	Death from thermal radiation	$Y = -46.1+4.82\ln J$
		$Y = -14.9+2.56\ln(t_e q''^{4/3}\cdot 10^{-4})$
10	Fatal injury from thermal radiation (unprotected by clothing)	$Y = -36.38+2.56\ln(t_e q''^{4/3})$
11	Fatal injury from thermal radiation (protected by clothing)	$Y = -37.23+2.56\ln(t_e q''^{4/3})$
12	First degree burns	$Y = -39.83+3.02\ln(t_e q''^{4/3})$
13	Second degree burns	$Y = -43.14+3.02\ln(t_e q''^{4/3})$

p_0 = peak overpressure in N/m^2; J = impulse in Nsm^{-2}; t_e = duration of radiation exposure in s; q'' = radiation intensity in W/m^2.

2. $Y = -26.36+2.854\ln(C{\cdot}t)$
3. $Y = -35.87+3.354\ln(C{\cdot}t)$
4. $Y = -25.87+3.354\ln(C{\cdot}t)$

Formaldehyde

1. $Y = -12.24+1.3\ln(C^2{\cdot}t)$

Carbon disulfide

1. $Y = -46.56+4.2\ln(C{\cdot}t)$

Phosgene

1. $Y = -27.2+5.1\ln(C{\cdot}t)$
2. $Y = -19.27+3.686\ln(C{\cdot}t)$

Phosphine

1. $Y = -2.25+\ln(C{\cdot}t)$

Sulfur dioxide

1. $Y = -15.67+2.1\ln(C{\cdot}t)$

Hydrogen sulfide

1. $Y = -11.15+\ln(C^{1.9}{\cdot}t)$

Toluene

1. $Y = -6.794+0.408\ln(C^{2.5}{\cdot}t)$

where $C(t)$, abbreviated as C, is the time-dependent concentration in ppm and time is in min (exception: * in mg/m^3 and min).

4. Acknowledgement

All Plant and Process Safety keywords were coordinated by Ulrich Hauptmanns.

References

1 U. Hauptmanns, W. Werner, *Engineering Risks—Evaluation and Valuation*, Springer Verlag, Berlin 1991.
2 S. Kaplan, B.J. Garrick: "On the quantitative definition of risk", *Risk Analysis* **1** (1981) no. 1, 11–27.
3 R.M. Cooke, *Experts in Uncertainty*, Oxford University Press, New York 1991.
4 G.M. Morgan, M. Henrion, Uncertainty—A Guide to dealing with Uncertainty in Quantitative Risk and Policy Analysis, Cambridge University Press, New York 1990.
5 T. Bedford, R. Cooke, *Probabilistic Risk Analysis: Foundations and Methods*, Cambridge University Press, Cambridge 2001.
6 Process Safety Management of Highly Hazardous Chemicals—Compliance Guidelines and Enforcement Procedures, CPL 02-02-045, Std. No. 1910.119; 1910.109, 1994.
7 U. Hauptmanns, J. Rodriguez, Untersuchungen zum Arbeitsschutz bei An- und Abfahrvorgängen von Chemieanlagen, Bundesanstalt für Arbeitsschutz, Fb 709, Dortmund 1994.
8 F.P. Lees: *Loss Prevention in the Process Industries. Hazard Identification, Assessment and Control*, vol. 1, Butterworth-Heinemann, Oxford 1996.
9 U. Hauptmanns: "Computer-aided valuation of safety management", *Trans IChemE. Part B* **76** (1998) 286–290.
10 IEC 60812 Ed. 2.0, Analysis techniques for system reliability–Procedure for failure mode and effects analysis (FMEA), 2006.
11 G. Wells: *Hazard Identification and Risk Assessment*, IchemE, Rugby 1996.
12 IEC 61882 Ed. 1.0 b:2001, Hazard and operability studies (HAZOP studies)—Application guide, International Electrotechnical Commission, 2001.
13 IVSS, Das PAAG-Verfahren, Geneva 2000.
14 U. Hauptmanns, P. Hömke, J. Huber, G. Reichart, H.-G. Riotte, Ermittlung der Kriterien für die Anwendung systemanalytischer Methoden zur Durchführung von Sicherheitsanalysen für Chemieanlagen, GRS-59, Köln 1985.
15 U. Hauptmanns: "Fault Tree Analysis for Process Plants" in A. Kandel, E. Avni (eds.): *Engineering Risk and Hazard Assessment*, vol. I, CRC Press, Boca Raton 1988.
16 DIN 25419:1985-11, Ereignisablaufanalyse; Verfahren, graphische Symbole und Auswertung (Event tree analysis; method, graphical symbols and evaluation).
17 M. Rausand, A. Høyland: *System Reliability Theory*, Wiley-VCH, Weinheim 2004.
18 DIN 25424-1:1981-09, Fehlerbaumanalyse; Methode und Bildzeichen (Fault tree analysis; Method and graphical symbols).
19 W.E. Vesely et al., *Fault Tree Handbook* (NUREG-0492), U.S. NRC, Washington, S.C. 1981.
20 W.E. Vesely et al., *Fault Tree Handbook with Aerospace Applications*, NASA, 2002.
21 U. Hauptmanns: "The impact of differences in reliability data on the results of probabilistic safety analyses", paper 00815, *8th World Congress of Chemical Engineering*, Montreal, August 23–27 2009.
22 L. Camarinopoulos, J. Yllera: "Advanced Concepts in Fault Tree, Modularisation", *Nucl. Eng. Des.* **91** (1986) 79–91.
23 R.E. Barlow, F. Proschan: *Statistical Theory of Reliability and Life Testing: Probability Models, To Begin With*, Holt, Rinshart and Winston, New York 1975.
24 R. Isermann: *Fault-Diagnosis Systems—An Introduction from Fault Detection to Fault Tolerance*, Springer Verlag, Berlin 2006.
25 A.A. Lakner, R.T. Anderson, Reliability: *Engineering for Nuclear and other High Technology Systems—A Practical Guide*, Chapman & Hall/CRC, London 1985.
26 I.A. Ushakov (ed.): *Handbook of Reliability Engineering*, Wiley Interscience, New York 1994.
27 D.R. Cox: *Renewal Theory*, Methuen, London 1962
28 IEC Standard 61508, Functional safety: safety related systems–7 parts, 2000.

29 IEC 61511, Functional safety—Safety instrumented systems for the process industry sector–3 parts, 2003.

30 VGB PowerTech e.V., Reliability Data for Nuclear Power Plant Components: Analysis for 2004, Centralized Reliability and Events Database (ZVGB), Essen 2004.

31 Center for Chemical Process Safety (CCPS): *Guidelines for Improving Plant Reliability Through Data Collection and Analysis*, Wiley-AIChE, New York 1998.

32 U. Hauptmanns: Reliability data acquisition and evaluation in process plants, paper 00814, *8th World Congress of Chemical Engineering*, Montreal, August 23–27, 2009.

33 P. Hömke, H.W. Krause, W. Ropers, C. Verstegen, H. Hüren, H. V. Schlenker, P. Dörre, A. Tsekouras: Zuverlässigkeitskenngrößenermittlung im Kernkraftwerk Biblis B, Abschlußbericht–GRS–A–1030/I-VI, Köln 1984.

34 H. Doberstein, U. Hauptmanns, P. Hoemke, C. Verstegen, J. Yllera: *Ermittlung von Zuverlässigkeitskenngrößen für Chemieanlagen*, vol. 1, 2, Gesellschaft für Reaktorsicherheit (GRS)mbH, Köln 1988.

35 SINTEF: *OREDA-Offshore Reliability Data Handbook*, 4th ed., DNV, Trondheim 2002.

36 SINTEF: *Reliability Data for Safety Instrumented Systems–PDS Data Handbook*, DNV, Trondheim 2006

37 American Institute of Chemical Engineers: Chemical Process Safety (CCPS), Guidelines for Process Equipment Reliability Data, with Data Tables, AIChe, New York 1989.

38 VROM (ed.): *Guidelines for quantitative risk assessment*, CPR 18E, The Hague, December 2005.

39 Health and Safety Executive, Offshore Hydrocarbon Release Statistics, 2001, HID Statistics Report, HSR 2001 02, January 2002.

40 K.C. Kapur, L.R. Lamberson: *Reliability in Engineering Design*, Wiley, New York 1977.

41 H.F. Martz, R.A. Waller: *Bayesian Reliability Analysis*, Krieger, Malabar 1991.

42 M. Abramowitz, I.A. Stegun (eds.): *Handbook of Mathematical Functions With Formulas, Graphs, and Mathematical Tables*, U.S. Department of Commerce, Washington 1972.

43 Deutsche Risikostudie Kernkraftwerke-Phase B, GRS, Köln 1990.

44 DIN 25424-1:1981-09, Fehlerbaumanalyse; Methode und Bildzeichen Fault tree analysis; Method and graphical symbols.

45 A. Mosleh, et al.: "Procedure for Treating Common Cause Failures in Safety and Reliability Studies", vol. 1, *Procedural Framework and Examples*, NUREG/CR-4870, February 1988; vol. 2, *Analytic Background and Techniques*, U.S.N.R.C., Washington, D.C. December 1988.

46 U. Hauptmanns: "The multiclass binomial failure rate model", *Reliab. Eng. Syst. Saf.* **53** (1996) 85–90

47 A.D. Swain, H.E. Guttmann: *Handbook of Human Reliability Analysis with Emphasis on Nuclear Power Plant Application*, Final Report, NUREG/CR-1278, Washington D. C. 1983.

48 J. Forester, A. Kolaczkowski, E. Lois, D. Kelly: *Evaluation of Human Reliability Analysis Methods Against Good Practices*, NUREG 1842, U.S. Nuclear Regulatory Commission, Office of Nuclear Regulatory Research, Washington, DC., September 2006.

49 J. Rasmussen: *On the Structure of Knowledge—A Morphology of mental Models in a Man Machine Context*, RISØ-M-2192, Roskilde, Denmark, 1979.

50 A.D. Swain: *Comparative Evaluation of Methods for Human Reliability Analysis*, GRS-71, Brussels April 1989.

51 G.W. Hannaman, D.H. Worledge: "Some Development in Human Reliability Analysis Approaches and Tools", *Reliab. Eng. Syst. Saf.* **22** (1988) 235–257.

52 D. Gertman, H. Blackman, J. Marble, J. Byers, C. Smith: *The SPAR-H Human Reliability Analysis Method*, NUREG/CR-6883, Office of Nuclear Regulatory Research, U.S. Nuclear Regulatory Commission, Washington, August 2005.

53 A. Richei, U. Hauptmanns, H. Unger: "The human error rate assessment and optimizing system HEROS—a new procedure for evaluating and optimizing the man-machine interface in PSA", *Reliab. Eng. Syst. Saf.* **72** (2001) 153–164.

54 U.S. Nuclear Regulatory Commission: Technical Basis and Implementation Guidelines for A Technique for Human Event Analysis (ATHEANA), NUREG-1624, Rev. 1, Washington, D. C., May 2000.

55 R.M. Cooke, L.H.J. Goossens: *Procedures Guide for Structured Expert Judgment*, Report EUR 18820 EN Prepared Under Contract FI4P-CT95-0006 for the European Commission, Directorate General for Research, Brussels 2000.

56 U. Hauptmanns, P. Pana, R. Stück, C. Verstegen, J. Yllera: *Nutzung sicherheits-technischer Untersuchungen aus der Prozeßindustrie für den Arbeitsschutz*, Bundesanstalt für Arbeitsschutz, Fb 619, Dortmund 1990.

57 W.G. Bridges, A.M. Dowell, III, M. Gollin, W.A. Greenfield, J. M. Poulsen, W. Turetzky: *Layer of Protection Analysis: Simplified Process Risk Assessment, Center for Chemical Process Safety*, AIChE, New York 2001.

58 U. Hauptmanns: "Semi-quantitative fault tree analysis for process plant safety using frequency and probability ranges", *J. Loss Prev. Process Ind.* **17** (2004) 339–345.

59 S.N. Anyakora, G.F.H. Engel, F.P. Lees: "Some Data on the Reliability of Instruments in the Chemical Environment", *The Chemical Engineer*, **255** (1971) 396–402.

60 V. Skala: "Improving Instrument Service Factors", *Instrum. Technol.* **21** (1974) no. 11 27–30.

61 M.R. Gibson: "Field Data from the Chemical Industry", *2nd National Reliability Conference*, Birmingham 1979, 2B/2/1–B/2/8.

62 P. Hömke, C. Verstegen et al.: *Zuverlässigkeitskenngrößenermittlung im Kernkraftwerk Biblis-B–Ausfallraten und ihre Einflußgrößen*, GRS-A-744, GRS Köln 1982.

63 E. Mai et al.: *Untersuchung der Zuverlässigkeit von Druckabsicherungen in Kernkraftwerken*, Forschungsbericht, BMI-Forschungsvorhaben RS II-510321/245 SR 214, Köln 1981.

64 B.D. Ripley: *Stochastic Simulation*, Wiley, New York 1987

65 U. Hauptmanns: "The impact of reliability data on probabilistic safety calculations, " *J. Loss Prev. Process Ind.* **21** (2008) 38–49.

66 U. Hauptmanns: "Different sets of reliability data and success criteria in a probabilistic safety assessment for a plant producing nitroglycol", *J. Haz. Mater.* **162** (2009) 1322–1329.

67 M.D. Moosemiller: "Development of Algorithms for Predicting Ignition Probabilities and Explosion Frequencies", paper 00813, *8th World Congress of Chemical Engineering*, Montreal, August 23–27, 2009.

68 Rijksinstitut voor Volksgezondheid en Milieu (RIVM), Centrum Externe Veiligheid, Handleiding Risicoberekeningen Bevi, Juli 2009.

69 M. Fingas (ed.): *The Handbook of Hazardous Materials Spills Technology*, McGraw-Hill, New York 2002

70 DNV Software: *Phast: Impact Theory*, DNV London, June 2007.

71 F.P. Lees, *Loss Prevention in the Process Industries—Hazard Identification, Assessment and Control*, vol. 1, Butterworth-Heinemann, Oxford 1996.

72 C.J.H. van den Bosch, R.A.P.M. Weterings (eds.): *Methods for the Calculation of the Physical Effects Due to Releases of Hazardous Materials (Liquids and Gases)—"Yellow Book"*, CPR 14 E, The Hague 2005.

73 D.M. Webber, S.E. Gant, M.J. Ivings, S.F. Jagger: *LNG Source Term Models for Hazard Analysis: a Review of the State-of-the-Art and an Approach to Model Assessment*, Final Report, The Fire Protection Research Foundation, Quincy, MA, USA, March 2009.

74 D.M. Webber: *Model for Pool Spreading and Vaporization and its Implementation in the Computer Code GASP*, SRD/HSE Report R507, Norwich September 1990.

75 U.S. EPA, U.S. DoT, Guidance for Hazard Analysis, December 1987.

76 U.S. EPA, Risk Management Program Guidance for Offsite Consequence Analysis, EPA 550-B-99-009, April 1999.

77 R.L. Smith, "Predicting Evaporation Rates and Times for Spills of Chemical Mixtures", *Ann. Occup. Hyg.* **45** (2001) no. 6, 437–445.

78 P.S. Cronin, J.A. Evans: *A series of experiments to study the spreading of liquid pools with different bund arrangements*, HSE Contract Research Report 405/2002, Norwich 2002.

79 A.M. Thyer: "A review of data on spreading and vaporisation of cryogenic liquid spills", *J. Hazard. Mater.* **A99** (2003) 31–40.

80 PVAP Theory Document, DNV Software, London, January 2006.

81 VDI Guideline 3783, Part 1, Ausbreitung von störfallbedingten Freisetzungen; Sicherheitsanalyse. Beuth Verlag, Berlin, 1987.

82 VDI Guideline 3783, Part 2, Dispersion of heavy gas emissions by accidental releases—Safety Study, Beuth Verlag, Berlin, 1990.

83 C. Wamser, J. Schröter, K. Hinrichsen: "Darstellung und Anwendung eines verbesserten, universell gültigen Ausbreitungskriteriums", *Staub-Reinhal. Luft* **40** (1980) 253–257.

84 VDI Guideline 3782, Part 3, Berechnung der Abgasfahnenüberhöhung. Beuth Verlag, Berlin 1985.

85 G. König-Langlo, M. Schatzmann: "Ausbreitung von störfallbedingten Freisetzungen schwerer Gase", *Staub-Reinhalt. Luft* **49** (1989) 241–247

86 J. McQuaid: "Large scale experiments on the dispersion of heavy gas clouds" in G. Ooms, H. Tennekes (eds.): *Atmospheric Dispersion of Heavy Gases and Small Particles*, Springer Verlag, Berlin 1984.

87 R.E. Britter, J. Mc Quaid: *Workbook on the Dispersion of Dense Gases*, Health and Safety Executive, Sheffield 1988.

88 L.A.M. Janssen: *Wind tunnel modelling of the dispersion of LNG vapour clouds in the atmospheric boundary layer*, MT-TNO Rep. 81-07020, Apeldoorn 1981.

89 G. König: *Windkanalmodellierung der Ausbreitung störfallartig freigesetzter Gase schwerer als Luft*, Hamburger Geophysikalische Einzelschriften, Verlag Wittenborn Söhne, Hamburg 1987.

90 K. Marotzke, M. Schatzmann: *Untersuchung von Hindernisstrukturen bei der Störfallausbreitung*, Forschungsbericht UBA 104 09 110, Meteorologisches Institut, Universität Hamburg, Hamburg 1993.

91 H.H. van Heugten, N.J. Duijm: "Some findings based on wind tunnel simulations and model calculations of Thorney Island Trial No. 008", *J. Hazard. Mater.* **11** (1984) 409–416.

92 D.H. Hall, E.J. Hollis, H. Ishaq: *A wind tunnel model of the Porton Down dense gas spill field trials*, Report LR 394 (AP), Warren Spring Laboratory, Stevenage 1982.

93 J.A. Havens, T.O. Spicer: "Gravity spreading and air entrainment by heavy gas instantaneously released in a calm atmosphere" in G. Ooms, H. Tennekes (eds.): *Atmospheric Dispersion of Heavy Gases and Small Particles*, Springer Verlag, Berlin 1984.

94 D.E. Neff, R.N. Meroney: *The behavior of LNG vapor clouds*, Report, Contr. No. 5014-352-0203, Gas Research Institute, Chicago 1982.

95 R.P. Koopmann et al.: Burro Series Data Report, LLNL/NWC 1980 LNG Spill Tests, Lawrence Livermore National Laboratory, Livermore, CA 1982.

96 J.S. Puttock, G.W. Colenbrander: "Dense gas dispersion—experimental research" in *Proceedings of the Heavy Gas (LNG/LPG) Workshop*, Toronto, Ontario, Canada, 1985.

97 J.S. Puttock, G.W. Colenbrander, D.R. Blackmore: "Maplin Sands Experiments 1980: Dispersion Results from Continuous Releases of Refrigerated Liquid Propane" in S. Hartwig (ed.): *Heavy Gas and Risk Assessment II*, Reidel, Dordrecht 1982.

98 M. Heinrich, E. Gerhold: *Praxisgerechte Bestimmung der Zündentfernung bei der Freisetzung schwerer Gase (LPG)*, 3. Zwischenbericht, TÜV Norddeutschland, Hamburg 1986.

99 S. Mannan: *Lee's Loss Prevention in the Process Industries*, vols. 1–3, Elsevier Butterworth-Heinemann, 3rd ed., Oxford 2005.

100 K.B. McGrattan, H.R. Baum, A. Hamins: *NISTIR 6546*, Fire Safety Engineering Division Biulding and Fire Research Laboratory, U.S. Department of Commerce, Boulder, Col. 2000.

101 K.S. Mudan, *Prog. Energy Combust. Sci.* **10** (1984) 59; K.S. Mudan, P.A. Croce in P.J. DiNenno et al. (eds.): *SFPE Handbook of Fire Protection Engineering*, 2nd ed., National Fire Protection Association (NFPA), Quincy, MA, 1995, chap. 11, pp. 3–197.

102 Methods for calculation of the physical effects ("Yellow Book"), 3rd ed., CPR 14E Part 2, chap. 6: Heat flux from fires, 6-1, 1997; 6. Methods for calculation of the physical effects ("Yellow Book"), Netherlands organization for applied scientific research (TNO), The Hague 1980.

103 M. Hailwood, M. Gawlowski, B. Schalau, A. Schönbucher, *Chem. Eng. Technol.* **32** (2009) 207.

104 A.G. Gaydon, H.G. Wolfhard: *Flames, Their Structures Radiation and Temperature*, 4th ed., Chapman & Hall, London 1979.

105 B. Lewis, G. von Elbe: *Combustion, Flames and Explosions of Gases*, 3rd ed., Academic Press, Amsterdam 1987.

106 A.M. Kanury: *Introduction to Combustion Phenomena*, Gordon & Breach Publishing Group, New York 1996.

107 K.K. Kuo: *Principles of Combustion*, Wiley-Interscience, New Jersey 2005.

108 *Proc. Combust. Inst*. biennial publication; vols. **1** (1928) to **33** (2012).

109 F.A. Williams, *Combustion Theory*, Westview Press, Boulder 1994.

110 K.S. Mudan, P.A. Croce: "Fire hazard calculations for large open hydrocarbon fires", *SFPE Handbook on Fire Protection Engineering*, 2nd ed., Quincy, MA, 1988, pp. 2–45.

111 K.S. Mudan, *Prog. Energy Combust. Sci.* **10** (1984) 59.

112 A. Schönbucher (ed.): *Berechnung von Quelltermen bei störungsbedingten Stoff- und Energiefreisetzung in der Prozessindustrie*, ProcessNet, Frankfurt 2012.

113 M.F. Modest: *Radiation Heat Transfer*, McGraw Hill, New York 1993.
114 R. Siegel, J.R. Howell: *Thermal Radiation Heat Transfer*, 2nd ed., Hemisphere, New York 1991.
115 N. Afgan, J.M. Beer (eds.): *Heat Transfer in Flames*, Scripta Book Company, Washington, D.C., 1974.
116 E.M. Sparrow, R.D. Cess: *Radiation Heat Transfer*, McGraw Hill, New York 1978.
117 W.H. McAdams: *Heat Transmission*, McGraw Hill, New York 1954.
118 D.Q. Kern: *Process Heat Transfer*, McGraw Hill, New York 1950.
119 H.C. Hottel, A.F. Sarofim: *Radiative Transfer*, McGraw Hill, New York 1967.
120 A.F. Sarofim, *Proc. Combust. Inst.* **21** (1986) 1.
121 J.P. Spinti, J.N. Thornock, E.G. Eddings, P.J. Smith, A.F. Sarofim: "Heat transfer to objects in pool fires", in B. Sundén, M. Faghi (eds.): *Transport Phenomena in Fires*, WIT Press, Boston 2008, chap. 3, p. 69.
122 T. Steinhaus, S. Welch, R. Carvel, J.L. Torero, "Large-Scale Pool Fires", *J. Therm. Sci.* **11** (2007) 101.
123 P. Joulain, *Proc. Combust. Inst.* **27**(2) (1998) 2783.
124 D.D. Drysdale: *Introduction to Fire Dynamics*, 2nd ed., Wiley, New York 1999.
125 V.I. Blinov, G.N. Khudiakov, *Academiia Nauk SSSR Doklady* 1957, 1094.
126 M. Hertzberg, *Combust. Flame* **21** (1973) 195.
127 H. Koseki, Y. Iwata, *Fire Technol.* **36** (2000) 24.
128 V. Babrauskas, *Fire Technol.* **19** (1983) 251.
129 V. Babrauskas: "Pool fires: burning rates and heat fluxes" in A. E. Cote, J.M. Linville (eds.): *Fire Protection Handbook*, 16th ed., National Fire Protection Association, Quincy, MA, 1986, p. 21.
130 E.E. Zukoski, B.M. Cetegen, T. Kubota, *Proc. Combust. Inst.* **20** (1984) 361.
131 W. Brötz, A. Schönbucher, *Chem.-Ing.-Tech.* **50** (1978) 573.
132 C. Balluff, W. Brötz, D. Göck, N. Schieß, A. Schönbucher, *Chem.-Ing.-Tech.* **57** (1985) 823.
133 A. Schönbucher, S. Schälike, I. Vela, K.-D. Wehrstedt in J. Schmidt (ed.): *Safety Technology Applying Computational Fluid Dynamics*, Wiley-VCH, Weinheim, 2012.
134 I. Vela, H. Chun, K.B. Mishra, M. Gawlowski, P. Sudhoff, M. Rudolph, K.-D. Wehrstedt, A. Schönbucher, *Forsch. Ingenieurwes.* **73** (2009) 87.
135 A. Modak, *Fire Res.* **1** (1978) 339.
136 V.I. Blinov, G.N. Khudyakov: *Diffusion Burning of Liquids*, U. S. Army Translation NTIS No. AD296762., Izdatel'stvo Akademii Nauk SSSR, Moscow 1961, p. 208.
137 A.R. Hall: *Pool Burning: A Review*, Rocket Propulsion Establishment, Westcott 1972.
138 L. Orloff, *Proc. Combust. Inst.* **18** (1981) 549.
139 J.A. Fay, *J. Hazard. Mater.* **B136** (2006) 219.
140 M. Muños, J. Arnaldos, J. Casal, E. Planas, *Combust. Flame* **139** (2004) no. 3, 263.
141 I. Vela, CFD prediction of Thermal Radiation of large, sooty hydrocarbon Pool Fires, PhD thesis, University Duisburg-Essen, 2009.
142 R.O. Carvel, A.N. Beard, P.W. Jowitt, *Civil Eng. Environ. Syst.* **18** (2001) 279.
143 H. Kurioka, Y. Oka, H. Satoh, O. Sugawa, *Fire Saf. J.* **38** (2003) 319.
144 V.B. Apte, A.R. Green: "Pool Fire Plume Flow in a Large-Scale Wind Tunnel", *3rd Int. Symp. Fire Safety Science*, Edinburgh, UK, 1991.
145 R. Carvel, A. Beard, P. Jowitt, *Fire Technol.* **41**(4) (2005) 271.
146 J.H. Burgoyne, L.L. Katan, *J. Inst. Pet.* **33** (1947) 158.
147 J.P Garo, J.P. Vantelon, H. Koseki, *Combust. Sci. Technol.* **178** (2006) 1217.
148 J. Hristov, E. Planas-Cuchi, J. Arnaldos, J. Casal, *Int. J. Therm. Sci.* **43**(3) (2004) 221.
149 P.J. Pagni, *Appl. Mech. Rev.*, **43** (1990) 153.
150 W.M.G. Malalasekera, H.K. Versteeg, K. Gilchrist, *Fire Mater.* **20** (1996) 261.
151 A. Schönbucher, B. Arnold, V. Banhardt, V. Bieller, H. Kasper, M. Kaufmann, R. Lucas, N. Schieß, *Proc. Combust. Inst.* **21** (1986) 83.
152 D.T. Gottuk, D.A. White: "Liquid fuel fires", *SFPE Handbook on Fire Protection Engineering*, 3rd ed., Quincy, MA, 2002, pp. 2–297.
153 K.S. Narasimhan, P.J. Foster, *Proc. Combust. Inst.* **10** (1965) 253.
154 J.L. Torero, S.M. Olenick, J.P. Garo, J.P. Vantelon, *Spill Sci. Technol. Bull.* **8** (2003) no. 4, 379.
155 N. Wu, G. Kolb, J.L. Torero, *Combust. Sci. Technol.* **161** (2000) no. 1-6, 269.
156 G.H. Markstein, *Proc. Combust. Inst.* **22** (1988) 363.
157 H.D. Ross, *Prog. Energy Combust. Sci.* **20**(1) (1994) 17.
158 W.L. Fowler, *Proc. Combust. Inst.* **22** (1988) 425.
159 B.J. McCaffrey, M. Harkleroad, *Proc. Combust. Inst.* **22** (1988) 1251.
160 Ü.Ö. Köylü, G.M. Faeth, *Combust. Flame* **89**(2) (1992) 140.
161 Ü.Ö. Köylü, G.M. Faeth, T.L. Farias, M.G. Carvalho, *Combust. Flame* **100** (1995) 621.
162 G.M. Faeth: *Microgravity Combustion: Fire in Free Fall*, Academic Press, New York 2001.
163 J.P. Gore, G.M. Faeth, *J. Heat Transfer*, **110** (1998) 173.
164 K.M. Leung, R.P. Lindstedt, W.P. Jones, *Combust. Flame* **87** (1991) 289.
165 J.B. Moss, C.D. Steward, *Fire Saf. J.* **30** (1998) 229.
166 P.K. Raj, *Process Saf. Prog.* **24** (2005) 192.
167 P.K. Raj, *J. Hazard. Mater.* **140** (2007) 280.
168 W.W. Yuen, C.L. Tien, *Proc. Combust. Inst.* **17** (1976) 1481.
169 J. de Ris, *Proc. Combust. Inst.* **17** (1978) 1003
170 N. Lallemant, A. Sayre, R. Weber, *Prog. Energy Combust. Sci.* **22** (1996) 543.
171 C.R. Shaddix, Á.B. Palotás, C.M. Megaridis, M.Y. Choi, N.Y. C. Yang, *Int. J. Heat Mass Transfer* **48** (2005) 3604.
172 C.W. Lautenberger, J. de Ris, N. Dambsey, J.R. Barnett, H.R. Baum, *Fire Safety J.* **40** (2005) 141.
173 G.H. Markstein, J. de Ris, *Proc. Combust. Inst.* **20** (1984) 1637.
174 K.A. Notarianni, D.D. Evans, W.D. Walton, D. Madrzykowski, J.R. Lawson, *Proc. Int. Conf. Fire Saf.* **6** (1993) 111.
175 H. Koseki, *Fire Technol.* **25**(3) (1989) 241.
176 H.C. Hottel, *Fire Res. Abstr. Rev.* **1** (1958) 41.
177 A. Nakakuki, *Fire Saf. J.* **23**(4) (1994) 339.
178 P. Joulain, *Fire Saf. J.* **26**(2) (1996) 99.
179 J.R. Howell, K. Daun, H. Erturk: *Annotated Bibliography of Thermal Radiation Validation Data for Fire Applications*, Sandia National Labs: Albuquerque, NM, USA, 2001, p. 96.
180 G.H. Markstein, *Combust. Flame* **27** (1976) 51.
181 H.R. Baum, R.G. Rehm, *Proc. Combust. Inst.* **30** (2005) 2247.
182 T.T. Fu, *Fire Technol.* **10** (1974) 54.
183 T. Yamaguchi, K. Wakasa, *Proc. Fire Saf. Sci.* **1** (1986) 911.
184 H. Koseki, *Fire Technol.* **25** (1989) 241.
185 H. Koseki, G.W. Mulholland, *Fire Technol.* **27** (1991) 54.
186 J.M. Suo-Anttila, L.A. Gritzo: *Thermal Measurements from a Series of Tests with a Large Cylindrical Calorimeter on the Leeward edge of a JP-8 Pool Fire in Cross-flow*, Sandia

National Laboratories, SAND2001-1986, Albuquerque, NM, USA, 2001, DOI10.2172/786626, p. 172.
187 J.J. Murphy, C.R. Shaddix, *Combust. Sci. Technol.* **178** (2006) no. 5, 865.
188 K.A. Jensen, J.M. Suo-Anttila, L.G. Blevins, *Characterization of Soot Properties in Two-Meter JP-8 Pool Fires*, Sandia National Laboratories, Albuquerque 2005.
189 D.D. Evans, G.W. Mulholland, H.R. Baum, W.D. Walton, K.B. McGrattan, *J. Res. Natl. Inst. Stand. Technol.* **106** (2001) 231.
190 W.D. Walton, D.D. Evans, K.B. McGrattan, H.R. Baum, W.H. Twilley, D. Madrzykowski, A.D. Putorti, R.G. Rehm, H. Koseki, E.J. Tennyson: "In situ burning of oil spills", *16th Arctic and marine oil spill program technical seminar*, vol. 2, Ottawa 1993.
191 T. Takahasi, H. Koseki, Y. Iwata: *Crude Oil Full Scale Pool Fire Experiments in Tomakomai*, NISTIR 6242, National Institute of Standards and Technology, Boulder, Col. 1998, p. 91.
192 J.J. Trelles, K.B. McGrattan, H.R. Baum, *AIAA J.* **37** (1999) 1588.
193 K.B. McGrattan, H.R. Baum, W.D. Walton, J.J. Trelles: *Smoke Plume Trajectory from In Situ Burning of Crude Oil in Alaska*, NISTR 5958; NIST SP 995, Boulder, Col. 1997, p. 2.
194 S. Hostikka, K.B. McGrattan, A. Hamins: "Numerical Modeling of Pool Fires using LES and Finite Volume Method for Radiation", *7th Int. Symp. Fire Safety Science*, International Association for Fire Safety, Worchester 2002.
195 A. Schönbucher, D. Goeck, A. Kettler, D. Krattenmacher, N. Schieß, *Proc. Combust. Inst.* **21** (1986) 93.
196 I. Vela, C. Kuhr, A. Schönbucher: *Validation of the semi-empirical radiation model OSRAMO II*, Workshop, 12–13 April, 2005, Livermore, USA.
197 H. Chun, K.-D. Wehrstedt, I. Vela, A. Schönbucher, *J. Hazard. Mater.* **167** (2009) 105.
198 I. Vela, M. Gawlowski, P. Sudhoff, A. Schönbucher: "CFD calculated SEP of large-sclae JP-8 pool fires", *Fire Model Validation and Soot Workshop*, Salt Lake City, Utah, USA, 20–21 September, 2007.
199 I. Vela, M. Gawlowski, P. Sudhoff, A. Schönbucher: "CFD modeling of a 1 m methane fires for different initial and boundary conditions—validation with Sandia data sets", *Fire Model Validation and Soot Workshop*, Salt Lake City, Utah, USA, 20–21 September, 2007.
200 I. Vela, M. Gawlowski, C. Kuhr, A. Schönbucher: *SAS and experiments of large methane and JP-8 pool fires and LES of helium plume*, 10–12 May, Institute for Combustion and Energy Studies (ICES), University of Utah, Salt Lake City, USA, 2006.
201 M. Gawlwoski, C. Kuhr, I. Vela, A. Schönbucher: *LES and experimental investigation of helium plumes and hydrocarbon pool fires*, 10–12 May, Institute for Combustion and Energy Studies (ICES), University of Utah, Salt Lake City, USA, 2006.
202 I. Vela, C. Kuhr, A. Schönbucher: "3D-simulation of large pool fires using ANSYS CFX", *Heat Transfer in Pool Fires*, 12–13 April, Livermore 2005.
203 I. Vela, C. Kuhr, A. Schönbucher: "3D-simulation of large pool fires using ANSYS CFX", workshop on Heat Transfer in Pool Fires? 15 April, ICES, University of Utah, Salt Lake City, USA, 2005.
204 M. Gawlowski, K. Kelly, L.A. Marcotte, A. Schönbucher, *Appl. Opt.* **48** (2009) 4625.
205 M. Gawlowski, K.E. Kelly, P. Sudhoff, I. Vela, A. Schönbucher: "Temperature measurements by real-time holographic interferometry in a tank fire–influence of species composition", *32nd International Symposium on Combustion*, Montreal 2008, 4P100.
206 M. Gawlowski, K.E. Kelly, P. Sudhoff, A. Schönbucher, I. Vela: "Simulation of small-scale helium plume and hexane tank flame. For validation with interferometric data sets", *Fire Model Validation and Soot Workshop*, University of Utah, Salt Lake City, 20–21 September, 2007.
207 I. Vela, C. Kuhr, A. Schönbucher: *Dissipative structures in tank flames–an experimental study of the dynamic behaviour using several methods*, 15th–16th of April, Institute for Combustion and Energy Studies (ICES), University of Utah, Salt Lake City 2005.
208 H.G. Werthenbach, *Verfahrenstechnik* **5** (1971) 115.
209 H.G. Werthenbach, *VDI-Z.* **115** (1973) 383.
210 A. Hamins, J.C. Yang, T. Kashiwagi, *Proc. Combust. Inst.* **24** (1992) 1713.
211 K.B. McGrattan, H.R. Baum, A. Hamins: "Thermal radiation from large pool fires", National Institute of Standards and Technology, NISTIR 6546, Boulder, Col. 2000.
212 N. Takahashi, M. Suzuki, R. Dobashi, T. Hirano, *Fire Saf. J.* **33** (1999) 1.
213 G.W. Mulholland, W. Liggett, H. Koseki, *Proc. Combust. Inst.* **26** (1996) 1445.
214 LASTFIRE (Large Atmospheric Storage Tank Fires), Resource Protection International, Aylesburg, Buckinghamshire 1997.
215 M. Greiner, A. Suo-Anttila, *J. Pressure Vessel Technol. Trans AFME* **126** (2004) 360.
216 N.L. Ryder, J.A. Sutula, C.F. Schemel, A.J. Hamer, V.V. Brunt, *J. Hazard. Mater.* **115** (2004) 149.
217 R.G. Rehm, H.R. Baum, *J. Res. Natl. Inst. Stand. Technol.* **83** (1978) 297.
218 K.B. McGrattan, H.R. Baum, R.G. Rehm, *Atmospheric Enviroment*, **30** (1996) no. 24, 4125.
219 P. Smith: *16th AIAA Computational Fluid Dynamics Conf.*, American Institute of Aeronautics and Astronautics, Orlando, Florida, 2003.
220 K.B. McGrattan: "Fire modelling: Where are we? Where are we going?", *8th Int. Symp. Fire Safety Science*, Beijing, China, 2005, p. 53.
221 P.E. DesJardin, T.M. Smith, C. Roy: *39th Aerospace Science Meeting and Exhibit*, Reno, NV, 2001.
222 B.E.A. Fisher, E. Metcalfe, I. Vince, A. Yates, *Atmos. Environ.* **35** (2001) 2101.
223 C. Kuhr, S. Staus, A. Schönbucher, *Progr. Comput. Fluid Dyn.* **3** (2003) 151.
224 K.A. Jensen: *Radiative Transfer Modeling of a large Pool Fire by Discrete Ordinates, Discrete Transfer, Ray Tracing, Monte Carlo and Moment Methods*, Sandia National Laboratories, Albuquerque, NM, USA, 14, 2004.
225 M. Gawlowski, H. Michel, A. Schönbucher, *Chem.-Ing.-Tech.* **78** (1996) 1259.
226 C. Baluff, D. Göck, C. Kuhr, I. Vela, A. Schönbucher: *Visible organized structures in large pool fires—types and time dependent properties*, 10–12 May, ICES, University of Utah, Salt Lake City, USA, 2006.
227 R. Fiala, D. Göck, X. Zhang, A. Schönbucher, *TÜ* **33** (1992) 219.
228 P.J. Pagni, S. Bard, *Proc. Combust. Inst.* **17** (1979) 1017.
229 K.-D. Paul, A. Schönbucher: *Praxis der Sicherheitstechnik 7*, DECHEMA, Frankfurt 2006, p. 175.
230 W. Kaiser, P. Rogazewski, M. Schindler, A. Acikalin, M. Albricht, M. Lambert, J. Steinbach: *Determination and calculation of hazardous incident scenarios in accordance with the*

3rd hazardous incident administrative instruction, Report No. UBA-FB 20409428 (II), 1999, p. 194.
231 N.C. Daish, P.F. Linden, V. Vieillard, D. Nedelka, T.A. Roberts, C.J. Butler: "A new unified investigation into vapour cloud fires", LNG13, *13th International Conf. and Exhibition on Liquefied Natural Gas*, Seoul, Korea, 2001.
232 Center for Chemical Process Safety (CCPS): *Guidelines for Evaluating the Characteristics of Vapor Cloud Explosions, Flash Fires, and BLEVEs*, American Institute of Chemical Engineers, New York 1994.
233 HSE, Hazardous Installations Directorate, Offshore Division Fire and Explosion Strategy, Issue 1, 2004.
234 F.P. Lees: *Loss Prevention in the Process Industries Hazard Identification, Assessment and Control*, vols. 1–3, Butterworth-Heinemann, Oxford 1996.
235 Q.A. Baker, A.J. Pierorazio, J.L. Woodward, M.J. Tang: "Guidelines to Evaluating Vapor Cloud Explosion, Pressure Vessel Burst, BLEVE and Flash Fire Hazards", *Process Saf. Progr.* **30** (2011) no. 3, 296–300.
236 V. Novozhilov: "Some aspects of the mathematical modelling of fireballs", *Proc. Inst. Mech. Eng., Part E* **217** (2003) no. 2, 103–121.
237 INERIS-Institut National de l'Environnement Industriel et des Risques: Méthodes pour l'évaluation et la prévention des risques accidentels (DRA-006) Le BLEVE, Phénoménologie et modélisation des effets thermiques, Ω-5, Verneuil-en-Halatte September 2002.
238 W.E. Martinsen, J.D. Marx: "An Improved Model for the Prediction of Radiant Heat from Fireballs", *International Conference and Workshop on Modeling Consequences of Accidental Releases of Hazardous Materials*, San Francisco, California, September 28–October 1, 1999
239 L.T. Cowley, A.D. Johnson: *Oil and Gas Fires: Characteristics and Impact*, OTI 92596, HMSO, London 1992.
240 A.D. Johnson, L.C. Shirvill, A. Ungut: *CFD Calculation of Impingent Gas Jet Flame*, OTO 1999011, HSE, April 1999.
241 R. Pula, F.I. Khan, B. Veitch, P.R. Amyotte, "Revised Fire Consequence Models for Offshore Quantitative Risk Assessment", *J. Loss Prev. Process Ind.* **18** (2005) 443–454.
242 DNV Software: *Phast*, London, June 2007.
243 HID-Safety Report assessment guide: LPG, PM/Technical 103 (table 6), http://www.hse.gov.uk/comah/sraglpg/lpg.pdf (accessed 2 June 2012) .
244 C.J.H. van den Bosch, R.A.P.M. Weterings (eds.): *Methods for the Calculation of the Physical Effects Due to Releases of Hazardous Materials (Liquids and Gases)—"Yellow Book"*, CPR 14 E, VROM, The Hague 2005.
245 A.R. Lopez, L.A. Gritzo, M.P. Sherman: *Risk Assessment Compatible Fire Models*, SAND97-1562, NITS, Springfield, VA July 1998.
246 D.A. Crowl: *Understanding Explosions*, Wiley-AIChE, New York 2003.
247 V. Raghunathan: "Recent Advancements in Vapor Cloud Explosion Modeling for Onshore Plants", *DNV Energy*, Høvik, Norway 25. Oct. 2006.
248 H.S. Ledin: A Review of the State-of-the-Art in Gas Explosion Modelling, HSL/2002/02 Sheffield 2002.
249 Q.A. Baker, M.J. Tang, E.A. Scheier, G.J. Silva: "Vapor Cloud Explosion Analysis", *AIChE Loss Prevention Symposium*, Atlanta, GA 1994.
250 J.S. Puttock, M.R. Yardley, T.M. Cresswell: "Prediction of Vapour Cloud Explosions Using the SCOPE Model", *J. Loss Prev. Process Ind.* **13** (2000) 419–430.
251 M. Fairweather, M.W. Vasey: "A Mathematical Model for the Prediction of Overpressures Generated in Totally Confined and Vented Explosions", *19th Symposium (International) on Combustion*, The Combustion Institute. Pittsburgh, Pennsylvania, 1982, pp. 645–653.
252 S. Chippett: "Modeling of Vented Deflagrations", *Combust. Flame* **55** (1984) 127–140.
253 D. Bjerketvedt, J.R. Bakke, K. van Wingerden, *Gas Explosion Handbook*, GexCon, Bergen, Norway.
254 Health and Safety Executive: *Buncefield Explosion Mechanism Phase 1*, Steel Construction Institute, RR718, Norwich 2009.
255 G.F. Kinney, K.J. Graham: *Explosive Shocks in Air*, Springer, Berlin 1985.
256 *Explosions in the Process Industries, A Report of the Major Hazards Assessment Panel Overpressure Working Party* (Major Hazards Monograph), IChemE, Rugby 1994.
257 Q.A. Baker, C.M. Doolittle, G.A. Fitzgerald, M.J. Tang, "Recent Developments in the Baker-Strehlow VCE Analysis Methodology", *Process Saf. Progr.* **17** (1998) 297–301.
258 J.A. Pierorazio, J.K. Thomas, Q.A. Baker, D.E. Ketchum: "An Update to the Baker-Strehlow-Tang Vapor Cloud Explosion Prediction Methodology Flame Speed Table", *Process Saf. Progr.* **24** (2005) 59–65.
259 W.J. Tang, Q.A. Baker, "A New Set of Blast Curves from Vapor Cloud Explosions", *Proc. Safety Progr.* **18** (1999) 235–240.
260 L. Mélanie, I. Sochet, X. Rocourt, S. Jallais: Review of methods for estimating the overpressure and impulse resulting from a hydrogen explosion in a confined/obstructed volume, vgr.ing.unipi.it/ichs/images/stories/papers/254.pdf (accessed 2 June 2012) .
261 A. Sari: *Comparison of TNO Multienergy and Baker–Strehlow–Tang Models*, Wiley, New York 2010, Wiley Online Library, wileyonlinelibrary.com, DOI 10.1002/prs.10424.
262 A.M. Birk, C. Davison, M. Cunningham, "Blast Overpressures from Medium Scale BLEVE Tests", *J. Loss Prev. Process Ind.* **20** (2007) 194–206.
263 R.H. Perry, D.W. Green (eds.), *Perry's Chemical Engineering Handbook*, McGraw Hill, New York 1998.
264 W. Bartknecht: *Dust Explosions*, Springer, Berlin 1998.
265 T. Forcier, R. Zalosh: "External pressures generated by vented gas and dust explosions", *J. Loss Prev. Process Ind.* **13** (2000) 411–417.
266 R.K. Eckhoff: *Dust Explosions in the Process Industry*, Elsevier Science, Burlington, MA, 2003.
267 R.K. Eckhoff: "Current status and expected future trends in dust explosion research" *J. Loss Prev. Process Ind.* **18** (2005) 225–237.
268 The Seveso II Directive 96/82/EC and Directive 2003/105/EC of the European Parliament and of the Council of 16 December 2003 amending Council Directive 96/82/EC.
269 Q.B. Nguyen, A. Mébarki, R. Ami Saada, F. Mercier, M. Reimeringer: "A Monte-Carlo method used to study the fragment impact effect on industrial facilities", *Int. J. Simul. Multidiscip. Des. Optim.* **2** (2008) no. 2, 119–122.
270 U. Hauptmanns: "A Monte-Carlo based procedure for treating the flight of missiles from tank explosions", *J. Probab. Eng. Mech.* **16** (2001) 307–312.
271 U. Hauptmanns: "A procedure for analysing the flight of missiles from cylindrical vessels", *J. Loss Prev. Process Ind.* **14** (2001) 395–402.
272 F.P. Lees: *Loss Prevention in the Process Industries—Hazard Identification, Assessment and Control*, vol. 1, Butterworth-Heinemann, Oxford 1996.

273 W.E. Baker, J.J. Kulesz, R.E. Ricker, R.L. Bessey, P.S. Westine, V.B. Parr, G.A. Oldham: Workbook for Predicting Pressure Wave and Fragment Effects of Exploding Propellant Tanks and Gas Storage Vessels, NASA CR-134906, NASA Scientific and Technical Information Office, Washington 1977.

274 C.M. Pietersen: Analysis of the LPG Incident in San Juan Ixhuatepec, Mexico City, 19 November 1984, Apeldoorn, TNO, 1985.

275 Center for Chemical Process Safety (CCPS): *Guidelines for Evaluating the Characteristics of Vapor Cloud Explosions, Flash Fires, and BLEVEs*, American Institute of Chemical Engineers, New York 1994.

276 P.L. Holden, A.B. Reeves: "Fragment Hazards from Failures of Pressurized Liquefied Gas Vessels", *IChemE Symp. Ser.* **93** (1985) 205–220.

277 M.R. Baum: "Failure of a horizontal pressure vessel containing a high temperature liquid: the velocity of end-cap and rocket missiles", *J. Loss Prev. Process Ind.* **12** (1999) 137–185.

278 M. Abramowitz, I. Stegun: *Handbook of Mathematical Functions with Formulas, Graphs, and Mathematical Tables*, Dover Publications, New York 1972.

279 F.P. Lees: *Loss Prevention in the Process Industries. Hazard Identification, Assessment and Control*, vols. 1–3, Butterworth-Heinemann, Oxford 1996.

280 The Director-General of Labour: *Methods for the Determination of Possible Damage to People and Objects Resulting from the Release of Hazardous Materials*—"Green Book", Voorburg, December 1989

281 J.F. Louvar, B.D. Louvar: *Health and Environmental Risk Analysis: Fundamentals with Applications*, Prentice Hall, Upper Saddle River, NJ, 1998.